HYDROGEN EMBRITTLEMENT OF ALUMINIUM-LITHIUM ALLOYS

by

C. Thakur

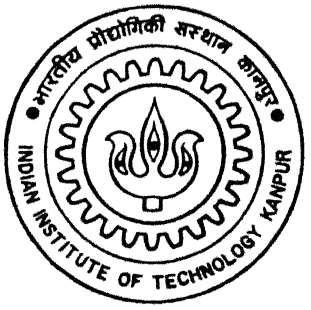

Department of Materials and Metallurgical Engineering

INDIAN INSTITUTE OF TECHNOLOGY KANPUR

APRIL, 1996

HYDROGEN EMBRITTLEMENT OF ALUMINIUM-LITHIUM ALLOYS

A Thesis Submitted
in Partial Fulfilment of the Requirements
for the Degree of
MASTER OF TECHNOLOGY

by

C THAKUR

to the

DEPARTMENT OF MATERIALS AND METALLURGICAL ENGINEERING

INDIAN INSTITUTE OF TECHNOLOGY KANPUR

APRIL 1996

MME-1996-M-THA-HYD

TO

MY SPIRITUAL MASTER

ANUKUL

CERTIFICATE

This is to certify that the work "Hydrogen Embrittlement of Aluminium-Lithium Alloys" has been carried out by Mr. C. Thakur under my supervision and that it has not been submitted elsewhere for a degree.

(R. Balasubramaniam)
Assistant Professor
Department of Materials and Metallurgical Engineering
Indian Institute of Technology
KANPUR

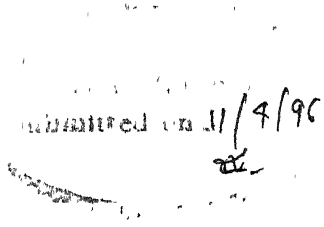

ACKNOWLEDGEMENTS

It is a pleasure for the author to express his deepest sense of gratitude and appreciation to Dr. R. Balasubramaniam for his esteemed guidance, valuable suggestions and encouragement throughout the study.

The present work is a part of the project sponsored by Aeronautical Research and Development Board, Ministry of Defense, Government of India. Their financial support is duely acknowledged. The author also wishes to acknowledge Dr. A.A. Gokhale of DMRL, Hyderabad, for providing the samples for the study. Valuable suggestions and discussions with Prof. A. Ghosh is also gratefully acknowledged.

Cooperation and help received from Dr.M.N. Mungole, M/s B.K. Jain, P.K. Pal, U.S. Singh, A. Sharma are thankfully acknowledged.

Author would also like to thank his friends Nunujee, Tapasda, Shyamjee, Arvind, Paddy, Rao and Basuda for their constant support, help and encouragement.

He had also the privilege to be associated with many other friends and well wishers whose names have not been mentioned here.

C. Thakur

INDEX

ABSTRACT

The aging behavior of Al-2.30Li-1.24Cu-0.80Mg-0.12Zr and Al-1.90Li-1.80Cu-1Mg-0.09Zr alloys (designated as 1440 and 1441) has been examined in detail by microhardness measurements of artificially aged specimens in varied conditions of heat treatment. The influence of solution heat-treatment temperature (SHT), percentage coldwork (CW), time and temperature of the artificial aging treatment and the influence of Li/Cu ratio on the aging behavior have been investigated. It has been found that solutionizing the alloys for 1 h above 530^{o}C provided satisfactory dissolution of the precipitates. Moreover, solutionizing at higher temperatures also provided higher hardness on subsequent artificial aging. Cold working the alloys prior to artificial aging hastened the kinetics of precipitation and also resulted in higher hardness. Higher Li/Cu ratio provided higher hardness on artificial aging. The aging behavior of the alloys at 150^{o}C, 170^{o}C and 190^{o}C has also been discussed. Artificial aging carried out at 170^{o}C for 16-18 h was found to be optimum for maximum strength, for both the alloys. The retrogression behavior of the peakaged alloys and the subsequent natural aging behavior of the retrogressed alloys were also studied. The critical immersion time for 1440 and 1441 alloys were found to be 60 sec at 270^{o}C and 40 sec at 235^{o}C, respectively. Possible structural hardening mechanisms of alloys have been discussed.

The hydrogen embrittlement (HE) of Al-Li alloys in different artificial aging tempers and after retrogression and reaging (RRA) treatments has been investigated by tensile testing hydrogen precharged specimens. Hydrogen precharging was performed in a 0.1M

NaOH solution at constant cathodic current density of 10 mA/cm^2, and at ambient temperature. The polarization behaviour of the alloys in this electrolyte was also studied with specific reference to film formation characteristics in this solution. The influence of RRA and hydrogen charging on the dislocation structure was studied by TEM. The under-aged temper was the most susceptible while the peak-aged temper was the most resistant to HE. The RRA treatment improved the HE resistance of all the tempers. This has been attributed to the reduction in dislocation density upon retrogression and reaging. The alloy with the lower Li content exhibited improved HE resistance. Flat fractographic features near the surface of the hydrogen charged specimen has been correlated to the depth of hydrogen penetration. Hydrogen concenteration profiles obtained by microhardness profiling have been utilized to determine hydrogen diffusivities in the alloys. The formation of $LiAlH_4$ and LiH in hydrogen charged Al-Li alloys has been confirmed by X-ray diffraction studies. The hydrogen-dislocation interaction and hydride cracking mechanisms of HE have been addressed.

LIST OF FIGURES

LIST OF TABLES

CHAPTER 1

INTRODUCTION

Hydrogen embrittlement (HE) is the loss of macroscopic ductility of a material due to the presence or interaction of hydrogen. This has been identified as one of the important mechanisms for explaining the failures in engineering materials due to environmental degradation.

Aluminium-Lithium alloys are candidate material for aerospace applications as they possess increased modulus to density ratio compared with conventional alumimium alloys. Rising energy cost has led to the development of more fuel efficient aircraft structures by reducing its weight. Al-Li alloys have been found promising in this regard. However, the use of Al-Li alloys has been restricted due to their low ductility and fracture toughness. The addition of Cu, Mg and Zr in advanced Al-Li alloys resulting in the precipitation of $T_1(Al_2CuLi)$, $S'(Al_2MgLi)$, S (Al_2CuMg), etc with an unrecrystallized microstructure has removed the above limitations. In the present study, the HE behaviour of two advanced Al-Li alloys (1440 and 1441) has been studied.

In addition to fuel efficiency, aircraft structures are also required to be corrosion resistant for safe and long service life. Therefore, the environmental degradation of these alloys by HE mechanism has received attention of several investigators. The present study was undertaken with following objectives. Firstly, an attempt has been made to understand the aging characteristics and retrogression behavior of these alloys. Secondly, the influence of grain boundary precipitates and dislocation density on the HE susceptibility of these alloys has been investigated.

Moreover, the validity of the hydride cracking mechanism of HE has been examined.

Microhardness measurements of the specimens in different heat treated conditions were used to characterize the aging behavior of these alloys. This technique was also used to determine the diffusivity of hydrogen in these alloys. A novel heat treatment, retrogression reaging (RRA), was used to vary the grain boundary precipitates keeping the δ' coherent matrix precipitate constant. Cathodic hydrogen charging followed by slow strain rate tensile test was employed to study the HE susceptibility to different heat treatment conditions of these alloys. X-ray diffraction (XRD) of hydrogen-charged specimens was employed to study the phase transformations near the surface region of the material due to the presence of hydrogen. Transmission electron microscopy (TEM) was used to study dislocation density structures in different heat treated specimens. Scanning electron microscopy (SEM) was used to observe the fracture morphology of precharged tensile specimens.

CHAPTER 2

LITERATURE REVIEW

2.1 *History of Alloy Development*

A historical perspective on the development of Al-Li alloys has been by Balmuth and Schmidt [1]. Its development began in Germany in the 1920s and was primarily concerned to increase the strength of aluminum alloys. In the 1950s, ALCOA developed the high strength Al-Cu-Li alloy designated as 2020. However, this alloy had low ductility and fracture toughness in the maximum strength temper. These limitations, as well as production problems, led to its withdrawal as a commercial alloy in 1969.

Since 1973, the rising energy costs has accelerated the development of more fuel efficient aircraft by reducing its structural weight and, consequently the development of advance Al-Li alloys obtained a renewed interest. Since aluminum alloys constitute nearly 80 pct. of the air frame weight, the advance Al-Li alloys can play a major role in the improvement of aircraft fuel efficiency. Besides beryllium, which is extremely toxic, lithium with a density of 0.53 gm/cc is the only alloying element that offers attractive combination of weight saving benefits and increased elastic modulus [2]. Each one percent weight addition of Li up to 4.2% increases the elastic modulus by 6% and reduces the density by 3% [3]. Moreover, additions of Cu, Mg and Zr to conventional Al-Li alloys have removed the limitation of low ductility and fracture toughness. Table 2.1 presents the composition of various commercial advanced Al-Li alloys.

Table 2.1 Composition of Advanced Al-Li Alloys [11,12]

Alloy Specification	Composition in weight percent			
	Li	Cu	Mg	Zr
2090	1.90-2.60	2.40-3.00	0.25	0.08-0.15
2091	1.70-2.30	1.80-2.50	1.10-1.90	0.04-0.16
8090	2.20-2.70	1.00-1.60	0.60-1.30	0.04-0.16
8090A	2.10-2.70	1.10-1.60	0.80-1.40	0.08-0.15
8091	2.40-2.80	1.80-2.20	0.50-1.20	0.08-0.16
X8092	2.10-2.70	0.50-0.80	0.90-1.40	0.08-0.15
X8192	2.30-2.90	0.40-0.70	0.90-1.40	0.08-0.15
CP-276	2.20	2.70	0.50	0.12
1440	2.30	1.24	0.80	0.12
1441	1.90	1.80	1.00	0.09
Weldalite 049 (Ag 04)	1.30	5.40	0.40	0.14
RX 818 Ag 0.4	0.80	3.50	0.40	0.13

2.2 *Physical Metallurgy of Alloy*

The Al-Li binary phase diagram is presented in Figure 2.1 [4]. About 4.2% Li can dissolve in aluminum at the eutectic temperature of 602^{o}C. However, due to certain restrictions regarding the maximum content of Li from a production and mechanical properties point of view, the maximum Li content present in commercial alloys is about 2.8% [5]. When Al-Li alloys containing more than 1% Li are quenched from the single phase field and aged at temperatures below the metastable δ′ solvus line, homogeneous precipitation of the metastable phase δ′ (Al_3Li) occurs. The atomic arrangement of aluminum and lithium in ordered δ′ ($L1_2$ structure) and its geometrical similarity to the fcc lattice of the solid solution facilitates the cube-cube orientation dependence observed. The close match between the lattice parameters of the precipitate and matrix results in a small misfit strain and leads to a homogeneous distribution of coherent spherical δ′ precipitates. The improvements in elastic modulus and density in the alloy occur irrespective of the presence of lithium in solid solution or δ′ precipitate. However, improvement in strength is dependent on volume fraction and size of δ′ [6]. The strength increase associated with δ′ is due to the magnitude of their resistance to dislocation motion. Although Al-Li alloys derive their strength from homogeneous precipitation of δ′, heterogeneous precipitation of the equilibrium δ (AlLi) phase is always possible below the solvus temperature [2]. Heterogeneous precipitation is enhanced at grain boundaries since they lower surface and strain energies and, thus, activation energy for precipitation. Consequently, δ precipitates at grain boundaries although it may be completely absent within the grains.

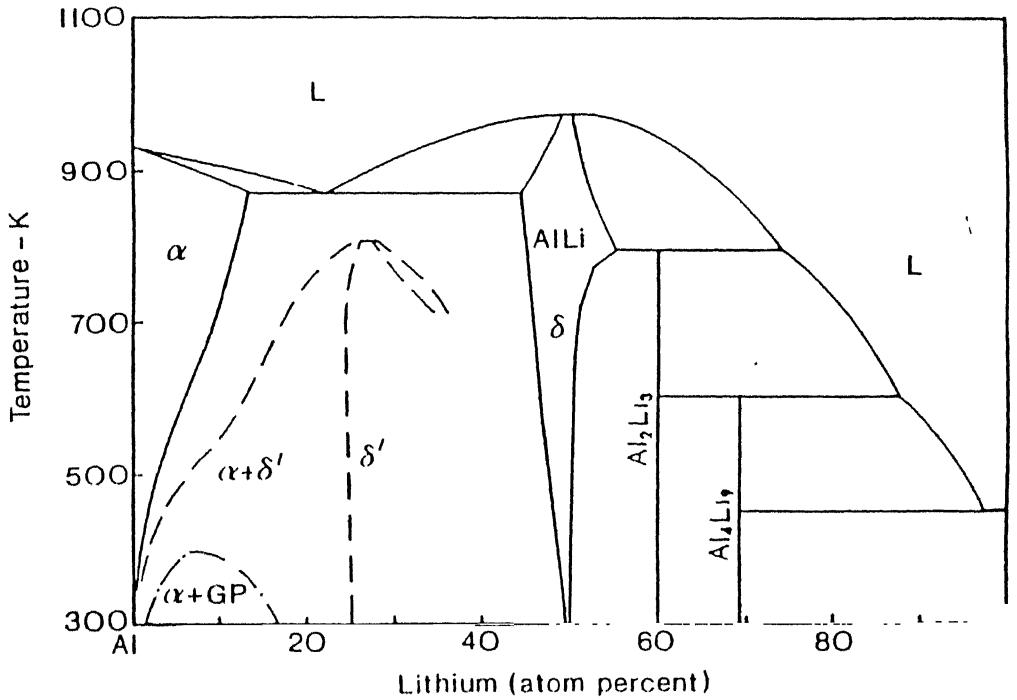

Figure 2.1 The binary phase diagram of aluminium-lithium alloy [4].

This results in a Li-depleted precipitate free zone (PFZ) adjacent to the grain boundaries.

The addition of Cu considerably increases the strength of Al-Li alloy without decreasing its ductility [7]. For the high lithium, low copper alloys, the T_1 (Al_2CuLi) phase forms directly in conjunction with δ' and the Al_2Cu precipitation sequence is absent [8]. The equilibrium T_2 (Al_6CuLi) phase may also form [9]. Copper addition in Al-Li alloys resulting in co-precipitation of T_1 with δ' aids in homogenizing deformation.

Magnesium increases the strength of Al-Li alloys by reducing the solubility of Li in the matrix, thereby enhancing the δ' precipitation [2]. Moreover, the precipitation of Al_2CuMg and Al_2MgLi phases further increase the strength of these alloys. Magnesium additions to a ternary AL-Li-Cu alloy provides solid solution strengthening and eliminates the formation of PFZ through the precipitation of S" and S' (Al_2CuMg) phases near the grains and subgrain boundaries [10]. Additionally, small amount of cold work (2% cold stretch) prior to aging enhances the precipitation of the above mentioned phases resulting in improved mechanical properties of the alloys [11].

In preference to manganese and chromium, zirconium addition has been used effectively to control recrystallization in Al-Li alloys [2]. Unlike manganese and chromium, Zr precipitates coherently as Al_3Zr. These Al_3Zr dispersoids inhibit the recrystallization by retarding subgrain boundary migration and coalescence. These dispersoids also help in avoiding the localization of planar slip, thereby improving the ductility of Al-Li alloys [11,12]. Moreover, Zr additions do not have any deleterious effect on corrosion resistance unlike Mn additions.

Therefore, Zr additions have been preferred to other dispersoid-forming elements for preventing recrystallization in Al-Li alloys.

The possible precipitates in Al-Li alloys and their crystal structures have been summarized in Table 2.2 [12].

2.3 *Heat Treatment of Alloy*

The mechanical properties and sensitivity to environmental degradation are function of the microstructure bearing different chemistry, size, volume fraction and distribution of precipitates. Microstructural features can be engineered through the variation of different heat treatment parameters. Precipitate size, volume fraction and distribution, and the width of PFZ are sensitive to a number of processing variables like [10,11], solutionizing temperature, quench rate, degree of cold deformation before aging, aging temp and aging time.

These experimental factors control the homogeneous precipitation of the equilibrium and metastable precipitates. In age-hardenable Al-Li alloys, the mechanical properties are essentially a function of the precipitate size and distribution [21], and therefore a strict control is required to obtain the optimum distribution while performing the thermal and thermomechanical treatments. For example, in order to obtain a homogeneous distribution of coherent, spherical $\delta'(Al_3 Li)$ precipitates in Al-Li alloys, aging has to be carried out at a temp below the δ' solvus. The phase diagram of Al-Li alloy showing the δ' solvus is shown in Figure 2.2 [22]. In Al-Li alloys, the δ' precipitates contribute to the strength of alloy in a significant way [12]. However, due to easy shearing of δ' precipitates by

Table 2.2 Possible Precipitates in Al-Li Alloys and Their Crystal Structure [12].

Precipitates in Al-Li Alloys	Crystal Structure	Lattice Parameters (nm)
Al_3Li (δ')	Cubic ($L1_2$)	a = 0.401
AlLi (δ)	Cubic (NaTl)	a = 0.638
Al_2CuLi (T_1)	Hexagonal	a = 0.496, c = 0.935
Al_6CuLi_3 (T_2)	Cubic	a = 1.391
$Al_{15}Cu_6Li_2$ (T_β)	Cubic (CaF_2)	a = 0.583
T'	Tetragonal	a = 0.575, c = 0.608
Al_2CuMg (S')	Orthorhombic	a=0.404, b=0.925, c=0.718
Al_2CuMg (S)	Orthorhombic	a=0.404, b=0.923, c=0.714
Al_2MgLi	Cubic	a = 2.000
Al_2Cu (θ')	Tetragonal	a = 0.404, c = 0.580
Al_2Cu (θ)	BCT	a = 0.607, c = 0.487
Al_3Zr (β) (dispersoids)	Cubic ($L1_2$)	a = 0.405
AlLiSi	Cubic	a = 0.594

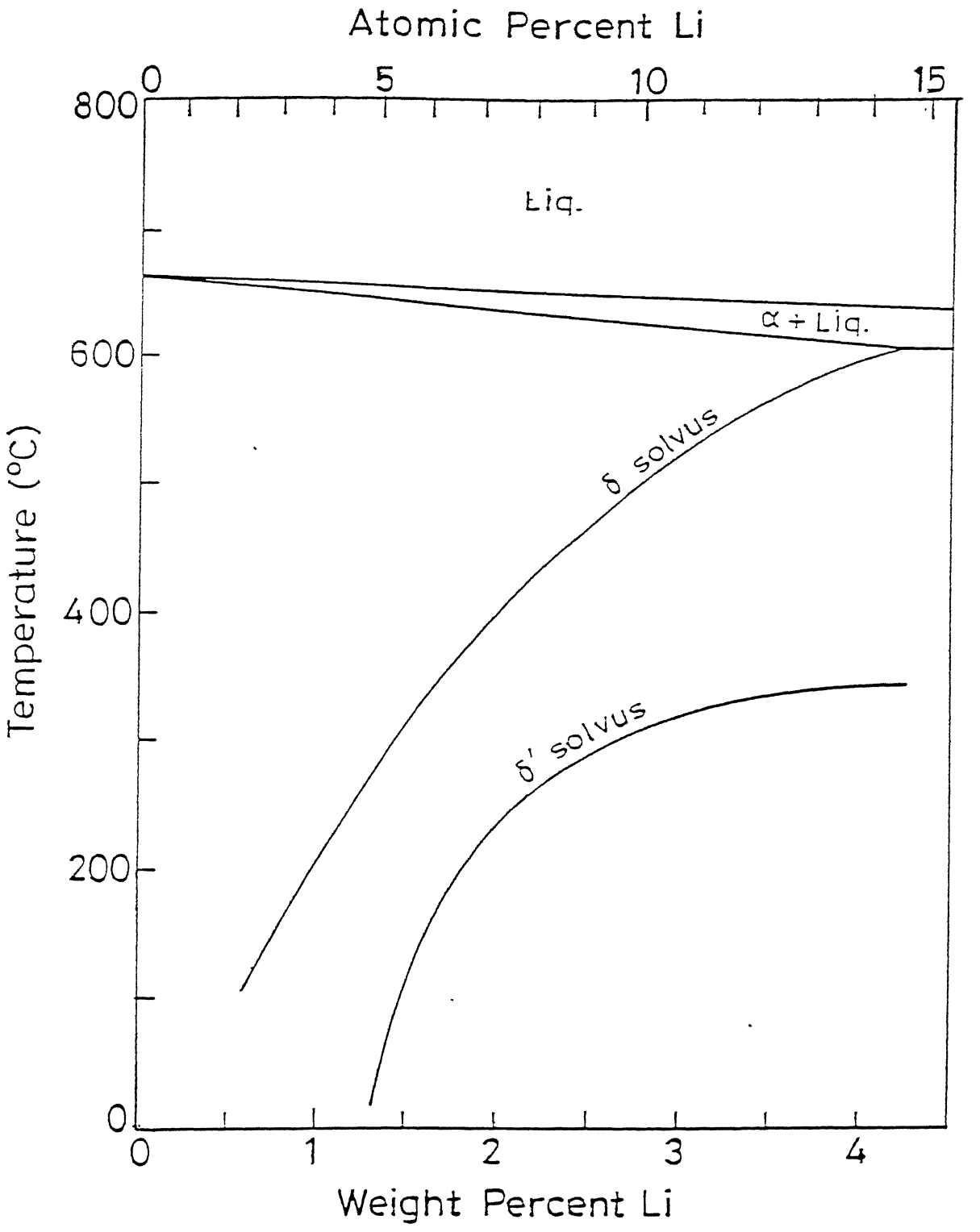

Figure 2.2 Al-Li phase diagram showing δ′ (Al_3Li) solvus [16]

dislocations, planar slip is promoted and this leads to strain localization. This reduces the ductility and toughness of the alloys [2,3,12,23]. To overcome the ductility problem, slip has to be homogeneously distributed within the matrix, which can be achieved by introducing dispersoids (like Al_3Zr) or semi-coherent or incoherent precipitates, {like $T_1(Al_2CuLi)$, θ' (Al_2Cu), S (Al_2LiMg) and $S'(Al_2CuMg)$} through copper, magnesium and zirconium additions.

The age hardening of Al-Li alloys involve continuous precipitation of $\delta'(Al_3Li)$ from a supersaturated solid solution. Precipitation occurs by nucleation and growth processes. Fluctuation in solute concentration provide small clusters of atoms in the lattice which act as nuclei for the precipitates. The rate at which these nuclei grow is controlled by the rate of atomic migration so that precipitation increases with increasing aging temperature. However, the size of the precipitates become finer as the aging temperature is lowered. Extensive hardening of the alloy is associated with a critical dispersion of precipitate. Beyond the peak aging time at constant temperature, coagulation of the particles occurs and numerous finely dispersed small particles are gradually replaced by a smaller number of more widely dispersed coarser particles. In this state the alloy becomes softer because the structure sensitive properties such as hardness, yield stress, etc. are extremely dependent on the structural distribution of the phases.

Since precipitation is controlled by the rate of atomic migration in alloy, temperature has a pronounced effect on the aging characteristics [21]. Moreover, precipitation is a thermally activated process and therefore, the period of aging is also

important. The growth of precipitate particles is directly related to the interfacial energy between matrix and particles. In case of coarser precipitates, matrix-precipitate interfacial energy is lower in comparison to the finer precipitates. This causes dissolution of small particles and simultaneous growth of coarser ones. In many alloys nucleation may occur both homogeneously and heterogeneously. Preferred sites for heterogeneous nucleation in such alloys are grain boundaries and slip planes. Since heterogeneous nucleation is easier than homogeneous one, precipitation tends to occur more rapidly at those sites. This introduces a time lag between aging responses in areas undergoing heterogeneous and homogeneous nucleations, and over aging frequently occurs at the grain boundaries long before precipitation in the matrix has had chance to develop fully. This may lead to the formation of precipitate free zone (PFZ) in the matrix [10] as is observed extensively in binary Al-Li alloys.

2.4 *Retrogression and Reaging (RRA)*

Grain boundary precipitates have been found to play a crucial role in HE susceptibility of Al-Li alloys [14]. In this regard, a novel heat treatment RRA has been employed to vary the size and the volume fraction of grain boundary precipitates. In conventional aluminum alloys, the over-aged (OA) T73 temper has been reported to be relatively less susceptible to environment induced cracking (EIC) [24]. However, overaging leads to a decrease in the strength of alloys. This problem was tackled, subsequently, through a heat treatment of peak-aged (PA) alloys called retrogression-reaging (RRA) [25]. RRA, a two stage heat treatment, combines the beneficial effects of both PA and OA

tempers. During the first stage of heat treatment (i.e. retrogression), the peak aged sample is maintained at a high temperature for a short duration (depending upon the alloy composition and sample thickness) to dissolve some of the coherent matrix precipitates while retaining the other precipitates at the grain and sub-grain boundaries. Immediately after retrogression, samples are subjected to reaging (second stage) during which the alloy regains its strength due to the precipitation of age hardening phases in the matrix. The microstructures of grain and subgrain boundary precipitates of RRA treated samples resemble approximately that of the over aged T73 temper. Resistance to HE increases after the RRA treatment due to the following reasons. Firstly, the grain boundary precipitates (size > 20 nm) have been proposed to act as irreversible hydrogen trapping sites which result in the improved HE resistance of RRA alloys [26,27]. However, it must be noted that these large grain boundary precipitates play a beneficial role in improving HE resistance only if they are large in number and homogeneously distributed. Secondly, the improvement of EIC resistance of RRA samples has been attributed to the decrease in dislocation density [28]. The relatively higher dislocation densities in the untreated samples result in additional stress fields leading to crack initiation. Moreover, dislocations also serve as rapid hydrogen diffusion paths, thereby enhancing the build up of hydrogen concentration to the critical limit beyond which HE of the alloy occurs.

The RRA treatment, devised by Cina [29], can be used to obtain the improved resistance to SCC/HE without sacrificing the strength of the peak-aged temper. Several RRA experiments carried out by a number of investigators [21,25,28-41] have been compiled

in Table 2.3. Their aim was to optimize the temperature and time of the heat treatments to obtain the best combination of strength and SCC/HE resistance in aerospace aluminum alloys. Longer retrogression times lead to a gradual loss of reaging responses [36]. Huang and Ardell [35] have used the retrogression and reaging heat treatments to dissolve δ' while retaining the T_1 precipitates in a nearly undisturbed condition. This is possible because T_1 is thermodynamically more stable than δ'. Slight growth of the former particles during the reversion anneal was also observed [35]. RRA treatments result in a significant decrease in stress corrosion crack growth rates [36]. The magnitude, interestingly, depends on the retrogression time [36]. According to Park [36] stress corrosion crack velocity decreased logarithmically with increase in the volume fraction of grain boundary precipitates in 7075 alloy. Coarsening of grain boundary precipitates occurs during the retrogression treatment, in contrast to the dissolution of the matrix precipitates, which also results in an increase in the volume fraction of grain boundary precipitates. This may also be the case with Al-Li alloys because the grain boundary precipitates (AlLi phase δ) are stable compared to the metastable matrix δ' precipitates. A coarse grain boundary precipitate distribution is favorable when the anodic dissolution mechanism of SCC is operative [33].

Rajan *et al.* [25] reported similar findings while studying the effect of RRA treatments on the SCC resistance of 7075. Their RRA treatment yielded coarse η' grain boundary precipitates and coherent θ' matrix precipitates. The latter provided high strength to the alloy while the coarse grain boundary precipitates provided enhanced SCC resistance.

Table 2.3 Salient features of retrogression and reaging (RRA)

Investigator(s) (year) [ref]	Alloy specifcation /composition (wt%)	Retrogression		Reaging		Remarks
		Temp. (^{o}C)	Time (min)	Temp. (^{o}C)	Time (h)	
B. Cina (1974) [29]	7075 T651	200-260	1-30	120	6	RRA heat treatment has been devised. RRA treatment claimed to increase SCC resistance of the 7075 alloy without sacrificing its YS and TS
I. Novikov (1978) [21]	Duralumin 2024 NA	250	0.80	-	-	Stability of GP zones and their dissolution temp estimated under diff aging conditions. Temp and time of reversion treatment must be individually selected for each alloy & their aging condition.
K. Rajan, W. Wallace and J.C. Beddoes (1982) [25]	7075 T6 Zn=5.1-6.1, Mg=2.1-2.9, Cu=1.2-2	220	5.00	-	-	Trade off between SCC resistance and YS in choosing between T73 and T6 temper can be eliminated by RRA treatment which is attributed to increase in GB ppt size keeping coherent matrix ppt const.
R.E.Swanson, I.M.Bernstein and A.W.Thompson (1982) [30]	7075 T6 Zn-5.68, Mg=2.48, Cu=1.63,	205 265	as per sample thickness	120	-	T6 RR treatmnet resists SCC crack initiation better than T6 temper but has about the same resistance to crack propagation. SCC resistance of notched T6 RR specimen is no better than T6 temper.
N.C. Danh, K. Rajan and W. Wallace (1983) [31]	7075 T6 Zn=6.1, Mg=2.1-2.9 Cu=1.2-2	200	5.00	120	24	RRA involves 3 main processes: 1. partial dissolution of GP zones, 2. formation and growth of η' particles & 3. coarsening of precipitates
J.K.Park and A.J. Ardell (1984) [32]	7075 T651	240	1.00	120	48	Effect of RRA on microstructure of 7075 T651 studied both in matrix and GB using TEM. Behaviour of ppt during RRA reported. Benificial effect of RRA attributed to increased overall ppt concn.
A.K. Vasudevan, J.Liu, and R.E.Ricker (1987) [33]	Al-Li alloys (a) Li=2.1, Cu=2.9	270	1.00	190	2	Contributions of GB ppt to SCC independent of matrix ppt. δ' in Al-Li alloys have been investigated using RRA technique. GB ppts play important role in SCC characteristics.
	(b) Li=2.9, Cu=1.1	325	1.00	190	2	
A.K. Vasudevan and R.D.Doherty (1987) [34]	Al-Li alloy Li=2.98 (a) Mn=0.49 (b) Zr=0.01	330	1.00	177	-	By RRA treatment it is possible to vary the amt. and size of GB ppt. keeping matrix microstruture const. YS of RRA treated alloy remained const. but toughness decreased due to increased GB ppt. RRA has been used as a tool to study the influence of GB ppts on GB fracture independent of δ' ppt

In most of the above investigations, Silicone-oil baths have been used, particularly for the low temperature heat treatments. However, for the high temperature retrogression treatments, molten salt or metal baths have been used. All the investigators quenched the samples in ice cooled water after retrogression treatments.

Table 2.3 continued

Investigator(s) (year) [ref]	Alloy specifcation /composition (wt%)	Retrogression Temp. (°C)	Retrogression Time (min)	Reaging Temp. (°C)	Reaging Time (h)	Remarks
J. C. Huang and A J. Ardell (1988) [35]	Al-Li alloy (a) Li=2 3, Cu=2 85	265	1.00	-	-	Seperate contribution of T1 & δ' to strengthening of Al-Li alloys investigated using RRA treatment Slight growth of T1 plates during reversion noticed. Very fine δ' ppt observed in reverted sample
	(b) Li=2.9, Cu=0.99	315	1.00	-	-	
J.K. Park (1988) [36]	7075 T6 Zn=5.43, Mg=2 38	200 220 240	30 00 5.00 1 50	120	48	Decrease in SC crack velocity without losing the max strength of RRA treated 7075 alloy attributed to increase in volume fraction of grain boundary precipitates.
M. Talianker and B.Cina (1989) [28]	7075, 7050 & 7278 T6 Zn=6.6-7 4 Mg=2.5-3.2 Cu=1.6-2.2	200 190	12.00 1-40	120 120	44 6-42	Presence of dislocations, rather than ppt structure, is the prime factor in determining the susceptibility to SCC of 7075 alloy. Improvement in SCC resistance by RRA treatment is caused by reduction in dislocation density
R.E Ricker, J.L. Fink and A K. Vasudevan (1991) [37]	Al-Li alloy (a) Li=3.0, Mn=0.5	338	1 00	177	1	Critical stress reqd to initiate SCC decreased with the increase in size and number density of GB ppts. SCC not observed in samples with higher Af of GB ppt because GBDF occured before the critical stress reqd for SCC could be reached However, the critical stress itself may be lower.
	(b) Li=2.0, Cu=1, Mn=0 5	288	1.00	177	0-0.5	
P.D. Pitcher, R.J Stewart, and S. Gupta (1992) [38]	8090	210	15 00	-	-	Problem of variable toughness in the ST direction of plates and LT of sheets of alloy studied Significant improvement in ST toughness achieved by RA. SANS and TEM employed to study the effect of RA on distribution of δ' ppt in the alloy SANS is ideal in contrast to TEM for the study of very fine spherical ppt.
C.P. Blankenship, Jr. and E.A. Starke, Jr (1993) [39]	AA8090 T8771 Li=2.55, Cu=1.2, Mg=0.7 Zr=0 11	210 230 250 275 300	5 00 5 00 5 00 5.00 5 00	100	145	ST fracture toughness improved by RRA treatments which produce transition from coarse planar slip to nomogeneous deformation leading to reduction in stress concn. across the weak high angle GB attributed to dissolution of δ' and growth of S'
D.C.Slavik,C.P Blankenship.Jr, E.A.Starke Jr, R.P Gangloff (1993) [40]	AA8090 Li=2.6, Mg=0.7, Cu=1.2, Zr=0.1	230	5.00	-	-	Influences of microstucture and deformation mode on inert environment intrinsic fatigue crack propagatiom studied. Amount of δ' ppt & extent of localized planar slip deformation reduced by increasing Cu/Li in alloy & by RA (reversion aging)
C. Thakur and R Balasubramaniam (1996) [41]	1440 PA 2.3Li-1.2Cu	270	1.00	170	2	RRA treatment of both the alloys in all aging tempers improved the HE resistance. TEM observation of RRA treated samples indicated the decrease in dislocation density.
	1441 PA 1.9Li-1.8Cu	235	0.66	170	2	

Danh *et al.* [31] observed the following microstructural changes during retrogression of an 7075 Al alloy:

(a) Partial dissolution of G.P. zones (first stage of retrogression) accompanied by a drop in strength of the alloy.

(b) Formation of η' particles (second stage of retrogression) accompanied by a recovery of strength.

(c) Coarsening of grain boundary precipitates after a critical retrogression time (third stage of retrogression) accompanied by a decrease in the strength of the alloy.

Vasudevan and Doherty [34] used the RRA experiment as a tool to independently control grain boundary precipitation while keeping the matrix strength constant in their study of toughness of Al-Li alloys. In this manner, they were able to attribute to reduced toughness of Al-Li alloys to the grain boundary precipitates. It has also been reported that the grain boundary δ phase can be deleterious to HE because it provides the necessary Li and Al for the formation of embrittling lithium alumino hydrides [42] at the grain boundaries. Ardell and Park [32] in a diametrically opposite view, suggested that coarsening of grain boundary precipitate by the RRA treatments was responsible for the improvement in the resistance of Al-Li alloys to SCC. Similar observations were made by Rajan et al. [25].

Cina [29] had originally proposed the RRA treatment with the objective of reducing the dislocation density of the system without causing overaging because Jacobs [43,44] had earlier suggested that dislocations developed during quenching from the solution treatment or during cold stretching before aging (and present adjacent to the grain boundaries) were responsible for susceptibility to SCC/HE.

There is fairly widespread agreement that hydrogen plays a major role in the SCC of engineering alloys [13,45,46]. Diffusion of hydrogen to, and along, grain boundaries, is expected to be accelerated by the presence of dislocations adjacent to the grain boundaries, and by the disordered nature of the grain boundaries itself. The microstructures, completely or partially free from dislocations after the retrogression and reaging treatments are relatively immune to SCC/HE in conventional Al alloys. The microstructural changes (involving the precipitate size and distribution changes) during the RRA treatment may then not be responsible for substantial change in SCC/HE susceptibility of 7075, as was first suggested by Talianker and Cina [28].

Jacobs and Dix [44,47] suggested, that during SCC, grain boundary precipitates dissolve and then act as crack initiation sites. Hence the resistance to SCC decreases as both the area covered by grain boundary precipitate and the number of particles per unit area of grain boundary increases. On the other hand, Ricker *et al.*[37] and Park and Ardell [32], for the specific case of Al-Li alloys, concluded that the increase in the volume of the grain boundary precipitates increases the resistance to SCC/HE. Thus, two opposite viewpoints on the effect of RRA treatment(s) on HE are available. It appears logical to explain the increased resistance to SCC of RRA treated alloys by the major changes in dislocation density rather than by the minor changes in precipitate structure [28]. Dislocations, at or adjacent to the grain boundaries, serve as trap sites for hydrogen produced either by dissolution of particles at the grain boundary or by hydrogen sweep-in by mobile dislocations. Mobile dislocations can capture hydrogen and carry them deep into the material at slow strain

rates [48] because it has been shown that strain rate should be lower than 10^{-4} per sec for hydrogen embrittlement effects to be observed [48]. Dislocation cores are strong hydrogen traps and about 3 to 5 times stronger than the Cottrell atmospheres [49]. Therefore any thermal treatment, causing a decrease in the density of dislocations and thereby, reducing the critical concentration of hydrogen for HE would improve resistance to HE.

2.5 *Hydrogen Embrittlement of Al-Li Alloys*

In addition to fuel efficiency, aircraft structures also require corrosion resistance properties. However, several studies have shown that Al-Li alloys are susceptible to environment induced cracking (EIC) [13-20]. In the following paragraphs, important role of HE in EIC of Al alloys has been discussed.

Thompson and Bernstein [46] suggested that hydrogen plays a dominant role in the SCC of Al alloys. Many others have since accepted the above mechanism of environmental degradation of Al alloys [13,50,61-71]. Green *et al.* [64] suggested an experiment for proving that hydrogen is important in SCC of aluminium alloys The material tested in an aqueous environment under tensile loading showed more susceptibility to hydrogen induced SCC compared to the material tested under torsional loading. In case of torsional loading the hydrostatic component of stress (which is believed to be responsible for driving hydrogen into the region ahead of the crack tip) is greatly reduced [72,73]. It has also been reported that significant improvement in both ductility and toughness and small decrease in yield strength could be achieved by reducing the hydrogen content from 43 to 14 ppm in Al alloys [74]. It has also been observed by Speidal and Hyatt [75] that an

increase in the total amount of solute (which is capable of being dissolved at high temperatures as a solid solution in the matrix) will increase susceptibility to SCC. Secondly, the presence of phase(s) at or near the grain boundaries (which are either anodic to the matrix [46] or strong hydride formers [42]) also give rise hydrogen embrittlement. Several studies have shown that HE is the main operative mechanism of EIC of Al-Li alloys [13-20]. The reversible nature of embrittlement [15], its strain rate dependence [48], the discontinuous nature of crack propagation [13], identification of brittle hydrides under HE condition [42] and the effect of cathodic overpotentials on hydrogen permeability resulting in enhanced embrittlement [17] are some of the evidences in support of HE as the probable mechanism of EIC compared to the anodic dissolution mechanism [13-20].

Therefore, attempts to improve EIC resistance of these alloys have focused attention on understanding the hydrogen embrittlement mechanism. In the study of HE susceptibility of these alloys, cathodic hydrogen precharging and slow strain rate tensile test have been generally utilized. The salient features of the previous HE studies have been compiled in Table 2.4 [15-20, 24,48, 50-60]. The weight saving and increased stiffness benefits of Al-Li alloys can be exploited by the aerospace vehicle designers only if the alloy is relatively immune to HE.

Aluminium alloys have low lattice hydrogen solubilities and diffusivities. This might lead to the erroneous conclusion that these materials are immune to HE. However, hydrogen solubilities can be enhanced by trapping and its diffusivity can be increased by dislocation transport. Hence, to understand the phenomena of HE, understanding of hydrogen-dislocation interactions is

Table 2.4 SALIENT FEATURES OF VARIOUS INVESTIGATIONS BY CATHODIC HYDROGEN CHARGING

Investigators	Experimental Conditions					Remarks
	sample specification	electrolyte	current density ($mA\ cm^{-2}$)	cathodic potential (mV vs SCE)	charging time (h)	
R.J Gest et al. (1979) [50]	7075 alloy, T 651 5.4 mm dia TS	3% NaCl soln pH = 6.5 - 7	-	-1500 to -1700	21 days	HE found to be the main mechanism of SCC in Al alloys Reversibility of embrittlement & discontinuous crack propagation observed in support of HE High cathodic pot led to H saturation No H saturation observed under anodic pot control due to pitting
T.F. Klimowicz et al. (1978) [51]	7075 alloy, 1.6 mm thick TS	(a) 3 5% NaCl, pH = 5.6-9 3 (b) H_2SO_4 and (c) Na_2SO_4 soln pH = 6 6-9.6 with and without 250 mg/l $NaAsO_4$	15	-1600	24	HE vs SCC of the alloys in aqueous Cl^- environment studied 2 test conditions (a) simultaneous deformation & charging (b) deformation of precharged samples Dominant role of HE supported by adverse effect of unstable surface film at higher alkanity presence of arsenate ions in the electrolyte
J. Albrecht et al (1979) [24]	7075 alloy, 5 3 mm dia TS	HCl soln., pH=1	-	-1500	10	Tensile testing in -200 to 20° C. Temp dependence of HE investigated UA found to be the most and OA least susceptible to HE. In OA max embrittlement shifted to lower temp HE correlated with slip planarity Transgranular fracture predominat in HE
D.A. Hardwick et al. (1982) [52]	2124 alloy, 5.4 mm dia TS	HCl soln , pH=1	-	-1500	10	HE of heat treated alloy investigated under precharging and SET conditions UA temper more susceptible to HE Degree of HE more for 7075 than 2124 alloys HE contributes to SCC in 2124 alloys
R E. Swanson et al (1982) [53]	7075 Al alloy, 5 38 mm dia, TS notched (root dia=3 86 mm)	HCl soln , pH 1 at room temp	-	over potential 150 mV	SET cross-head speed=10^{-4} cm/s	SCC of alloy of PA (T6) and IA-RRA (T6-RR) tempers investigated RRA did not improve SCC resistance of notched T6 samples T6-RR temper resists crack initiation better than the conventional T6 temper, but resistance to crack propagation is almost the same for the two tempers
P.P. Pizzo et al (1984) [54]	Al-Li alloy, 1.4 mm thick TS	3 5% NaCl soln	-	-1075	16	Role of H in SCC suggested Stringers of second phase particles along extrusion direction attacked rapidly during hydrogen charging attributed to play an important role in SCC. Susceptibilty to SCC of alloy influenced by electrochemical conditions and its microstructure
F. Binsfeld et al. (1987) [15]	Al-Li alloy, 0.8 & 1.6 mm thick TS	molten salt at 190°C	-	-1500 mV/Ag -2000 -2500 -3000		HE favoured in OA temper Intergranular failure observed H may promote dislocation density

Table 2.4 continued

Investigators	Experimental Conditions					Remarks
	sample specification	electrolyte	current density (mA cm^{-2})	cathodic potential (mV vs.SCE)	charging time (h)	
T. Magnin et al. (1987) [20]	Al-Li-Cu alloy, 5 mm dia TS	3.5% NaCl, pH=6	-	-1400	12	In PA temper CP 271 alloy found to be less susceptible to HE than conventional Al-Zn-Mg alloy HE may occur even at free corrosion potential when microcracks are formed during CF, in SCC by AD and tensile tested at very slow strain rate
S.S. Kim et al et al. (1988) [55]	2090 alloy, 1 mm thick TS	0.1N NaOH+ small amount of As_2O_3 as hydrogen recombination poison	varied from 1 to 100	-	varied from 1 12	Fracture strain decreased with increase in the relative hydrogen content Specimen with tensile orientation normal to rolling direction is more susceptible to HE than that of parallel to rolling direction H charging promoted delamination of alloys.
J.W Watson et al. (1988) [56]	pure Al 0.75 mm thick TS	75% methanol + 22.4% H_2O + 2.6% H_2SO_4 soln. containing 10 mg/l As_2O_3	30	-		Severely hardened surface region commensurate with an increased dislocation density which moved towards the core at approximately the diffusivity of Hydrogen in Al
T. Ohnishi et al. (1988) [16]	AA 8090 alloy 2 mm thick TS	2N H_2SO_4 with 1 Kg/m^3 Na_2HASO_4 $7H_2O$ at 293 K	5	-	30 min	Effect of cathodic H charging on mech prop of alloy aged at 453K studied Significant H permeation for UA and limited for OA conditions 2 step hardening behaviour on aging In step 1 sol hardening & in step 2 tendency of embrittling due to H charging
G. Disson et al (1989) [57]	2091 alloy, 1.6 mm thick TS	3 5% NaCl		≤ -1550	few hours	Both AD and HE mechanisms of SCC have been investigated in diff corrosive conditions In general, AD & HE both are operative However, under cathodic polarization embrittlement solely due to Hydrogen
E I. Meletis et al. (1989) [17]	Al-Li-Cu alloys 3 mm dia TS	(a) 0.1N HCl pH=1 (b) 0 5N H_2SO_4	-	-3000	10	SSRT in various environments to study HE Alloys susceptible to HE under cathodic charging or pre-exposing in NaCl soln Mainly transgranular fracture, some intergranular cracks too.
R. Balasubramaniam (1990) [18]	Al-Li & Al-Li-Cu alloys 3 mm dia TS	0 5M NaCl aerated pH=2 at temp 23°C	-	-1100 -1500	CERT strain rate $10^{-6}s^{-1}$	HE susceptibility increased with aging Instability of oxide film, dependent on pH, play important role in determining the degree of HE HE depends also on strain rate Cu bearing Al-Li alloy more prone to HE
A. Ravindra et al. (1991) [58]	8090 T6 alloy 2&1.5 mm thick TS	3 5% NaCl soln pH = 6, at 300 K	0 15	-	15	SCC/HE susceptibility to different orientation of TS w.r t the rolling direction investigated TS with orientation normal to RD showed higher SCC susceptibility than TS with orientation parallel to RD

Table 2.4 continued

Investigators	Experimental Conditions					Remarks
	sample specification	electrolyte	current density ($mA\ cm^{-2}$)	cathodic potential (mV vs SCE)	charging time (h)	
Z.F. Wang et al. (1992) [19]	Al-Li-Cu Mg-Zr alloys 2 mm thick TS	3.5% NaCl soln. pH = 6.9	-	-1050	-	SCC of alloy with variable orientation of samples & applied pot studied. SCC susceptibility highest in PA than that of NA and OA tempers TL samples more prone to SCC than LT samples HE predominat above a critical H concn below it LAD becomes important
A Bandyopadhyay et al. (1992) [59]	2091 & 2014 alloy 2 mm thick TS	3 5% NaCl soln., pH = 6 2 at 45°C	1 - 10	-	10	Elongation, UTS and YS decreased with increase in ccd. Transition in fracture mode from surface (brittle) to the core (ductile) observed. Presence of hydrogen increased surf hardness (soln strengthening) & it decreased with depth due to H conc. grad
L. Chen et al. (1993) [48]	8090 alloy 2 mm thick TS	0.1N NaOH soln. containing 250 mg/l As_2O_3	10	-	6	Effect of H and Strain-Rate(SR) on mech prop. and fracture mechanism investigated Linear decrease in UTS, YS and El with decreasing SR reported. SIMS revealed decrease in atomic BE of Al & Li in alloy
C Thakur et al. (1995) [60]	1440 & 1441 alloys 2.6 & 1.6 mm thick TS	0.1N NaOH soln. containing 100 ppm arsenate ion 10 ml/l	10	-1680	12	HE susceptibility to different heat-treatment cond. investigated PA temper was found to be less prone to HE and UA the most Moreover, PA+Retrogressed+UA was least susceptible to HE Alloy bearing more Li showed more susceptibility to HE

required. The deleterious effects of hydrogen are multi-faceted and complex. Therefore, several mechanisms of HE should be considered simultaneously in the case of Al-Li alloys.

Tien et al [79] observed that dislocation transport of hydrogen in Al alloys can be several orders of magnitude higher than the lattice diffusion of hydrogen. Therefore, the observation that environmental cracking rates exceed the rate of hydrogen diffusion [13] does not rule out the possible role of hydrogen in the SCC/EIC of Al-Li alloys. Moreover, environment sensitive crack growth occurs at relatively low stresses compared to those required for cracking under static loading conditions [45].

In fcc structures, the diffusivity of hydrogen is lower in comparison to bcc structures. Hence, the transport phenomena are of fundamental importance in describing the mechanisms by which metal loses its ductility. Hydrogen transport towards the crack tip can be accelerated simultaneously by a triaxial stress (through its effect on the chemical potential) and by a dislocation interaction effect.

In practice, the source of hydorogen for HE under humid atmosphere may be the condensation of moisture over the surface of alloy leading to hydrogen absorption by the following reaction.

$$Al + 3H_2O = Al_2O_3 + H^+ + 6e^- \qquad (2.1)$$

In aqueous solutions the following sequence of reactions may result in hydrogen uptake.

$$\underset{\text{(bulk liquid)}}{H^+} \longleftrightarrow \underset{\text{(on metal surface)}}{H^+} \longleftrightarrow \underset{\text{(adsorbed)}}{H} \longleftrightarrow \underset{\text{(near surface)}}{H_2} \qquad \text{(absorbed)} \qquad (2.2)$$

Hydrogen embrittlement of alloys depends upon the following

steps:

(a) Generation of atomic hydrogen

(b) Adsorption of atomic hydrogen

(c) Absorption of hydrogen

(d) Recombination of atomic hydrogen or its diffusion into the matrix

(e) Critical concentration of atomic hydrogen ahead of crack tip

In addition, the following factors would also be effective in the determination of HE susceptibility of alloys.

(a) Interactions with

(i) dislocation

(ii) grain boundary impurities (e.g. Mg)

(iii) grain boundary precipitates and their chemistry, size and distribution

(b) Volume fraction of irreversible and reversible traps present in the alloy

(c) Distribution pattern of the hydrogen traps.

There are contradictory reports in the literature between SCC susceptibility and degree of aging. Holroyd *et al.* [14] and Dorward and Hasse [76] observed that the SCC resistance of 8090 is improved in the OA condition as indicated by a reduction in the kinetics of crack initiation and crack propagation. It is interesting to note that Christodoulou *et al.* [13], and Ricker *et al.* [37] also explained the favorable SCC resistance of the OA condition using the anodic dissolution model of SCC. According to Christodoulou *et al.*, in the OA condition, the zone around the grain boundary is almost entirely and continuously deformed, and thus is more anodic. Consequently the difference in

electrochemical potential between the grain boundary δ and the surrounding Al matrix is reduced, and the zone itself becomes the corrosion path. This path is wider than the corrosion path produced by δ dissolution alone. The OA treatment leads to crack blunting by increasing the precipitate size at the grain boundaries (i.e. by increasing the radius of curvature of the advancing crack tip). This reduces SCC susceptibility of the OA temper to levels which are below detection by the experimental technique employed.

It is also suggested that UA and PA Al-Li alloy microstructures are susceptible to SCC because of coherent precipitates are easily sheared leading to planar slip and its associated problems [46]. On the other hand, the OA microstructure contains precipitates which can be easily bypassed (during deformation) by cross-slip [77,78]. Tien et al [79] have observed that planar slip conditions favor dislocation hydrogen transport and this could be one reason for the poor HE resistance of the UA and PA tempers. Moreover, planar slip produces a higher number of slip steps on the surface resulting in larger areas of exposed bare metal. This indirectly provides more sites for hydrogen reduction (i.e. hydrogen generation) on the surface. In case of Al-Li alloys Niskanen *et al.* [80] observed that the δ phase which is anodic to the matrix has a deleterious effect on the corrosion behaviour (considering active path mechanism for the crack propagation). In addition, Meletis [81] suggested that the presence of more active phases at grain boundary and the development of grain boundary strain due to microstructural changes involving θ' and δ' phase interactions, θ' to T_1 transformation and formation of more δ precipitates, would

reduce the SCC/HE resistance of the Al-Li alloy (2090 alloy) in its over aged temper. However the observations made by Meletis are in strong contradiction with Holroyd *et al.* [14] and Dorward *et al.* [76]. Therefore, OA tempers should be more susceptible to SCC/HE in Al-Li alloys in contrast to conventional Al alloys in which the OA tempers are resistant to HE/SCC.

Some observations about the fractography features of HE in Al-Li alloys are presented below. Al-Li alloys are more resistant to SCC in the long transverse direction relative to that in short transverse direction due to anisotropy. Hydrogen induced fracture is usually brittle, and intergranular fractures are, in fact, commonly observed [13], though in some cases ductile fracture is observed in the presence of hydrogen [48]. The tensile fracture morphology of hydrogen charged specimens tested at slow strain rates is grain boundary brittle fracture (GBBF), while that of at faster strain rates is grain boundary ductile fracture (GBDF)

Transgranular cracking in Al-Li alloy is associated with HE while intergranular cracking is due to either hydrogen embrittlement or anodic dissolution depending upon the externally applied electrochemical potentials [13]. At low strain rates, dislocations interact with hydrogen atoms to form core hydrogen atmospheres thereby carrying the hydrogen atoms into the PFZ to cause cracking. This also enhances slip of dislocation on the slip plane in the PFZ and usually results in a microscopically smooth grain boundary fracture. Therefore, this kind of fracture is pseudo-intergranular fracture, because the fracture cracks do not nucleate and propagate along grain boundaries but in the PFZ adjoining the grain boundaries.

Binary Al-Li alloys show grain boundary ductile fracture

(GBDF) because of their low tensile ductility. Strain localization (either in the matrix {111} slip planes or in the wide grain boundary PFZ) result in micro voids nucleation and coalescence at the grain boundaries, which is one of the reasons for the reduced tensile ductility of Al-Li alloys. However, the large sized closely spaced grain boundary precipitates (which is a special feature of Al-Li alloys in contrast to conventional Al alloys) affects GBDF in a significant way [34]. The above special characteristic of Al-Li alloys has been explained by Jensrud and Ryum [22] as follows. The wide difference in the solubilities of Al and Li (between grain boundary and matrix phases) is responsible for the excessive growth of grain boundary precipitates. Moreover, in order to achieve the peak strength temper, large size of δ' precipitates are required in the matrix which requires higher aging temperatures. This provides an additional opportunity for grain boundary precipitates to coarsen.

It is important to note that micro voids formation at grain boundary leads to GBDF. Rogers [82] suggested that high density of incoherent precipitates at the grain boundaries can give rise to a microscopically ductile fracture surface but macroscopically the fracture seems brittle. This is more severe, particularly, if the particles are in planar array on the grain boundaries. Thus a high area fraction of grain boundary precipitates leads to GBDF. Planar slip appears to be important in transgranular fracture.

2.6 *Mechanism of HE in Al-Li Alloys*

The complexity of HE phenomena in Al-Li alloys arises from factors such as nature and distribution of hydrogen trapping sites, possibility of hydride formation and possible reaction

between hydrogen and dislocations, impurities and/or alloying elements. Assuming a critical hydrogen concentration within the alloy lattice, the various mechanisms of HE reported in the literature for Al alloys are hydrogen pressure theory [84], decohesion model [83], hydrogen enhanced localized plasticity (HELP) [84], hydride cracking [42], and hydrogen-dislocation interactions [83]. Disparities amongst the findings of different investigations may be partly due to the different test conditions employed in the studies and partly to their consideration of single HE mechanism. Moreover, the variation in susceptibility of Al-Li alloys in different aging tempers to HE indicates that a universal HE mechanism is quite unlikely. Hence, in the analysis of HE susceptibility of Al-Li alloys to different heat treatment conditions, two or more mechanisms should be considered simultaneously instead of a single one.

2.6a *Decohesion Model*

The fracture stress (σ_c) necessary to cause the spread of an elliptical crack length (2C) is given by

$$\sigma_c = \left(\frac{2 E \gamma_s}{\Pi C} \right)^{\frac{1}{2}}$$

where γ_s is the specific surface energy of the new interface created by the advancing crack and E is the young's modulus of matrix [45]. Hydrogen adsorption on the crack surfaces is hypothesised to reduces the γ_s, which results in the lower value of σ_c in the presence of hydrogen [45]. This increases crack growth rate in the presence of hydrogen. Atomically dissolved hydrogen thus lowers the maximum cohesive force (force required

for the separation of the metal atoms) in the system. Chen *et al.* [48] showed that atomic binding energies of Al and Li in 8090 Al-Li alloy decreased after hydrogen charging by SIMS. They explained the HE of 8090 Al-Li alloy based on the decohesion model. However, their fractographs do not support such a mechanism. Extensive planar slip (which can be observed in their fractographs) may lead to the accumulation of hydrogen at the grain boundaries which may either reduce the cohesive strength or induce hydride formation. The authors have not discussed the second aspect (i.e. hydride formation) in their paper. It must be remembered that this could also result in intergranular separation under applied tensile stresses and the fractographs do not support this mode of failure. According to the decohesion model, transgranular cracking is equally probable, which does not occur in Al-Li-Cu-Mg-Zr alloys [45] (the fracture is highly intergranular under HE condition). It must also be mentioned here that several investigators have proposed the slip dissolution model to explain SCC of Al-Li alloys. Planar slip promotes coarse slip steps on the surface which lead to increased SCC susceptibility, whereas homogeneous slip (which produces closely spaced slip steps) leads to lower SCC susceptibility. The latter is less likely to rupture the passive film on the surface, which is a necessary event for SCC propagation by the slip dissolution model. Localized dissolution is often concentrated in grain boundary because of electrochemical heterogeneity at these locations due to the presence of active phases [13,45,85].

2.6b *Hydrogen-Enhanced Localized Plasticity (HELP)*

This mechanism postulates a ductility enhancement at crack tips which facilitates the initiation and propagation of fracture [84]. In a system under tensile stress, the defects are often near strain-singular points such as crack tips. Rapid accumulation of hydrogen at the crack tips results in a strongly inhomogeneous hydrogen concentration associated with local plasticity variations. Under tensile stress fracture would occur at these hydrogen saturated weak links, while the bulk of the matrix is not strongly affected. Fracture morphology is indistinguishable from brittle fracture. The regions of high local stress are relaxed by forming cracks. Presence of such cracks with ductile tip lowers the critical tensile stress substantially when compared to the defect-free system [84]. In real situation, crystal deformation occurs by dislocation motion. The locally increased plasticity near hydrogen loaded dislocations clearly lowers the friction stress for dislocation motion and hence, the material becomes resistant to cleavage.

2.6c *Hydride Cracking*

Hill, William and Mobley [86] first proposed that the poor ductility of Al-Li alloys might be due to the formation of a soluble hydride of either Li i.e.(LiH) or of Li and Al (i.e. Li_3AlH_6). Dickenson et al [87,88] observed LiH formation in Al-Li alloys when they were heat treated in moist air or in hydrogen, and that the morphology of LiH precipitates were highly faceted in commercial Al-Li alloys. Nucleation of LiH appeared to occur heterogeneously at grain boundaries and intermetallic grain

boundary particles. Recently, a hydride cracking mechanism of SCC has been elucidated by Balasubramaniam et al [42] for Al-Li alloys. Cleavage may occur either in the matrix or at the grain boundary through a precipitated hydride phase in the presence of hydrogen. Repeated formation and cleavage of hydrides ahead of the crack tip may explain nearly all the observed features of SCC fracture in Al-Li alloys (i.e. the hydride cracking mechanism). The low fracture toughness of the hydride facilitates crack growth by cleavage. Cracks arrest at the grain boundary when a relatively tougher matrix is encountered. Another particle of hydride then forms in the region ahead of the crack tip and the process of cleavage, and crack growth and arrest are repeated, resulting in discontinuous crack growth.

Regardless of the different mechanisms discussed above in the review, however, the facts that presence or interaction of hydrogen in the alloys degrades their mechanical properties and HE plays a dominant role in EIC have become well established. Two or more of the hydrogen embrittlement mechanisms may be operative simultaneously. It may be concluded from the above discussions that HE susceptibility of Al-Li alloys is a complex phenomena and is a function of microstructure of alloys, dislocation structure and, the nature and distribution of hydrogen traps.

CHAPTER 3

EXPERIMENTAL PROCEDURE

3.1 *Material*

The materials used in the present study, Al-Li alloys 1440 and 1441, were supplied by Defense Metallurgical Research Laboratory, Hyderabad. The two alloys were supplied as rolled sheets 2.9 mm and 1.8 mm thick respectively. The chemical compositions of these alloys are presented in Table 3.1. The 1440 alloy was supplied in the hot rolled condition, whereas, the 1441 alloy had been further solution treated at 530°C, cold stretched by 2 % and age hardened at 170°C for 24 hours to provide the peak aged temper as designated by the supplier. All these alloys were resolutionised in the present study before subsequent aging heat treatments. Figure 3.1 provides typical microstructures of the as-received 1441 Al-Li alloy in the rolling, long transverse and short transverse directions.

3.2 *Specimen Preparation*

3.2a *Solutionizing*

Samples from each alloy were cut in the form of strips (10 cm by 1 cm) and were enclosed in an evacuated glass tube for the solution heat treatment.

3.2b *Aging*

The individual solutionized and cold stretched strips were cut into one square centimeter coupons for the artificial aging treatments.

Table 3.1

Chemical composition (in wt %) of Al-Li alloys used in the present investigation

Alloy Specification	Li	Cu	Mg	Zr	Fe	Si	Al
1440	2.30	1.24	0.80	0.12	0.09	0.04	bal
1441	1.90	1.80	1.00	0.09	0.10	0.05	bal

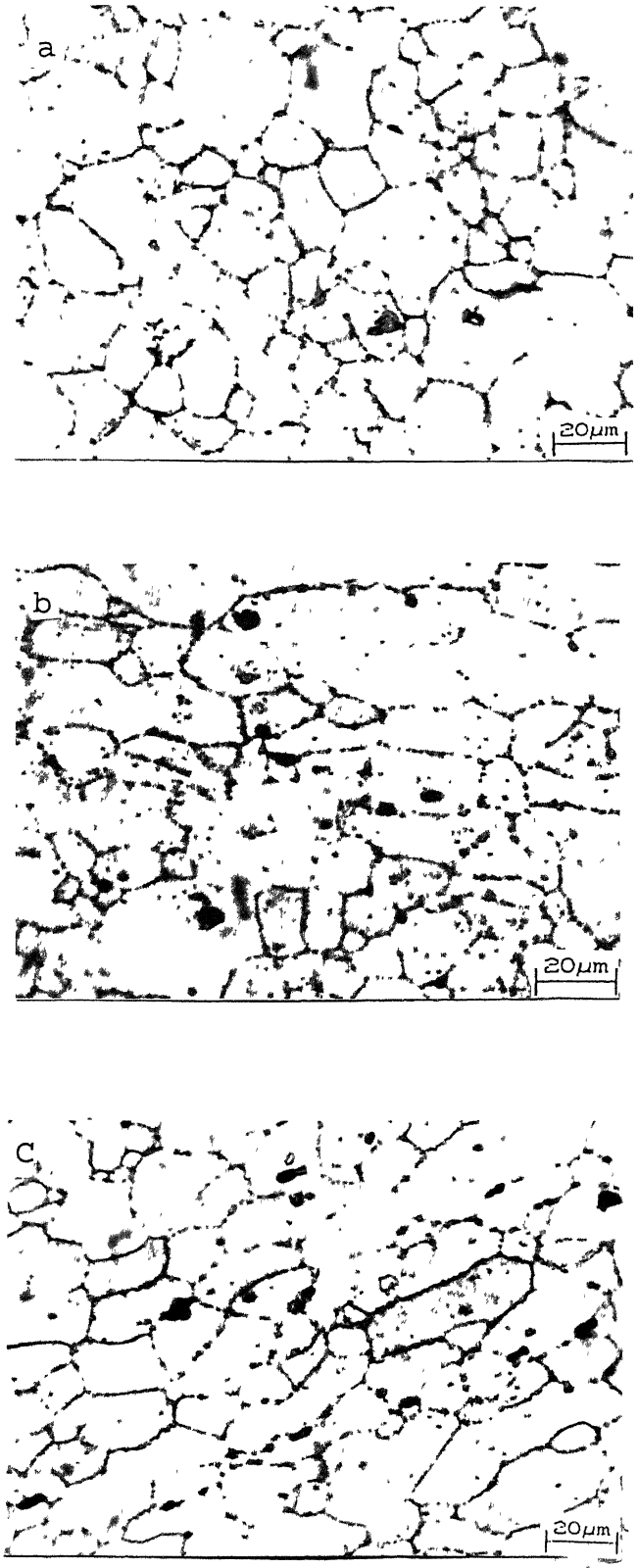

Figure 3.1 As received microstructures of 1441 Al-Li alloy in the(a) rolling, (b) long transverse and (c) short transverse directions.

3.2c *Microhardness Measurements*

In order to characterize the aging behavior of samples after different heat treatments microhardness measurements were obtained from each sample. Before the hardness measurement, all the heat treated samples were mounted in cold setting epoxy, and initially ground on 600 grit wet polishing paper in order to remove the Li depleted zone from near the surface [106-109]. The surfaces were then ground and polished metallographically to one micron surface finish for microhardness measurements.

3.2d *Tensile Testing*

As the 1440 and 1441 alloys had different thicknesses, the tensile specimens had to made with different dimnsions as per ASTM standard. Flat tensile specimens of 16.5 mm gauge length, 5 mm width and 4 mm R value were machined form the heat treated strips of 1440 alloy with tensile axis parallel to the rolling direction. Similarly, tensile specimens of 13.5 mm gauge length, 5 mm width and 3 mm R value were cut from the 1441 alloy heat treated strips. For each heat treatment conditions 4 identical tensile specimens were prepared form each alloy strips.

3.2e *XRD Analysis*

Specimen coupons (1 cm^2 cross-sectional area) were sectioned from the sheet and later all the surfaces were ground and polished to 1 micron surface finish. Similar preparation was done for the specimens used for SEM study, except the surfaces were polished to 0.05 micron surface finish on slow speed cloth polishing machine.

3.2f *TEM Analysis*

Transmission electron microscopy (TEM) was used to characterize the dislocation structure in few heat treated samples before and after the cathodic hydrogen charging. Thin foils of 0.2 mm thickness were prepared by mechanical polishing of the samples. Discs of 3 mm diameter were then punched from the thin foils. Twin jet electropolishing of the foils was carried out in a 1:3 mixture of nitric acid in methanol at -20°C and at 20 Volts potential difference. The specimens were examined in a JEOL 2000FX transmission electron microscope operating at 100 kV.

3.3 *Heat Treatment*

3.3a *Solutionizing and Cold Stretching*

In order to study the effect of solution heat treatment temperature (SHT) on the artificial aging behavior, samples were solutionised at three different temperatures (510,530,and 550°C) for one hour followed immediately by water quenching. The solution treated samples were refrigerated to avoid any appreciable natural aging before the commencement of artificial aging heat treatments. Care was taken during subsequent cold stretching operations not to keep the samples (taken out of the refrigerator) for more than half an hour to prevent natural aging. One of the two solutionised alloy strips was cold stretched in a 1195 INSTRON tensile testing machine to 1.5% prior to the artificial aging heat treatments while the other alloy strip was directly subjected to aging heat treatment without any prior cold deformation. The solutionizing treatment at 530°C for 1 h was used for sample pretreatment in all the investigations of the present study.

3.3b *Aging Treatment*

Artificial aging treatments were carried out using a constant temperature silicon oil bath controlled to within ±2 °C. Artificial aging was carried out at three different temperature of 150, 170, and 190 °C for periods of time varying from 2 to 96 hours. After heat treatment, the samples were removed from the furnace and air cooled to room temperature. The aging temperature of 170°C and aging time, 16 h for 1440 and 18 h for 1441 was used for sample pretreatment to obtain PA temper in all the investigations of the present study.

3.3c *Retrogression*

Peak aged samples of both the alloys were subjected to retrogression treatment. The retrogression heat treatment procedure adopted in the present study is as follows. The retrogression temperatures for the two alloys were estimated first from the δ' solvus of the Al-Li phase diagram [22]. The temperature was chosen 5°C above the solvus temperature of δ' (Al_3Li) phase. The retrogression temperatures used in the present study were 270°C and 235°C for 1440 and 1441 alloys, respectively. The samples in the peak aged temper were immersed in a constant temperature silicone oil bath for precise periods of 10, 20, 30, 40, 60, and 90 secs. The retrogression treatment was followed by an immediate ice cold water quench. Thereafter, the samples were preserved in the refrigerator. Finally, microhardness measurements of each sample were obtained.

3.3d *Natural Aging*

Moreover, the samples retrogressed for different times were subjected to natural aging at room temperature (25^{o}C) for one to ten days. In addition to this, the solution treated and cold stretched samples of both the alloys were also subjected to natural aging at ambient temperature for sixty days. Retrogressed samples were naturally aged and the variation in their microhardness values were recorded daily till a constant value was obtained. Similarly, solution treated and cold stretched samples were naturally aged and microhardness measurements recorded in the same way as mentioned before.

3.3e *Baking of hydrogen charged specimens*

In order to understand the stability of the phases formed on hydrogen charging, the hydrogen-charged specimens were further subjected to baking treatments at 25^{o}C (for 1 day), 160^{o}C, 395^{o}C, 510^{o}C and 550^{o}C for 25 minutes in a vertical tube furnace under atmospheric conditions. The same hydrogen-charged sample was successively baked at the above mentioned temperatures in steps and XRD patterns were obtained after every baking treatment. Additionally, one sample of each alloy was baked directly at 550^{o}C after hydrogen charging and the XRD study conducted.

3.4 *Cathodic hydrogen charging of heat treated samples*

In actual practice, hydrogen may be absorbed during the cathodic protection or reaction with moisture by these alloys. Condensation of moisture over the surface of alloy may lead to hydrogen absorption by the following reaction.

$$2Al + 3H_2O = Al_2O_3 + 6H^+ + 6e^- \quad (3.1)$$

In an attempt to approximately simulate the above condition, during the present investigation atomic hydrogen has been charged into the heat treated samples of alloys by the electrochemical means. Moreover, cathodic hydrogen charging was preferred as it gives the most severe charging conditions leading to the most deleterious effect of HE of alloys [11]. Cathodic charging of hydrogen was performed in a polarization cell using a potentiostat interfaced with a personal computer. Tensile samples of both the alloys were subjected to cathodic charging of hydrogen. All the surfaces of the tensile specimen, except for the gauge length, was covered with teflon during cathodic charging. For phase transformation studies by XRD and microhardness profiling, 1 cm^2 coupon of 1441 alloy was charged in a similar manner. A 0.1 mol/l NaOH solution in which 10 ml of 100 ppm arsenate ion was added as a hydrogen recombination poison was used as electrolyte. The pH of electrolyte was 13 at which hydrogen absorption in to the alloys is facilitated due to unstable surface film. The temperature of electrolyte was maintained constant at 25 ^oC with a thermostatically controlled water bath. A platinum foil was used as the counter electrode and the potential of the specimen was measured versus saturated calomel electrode (SCE). Charging of hydrogen was performed at a constant current density of 10 mA/cm^2. This current density, polarized the specimen to -1680 mV vs SCE, confirmed by potentiodynamic polarization studies (Appendix). Cathodic charging of hydrogen was carried out for 12 hours.

3.5 *Mechanical Testing*

3.5a *Microhardness Measurement*

Microhardness measurements were obtained using a microhardness tester (mhp 160) attached to a vertical incident light microscope (Carl Zeiness Jena). A load of 20 grams and indentation time of 10 secs were used in all measurements. Indentations were made at five different random places in each sample and the hardness reported in the study is the average of five hardness readings.

3.5b *Tensile Testing*

Out of four tensile specimens two were tested in uncharged condition for reference properties and the remaining two were tested after hydrogen charging. Duplicate tensile testing was maintained for all heat treatment conditions. The tensile specimens before and after hydrogen charging were immediately tested in a 1195 Instron tensile machine at a constant strain rate 10^{-4}/sec. The average value of the two tensile test results for each condition has been considered in the analysis. Generally, the results were reproducible and the duplicate values resembled each other. The base values of each type of heat treated sample were compared with the corresponding values of hydrogen charged samples. The base values of each alloy were subsequently compared to the yield strength, ultimate tensile strength and percentage plastic elongations values of the corresponding hydrogen charged samples. The percentage decrease in the plastic elongation (tensile ductility) values upon hydrogen charging has been taken as the measure of the hydrogen embrittlement.

3.6 *Characterization*

3.6a *X-ray Diffraction*

XRD patterns were obtained before and after hydrogen charging from the coupons of 1440 and 1441 alloys in a Rich Seifert X-Ray Diffractometer 2002 using Cu K_{α} radiation. In all the XRD experiments, the intensity of scaling, recorder chart speed, and sample rotation rate were maintained constant. A similar procedure was also adopted for baked samples.

3.6b *Transmission Electron Microscopy*

The peakaged and RRA treated specimens of the 1440 alloy, before and after hydrogen charging, were examined in a JEOL 2000FX transmission electron microscope operating at 100 kV.

3.6c *Scanning Electron Microscopy*

Fractured surfaces after tensile testing of some of the samples were observed with a scanning electron microscope (JEOL JSM 840A) for obtaining the fractographic features of failure. The specimens of 1441 PA alloy before and after hydrogen charging were observed for microstructural features. Kellars reagent (95 ml H_2O + 2.5 ml HNO_3 + 1.5 ml HCl + 1 ml HF) was used as the etchant.

CHAPTER 4

RESULTS AND DISCUSSION

4.1 *Heat Treatment Characteristics*

Precipitation hardening from a supersaturated solution is a diffusional process. Therefore the extent of precipitation, the type, size and shape of precipitate depend on both the temperature and time of aging history of the alloy and its composition. Moreover, the structure of an age hardenable alloy may be influenced by impurities, temperature of heating, rate of cooling, plastic deformation before aging, time of storage of the quenched alloy at room temperature before artificial aging and many other factors. In the following sections the effect of some of these parameters on the aging behaviour of Al-Li alloys (1440 and 1441) has been presented and discussed.

4.1a *Solution heat treatment temperature*

. Optimum solution treatment followed by rapid cooling via a water quench produces a solid solution supersaturated with solute elements and vacancies. Subsequent aging characteristics are affected by the solution treatment parameters.

Figures 4.1 and 4.2 present the influence of solution heat treatment temperature on precipitation hardening behaviour 1440 and 1441 Al-Li alloys, respectively. An increase in the solution heat treatment temperature (SHT) from 510 to 530 $^{\circ}$C resulted in higher hardness for all the artificially aged samples, which is evident from Figs. 4.1 and 4.2. However, increasing the SHT

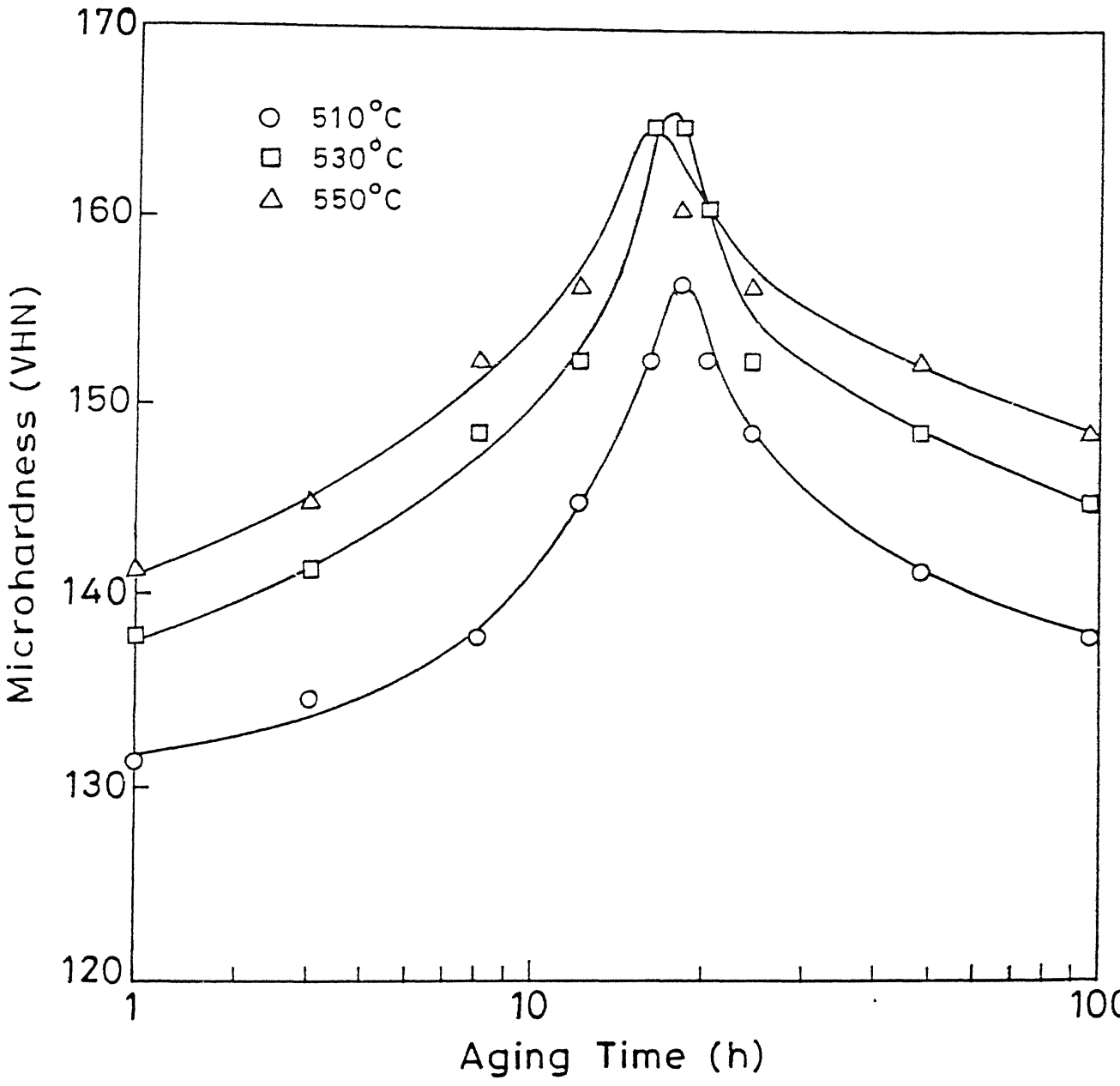

Fig.4.1 Effect of solution heat treatment temperature on subsequen artificial age hardening at 170°C for 1440 alloy.

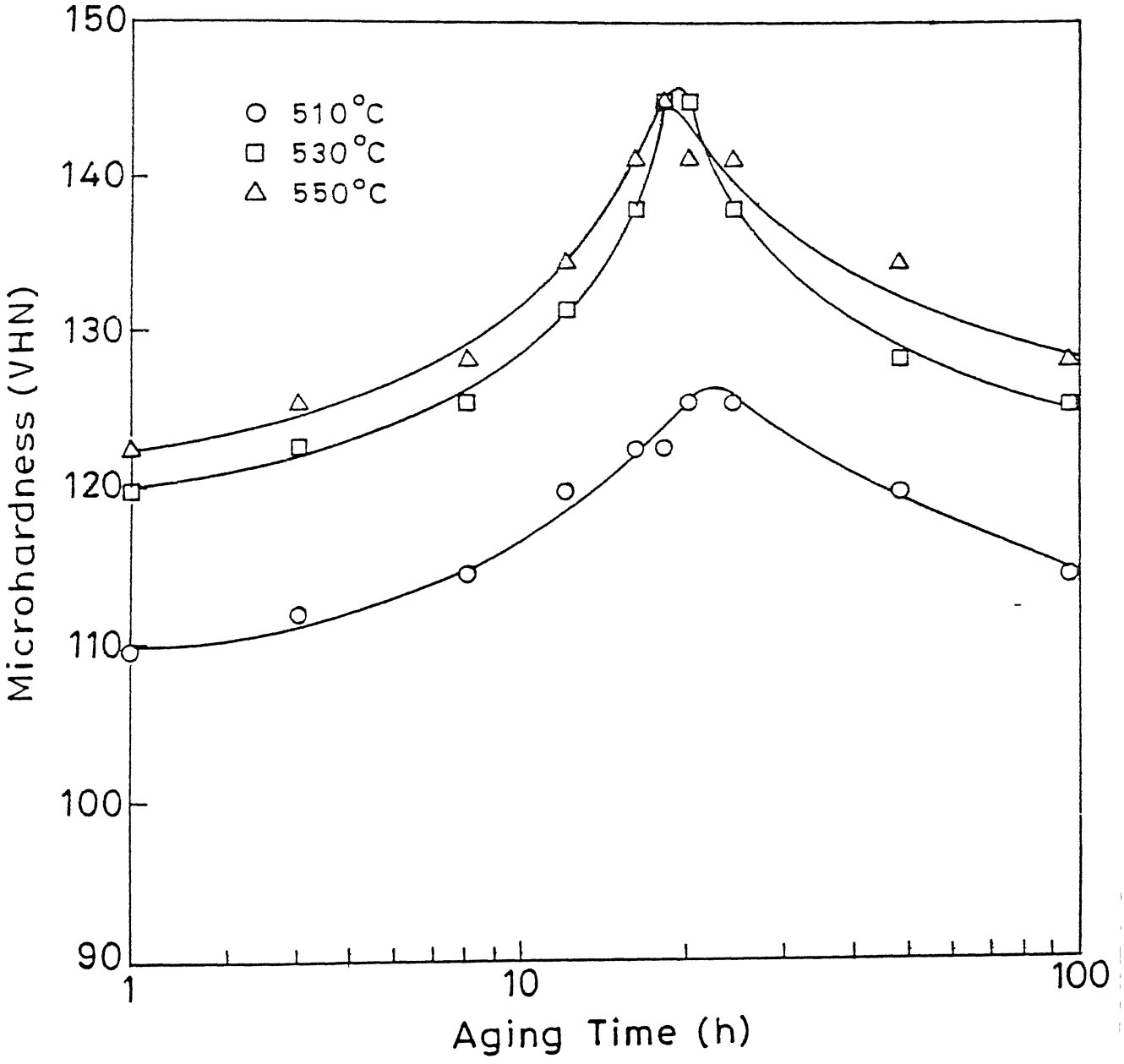

Fig 4.2 Effect of solution heat treatment temperature on subsequent artificial age hardening at 170°C for 1441 alloy.

further from 530 to 550°C did not yield any significant improvement in hardness, although the underaged and overaged conditions exhibited higher hardness for SHT at 550°C. SHT temperature affects dissolution of hardening precipitates back into the alloy. The microstructures of the 1441 alloys solution heat treated at 510°C, 530°C and 550°C for 1h are presented in Figures 4.3(a), 4.3(b) and 4.3(c) respectively. SHT temperature affects dissolution of hardening precipitates back into the alloy. The microstructure of 1441 alloy solution treated at 530°C for 1 hour followed by water quench presented in Figure 4.3(b) reveals that an increase in SHT yielded better dissolution of precipitating phases into the alloy.

Normally the commercial solution heat-treating temperature is determined by the composition of the alloy and an allowance provided for unintentional temperature variations. Broader ranges may be allowed for the alloys with greater intervals of temperature between their solvus and eutectic melting temperatures. The alloys used in the present study are complex quaternary systems for which the temperature- composition correlation is not exactly known. Avoiding both the overheating and underheating SHT, the objective is to take into solid solution the maximum practical amount of the hardening precipitates in the alloy and simultaneously create maximum number of vacancies. The maximum temperature may also be set with respect to grain growth, surface effects and economy of operation. The soaking time should be sufficient to achieve a nearly homogeneous solid solution. Soaking times for alclad sheets must be small because excessive diffusion of alloying elements from the core into the cladding reduces the corrosion protection offered by the cladding. Salt

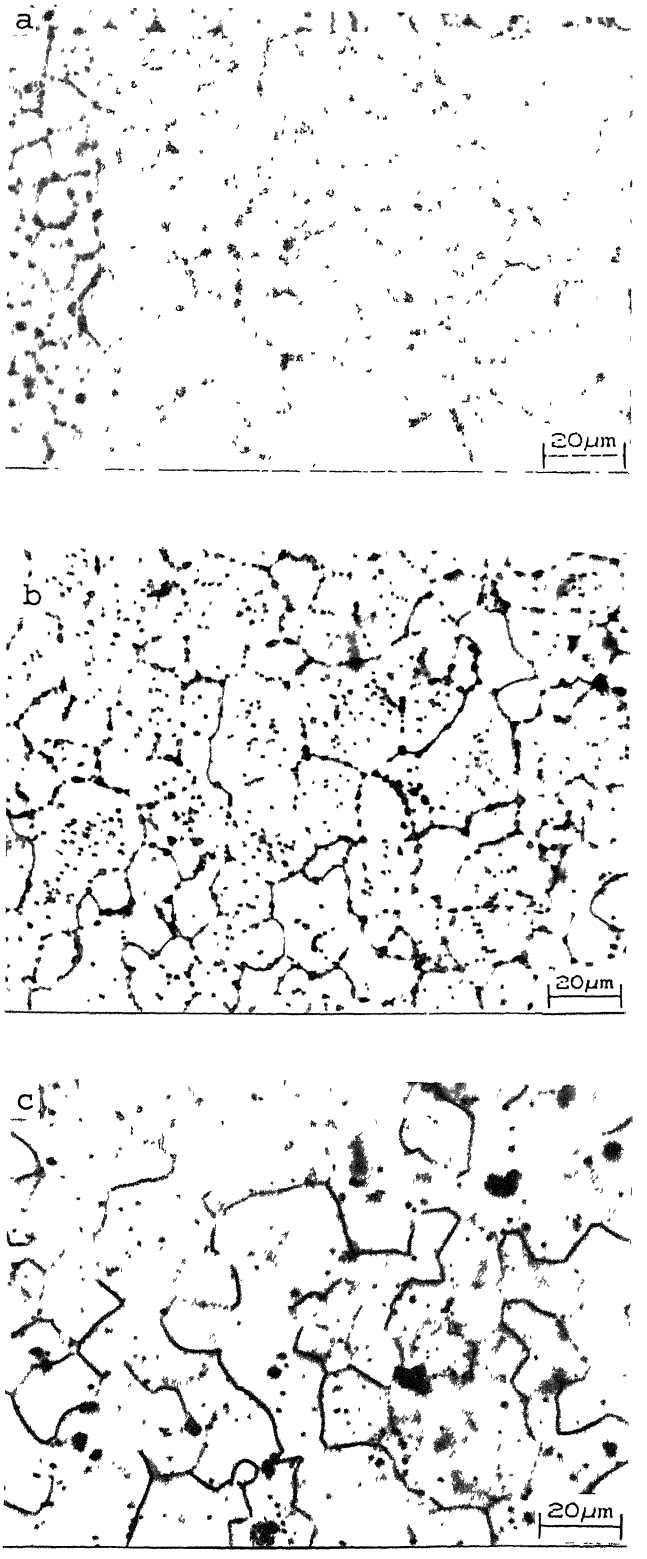

Figure 4.3 Microstructures of 1441 alloy, solution treated at 510^{o}C, 530^{o}C and 550^{o}C for 1h + WQ.

baths permit the immersion times to be monitored precisely. Whereas, soak time in air furnaces does not begin until all the furnace instruments attain their set temperature.

In the present study satisfactory dissolution of precipitates in the matrix was obtained for SHT above 530 °C. Microstructural observations presented in Figure 4.3 reveal satisfactory dissolution of precipitates for specimen solution treated at higher temperatures. The present observation are consistent with earlier observation on the influence of SHT on the aging characteristics of Al-Li alloys [10,11].

4.1b *Cold stretch on artificial aging behaviour*

The influence of cold deformation on precipitation hardening of these alloys are presented in Figures 4.4 and 4.5 respectively. From the above figures it is evident that samples cold stretched prior to artificial aging show higher hardness after the artificial aging treatment at 170 °C as compared to the unstretched samples. Hence, both the alloys are affected by cold work between the quenching and aging treatments and this characteristic is the basis for obtaining the high strength T8 tempers.

The strength improvement accruing from the combination of cold working and precipitation heat treatment is a result of nucleation of additional strengthening precipitates in the case of cold worked samples. It is believed that dislocations are necessary for the nucleation of the age hardening phases in Al-Li alloys like the T_1 (Al_2CuLi) phase, S′ (Al_2LiMg) and δ(AlLi) precipitates in Al-Li-Cu-Mg alloys [10,12,113,119]. Deformation prior to aging is often used to increase the dislocation density

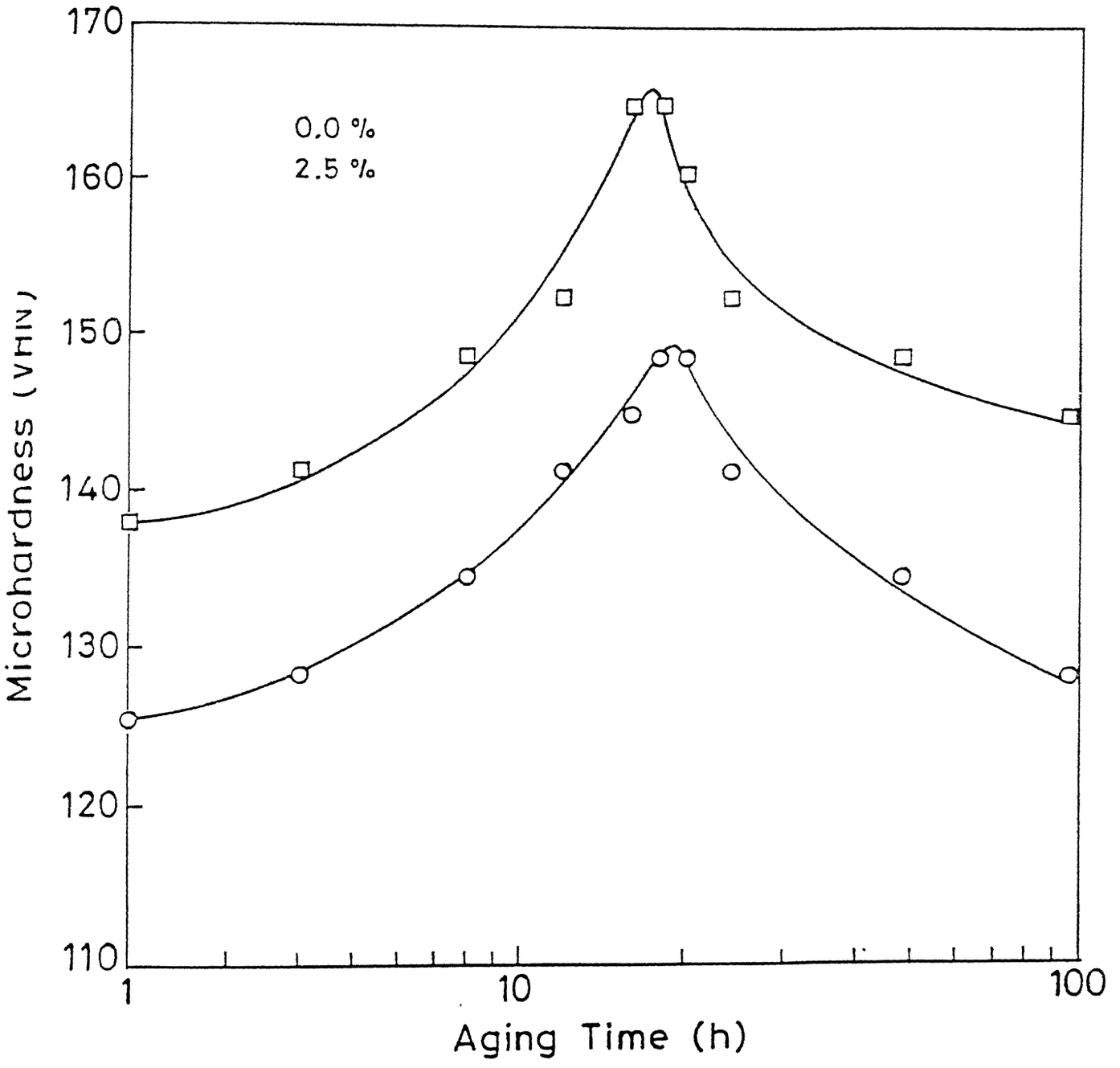

Fig.4.4 Effect of percentage prior cold stretch on the artificial aging behaviour of 1440 Al-Li alloy at 170°C.

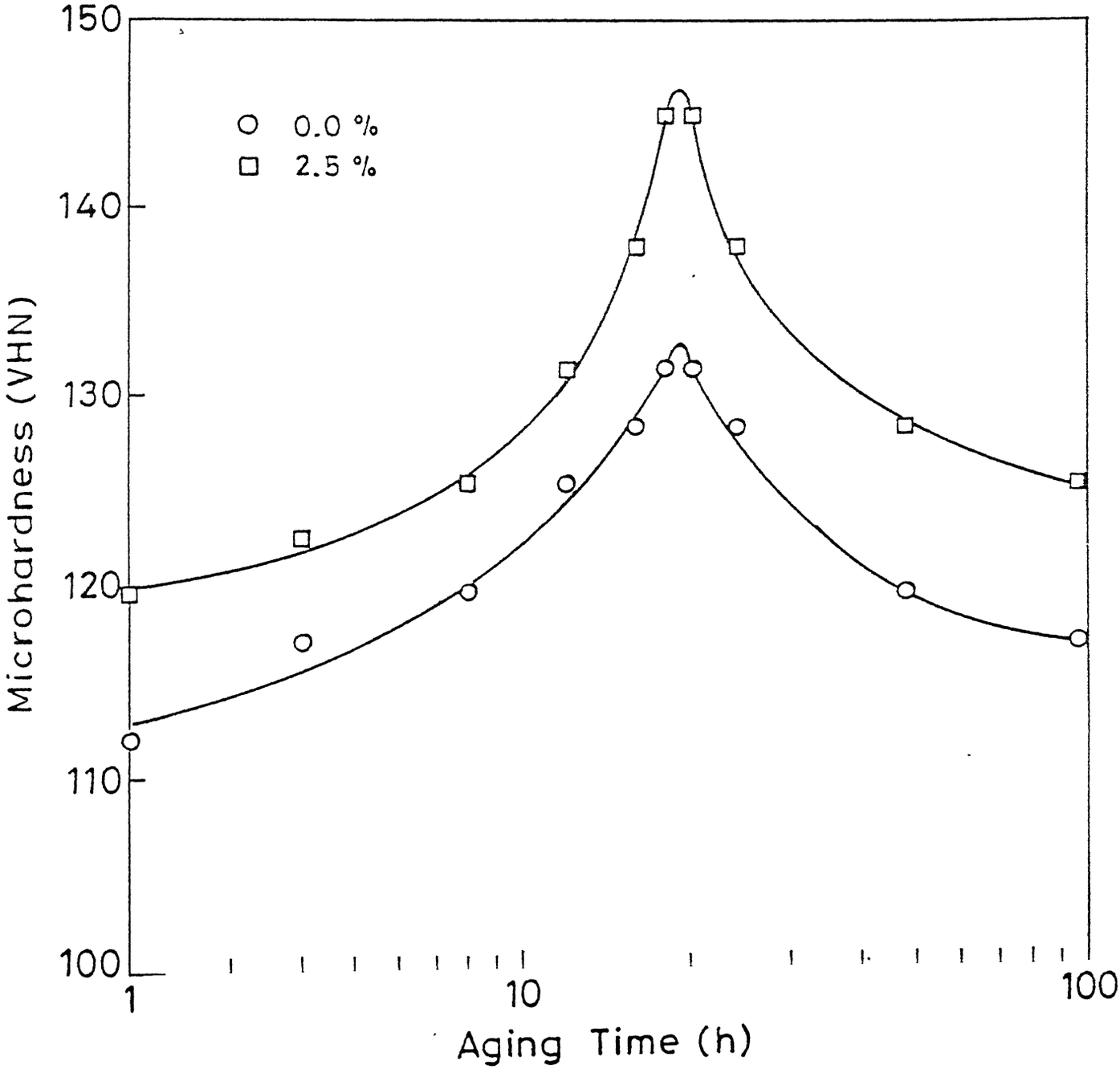

Fig.4.5 Effect of percentage prior cold stretch on the artificial aging behaviour of 1441 Al-Li alloy at 170°C.

and vacancy concentration and thereby the nucleation sites for strengthening precipitates. It is well established that the strength of age hardened Al alloys depends on both the size and volume fraction of the strengthening precipitates [10-12]. Hence, the aging response is very sensitive to the degree of deformation prior to artificial aging.

Introduction of vacancies by the cold stretch prior to aging plays an important role in the kinetics of precipitation hardening. In general, cold working the alloy prior to aging causes a decrease in the rate of formation of GP zones. It implies that the dislocations introduced by cold work are more effective as vacancy sinks than as vacancy sources. Cold working or rapid quenching, therefore have opposing effects on the formation of GP zones. Excess vacancies, by condensing to form dislocation loops, can also provide nucleation sites for intermediate precipitates. It is also interesting to note that screw dislocations, which are not normally favorable sites for nucleation can also become sites for preferential precipitation when they have climbed into helical dislocations by absorbing vacancies, and have thus become of mainly of edge character. In the present study increase of hardness was observed in the case of rapidly quenched alloy subjected to cold stretch and artificial aging compared to artificial aging of the same alloy without any prior cold stretch. This leads to the interesting observation in Al-Li alloys that cold working or rapid quenching have the same effect on the formation of matrix strengthening phases.

Trace impurities significantly modify the precipitation process. The interaction of trace impurities with vacancies inhibit zone formation by which age hardening process at room

temperature is delayed. On the other hand, density of metastable strengthening precipitates is increased due to the increase in vacancy loops and helixes which act as nuclei for precipitation and by segregating to matrix-δ' interfaces thereby reducing the interfacial energy [116].

Since grain boundaries absorb vacancies there is grain boundary zone relatively free from precipitation. Many precipitation hardening alloys suffer from the precipitate free zone (PFZ) at the grain boundaries. Any trace additions which stabilize vacancy clusters near the grain boundary and also increase the stability of the GP zone, therefore raising the G.P. zone solvus temperature will eliminate the PFZ. In Al-Li alloys, the S' (Al_2CuMg) precipitates are homogeneously nucleated, giving rise to improved and more uniform properties.

4.1c *Aging time and temperature*

The strength of an age hardening alloy is governed by the interaction of moving dislocations and precipitates. The obstacles in precipitation hardened Aluminium alloys hindering the motion of dislocations may be either (1) strains around GP zone precipitates (2) zones and precipitate themselves, or both. Dislocations will either cut through the zones/precipitates or go round them. Thus there are three kinds of hardening (i) internal strain hardening (ii) chemical hardening which involves dislocation cutting through precipitates (iii) dispersion hardening which involves dislocation going round the precipitate (orowan looping). Strain associated with a nucleus will enlarge as its size increases, but not indefinitely. Loss of coherency on the formation of interface would greatly reduce the state of strain associated with the

:ecipitate particles.

The basic idea of all heat treatments is to seed a uniform istribution of stable nuclei at the low temperature which can nen be grown to optimum size at the higher temperature. Alloys uenched below the GP zone solves and aged above it, is the most ommon practical situation to yield higher hardness values. Aging oes not have the same effect on the properties of all alloys due iffering effects of the precipitates on lattice distortion. If he precipitation involves extensive changes in the lattice a arge amount of distortion occurs with major changes in mechanical)roperties. Enhanced mechanical properties are often obtained in quaternary systems.

The effect of aging temperature on the artificial aging)ehavior of 1440 and 1441 alloys are presented in Figures 4.6 and 4.7, respectively. At aging temperature of 170 °C, an aging time 16 to 18 hours yielded the maximum hardness for 1440 alloy. On the other hand, the 1441 alloy took about two hours more to reach its peak hardness value. Moreover, the 1441 alloy exhibited relatively lower peak hardness values as compared to the 1440 alloy.

The diffusion rate is slow while aging at 150 °C, and therefore, the precipitation is delayed for both the alloys. Notice, that there is a slight increase in the peak hardness value for aging at 150°C than that for aging at 170°C. Aging at 190°C,hardening occurs quickly due to rapid diffusion, and the time to complete the precipitation is short. Hence, the peak hardness value is reached faster than aging at 170 °C or 150 °C. However, due to relaxation of elastic strain (coherency) energy at higher aging temperature, the peak hardness value is lower than that after aging at 170 °C and 150 °C. The optimum aging

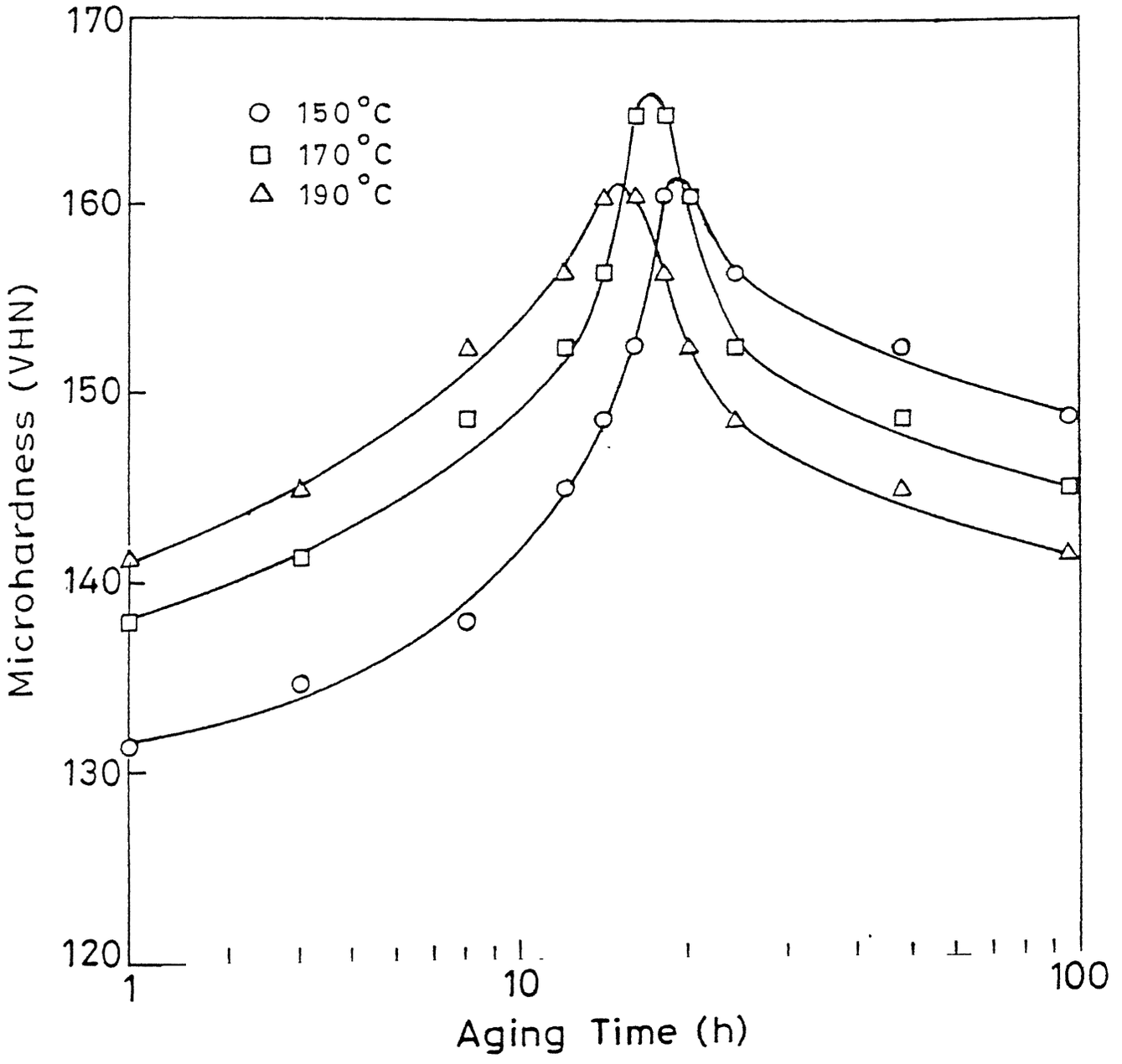

Fig.4.6 Effect of aging temperature on the precipitation behaviour of 1440 Al-Li alloy solution treated at 530°C for 1h+WQ+2.5% CW.

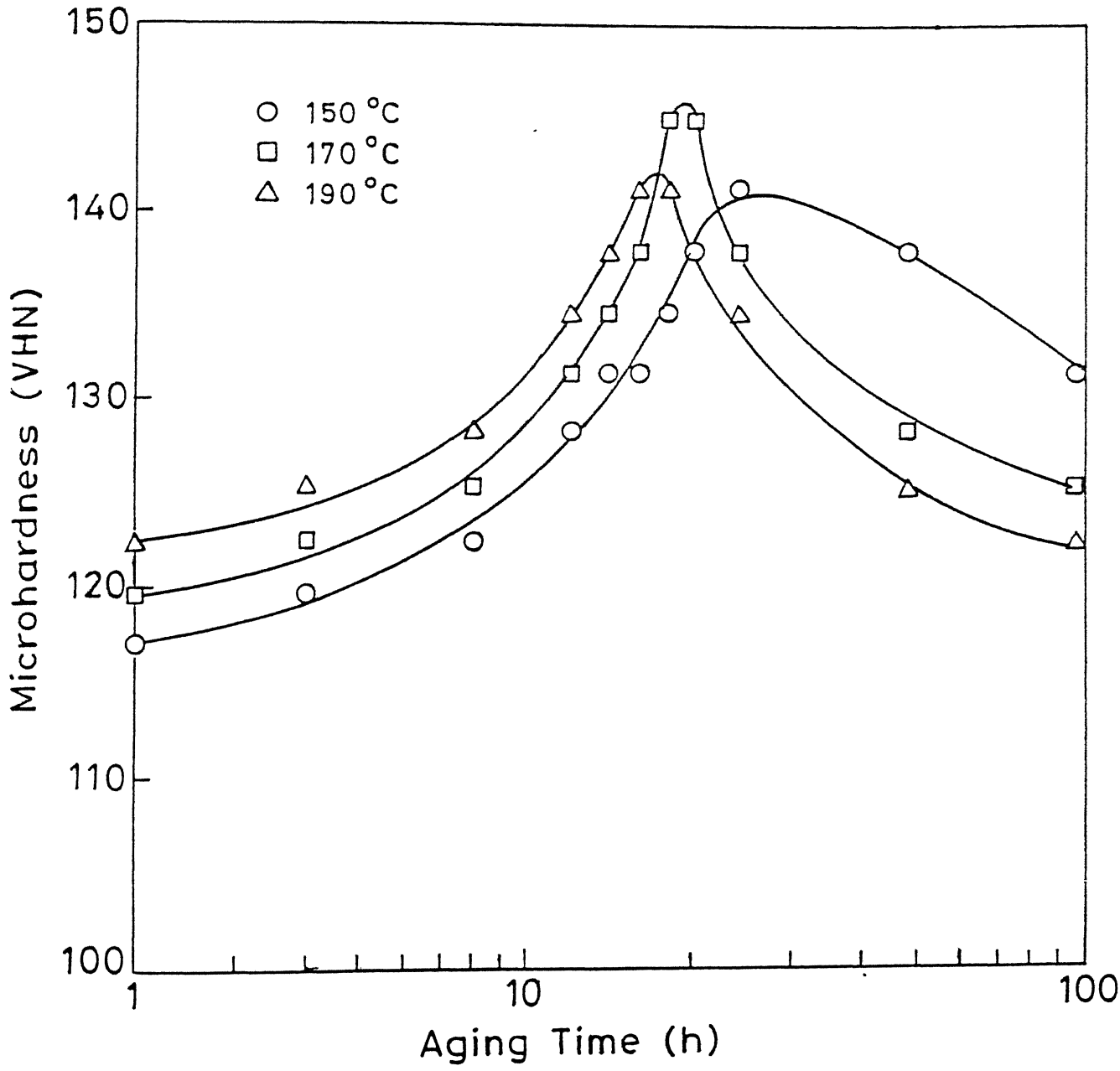

Fig.4.7Effect of aging temperature on the precipitation behaviour of 1441 Al-Li alloy solution treated at 530 °C for 1h+WQ+2.5% CW.

temperature seems to be 170 °C, at which peak hardness is obtained within a reasonable length of time. Higher precipitation temperatures usually are associated with lower nucleation rates and thus, a coarser precipitate distribution [10]. However, higher the aging temperature, higher the rate of precipitation, and hence the time to attain peak or maximum hardness would be smaller. Results shown in Figs. 4.6 and 4.7 confirm the above arguments. Maximum hardness does not correspond to formation of the equilibrium phases, but due to formation of metastable, transition phases, which precipitate in a considerably finer distribution [101]. It has been observed that as the temperature of aging is increased, the the over aged stage is attained earlier, the higher the aging temperature [8,92,94,96].

4.1d *Li/Cu ratio*

Figure 4.8 presents the influence of Li/Cu ratio on precipitation hardening behaviour of the above mentioned alloys. In Figure 4.8, it is seen that the 1440 alloy having a higher Li/Cu ratio compared to the 1441 alloy provides higher hardness on artificial aging at 170 °C. This is because of the greater amount of hardening element dissolved in excess of the saturation limit for 1440 alloy and hence the larger number of precipitating phases.

It is also evident from Figure 4.8 that the alloy having the higher Li/Cu ratio shows higher hardness. Also, the peak hardness of alloy containing higher Li/Cu ratio is reached in a shorter duration. In the present study, the 1440 and 1441 alloys have Li/Cu ratios approximately equal to 2 and 1, respectively. Owing to higher supersaturation and presence of Li in higher proportion,

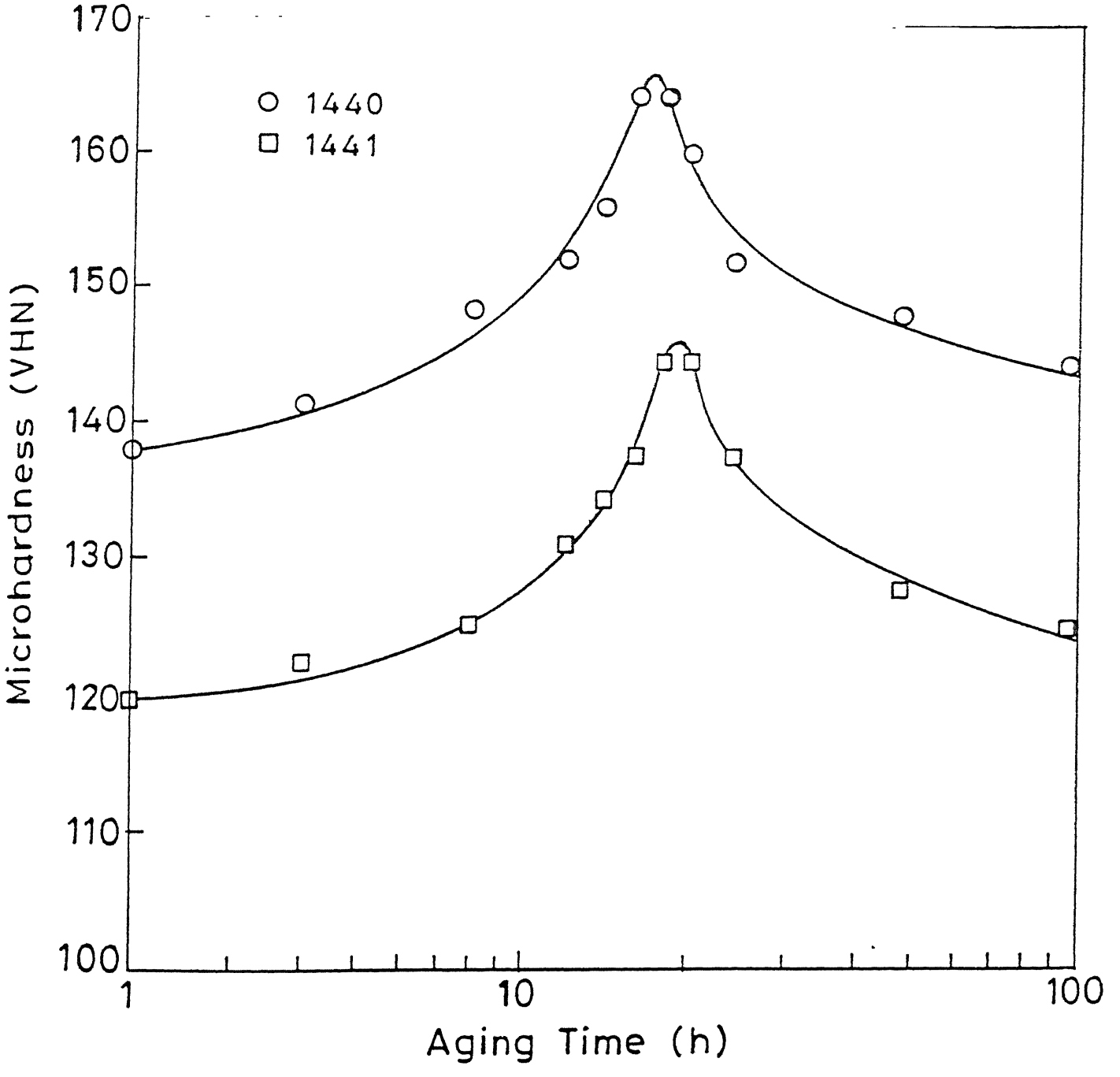

Fig.4.8 Effect of Li/Cu ratio on the artificial aging behaviour of 1440 and 1441 Al-Li alloys, solution treated at 530°C for 1h + WQ + 2.5% cold stretch and age hardened at 170°C.

precipitation from the solution takes place faster for the 1440 alloy. Hence, the maximum strengthening is attained in a shorter aging time for this alloy.The strength of an aged alloy depends on the initial level of strength in the alloy as quenched. In case of 1440 due to higher Li content, more amount of $\delta'(Al_3Li)$ precipitation is expected. The increased proportion of $\delta'(Al_3Li)$ in the matrix results in higher hardness values, as has been reported by other investigators [101,104].

4.1e *Retrogression heat treatment*

It is evident from Figure 4.9 that the 1440 alloy exhibited minimum hardness at 60 sec immersion time, whereas the same for the 1441 alloy was observed at 40 sec immersion. In the case of Al-Li alloys, preferential dissolution of shearable coherent matrix δ′ precipitates occurs during retrogression whereas other precipitates like T_1, T_2, δ and S′ remain undissolved [93]. Moreover, growth of other precipitates, particularly S′, can also occur to some extent during the short holding time at the retrogression temperature [94]. The alloy partially loses its strength due to dissolution of some coherent matrix precipitates that occurs during retrogression. It can be noted in Figure 4.9 that microhardness decreased with increase in immersion time up to a critical value. The minima in the retrogression curve is indicative of the maximum dissolution of δ′ precipitates [95]. Prolonged immersion time can cause slight hardening owing to the onset of structural age hardening effect. The microhardness increases slightly after 60 seconds for 1440 and 40 seconds for the 1441 alloys. The present results confirm the findings of Rajan *et al.* [103] that, initially, the dissolution rate is greater than

the precipitation rate but beyond a critical point, the precipitation rate leads the dissolution rate. This explains the slight increase of hardness following the initial decrease. In all the retrogression treatments provided to the 1440 and 1441 tensile specimens, 60 seconds at 270^{o}C and 40 seconds at 235^{o}C were employed, respectively.

In Al-Li alloys, δ' is the prime strengthening metastable phase. During retrogression heat treatment, δ' is preferentially dissolved into matrix while the grain boundary equilibrium precipitates are deliberately retained. The critical retrogression temperature for 1440 and 1441 alloys are 270 °C and 235 °C, respectively which was obtained from the Al-Li phase diagram and δ' solvus [22]. Short immersion time is insufficient for the formation of metastable and stable phases. The subsequent quick cooling fixes the supersaturated solid solution. The above selective dissolution is accomplished by selecting retrogression temperature above the solves of δ' but below the solves of δ (Al Li), T_1 (Al_2CuLi) and S (Al_2CuMg) precipitates. During reaging a constant volume of matrix strengthening phase is obtained for different samples of alloys. Thus retrogression reaging (RRA) heat treatment provides varying amount of grain boundary precipitates at constant matrix strength.

The retrogression behavior of 1440 and 1441 is presented in Figure 4.9. Immersion times of 60 sec. and 40 sec. have been found to be critical for retrogression treatment for 1440 and 1441 alloys, respectively. Amount of δ' (Al_3Li) dissolved into matrix during retrogression were assessed as a function of immersion time in terms of microhardness since δ' is the prime phase contributing to the strength as well hardness of the alloy. Note

that in Figure 4.9 microhardness decreased with increase in immersion time up to a critical value. Short holding time is insufficient for the formation of metastable and stable phases. However, prolonged immersion time can cause slight hardening owing to the onset of structural age hardening effect. But it is followed by immediate softening due to coarsening of precipitates. The above phenomena was also observed (Figure 4.9) beyond the critical immersion time after the lowest hardness values were attained. Retrogression treatment predicts the stability of matrix strengthening. Metastable phase of the alloy was considered under different aging conditions. Thus the retrogression temperature and the immersion time of alloys are greatly affected by the preceding heat treatment yielding the metastable phases of varying stability. Longer times at aging temperature produce larger and stabler strengthening phases which require a higher temperature for full dissolution. The critical temperature for retrogression of the alloys 1440 and 1441 (which were peak aged at 170 ^{o}C for 16 hours and 18 hours, respectively) are 270 and 235^{o}C.

Observations made in the Figure 4.9 are consistent with the results of Park and Ardell [32] on the retrogression of 7075-T651 aluminium alloy. Our results confirm those of others [32,35] that initially dissolution rate is greater than the precipitation rate below critical point but beyond that, precipitation rate leads the dissolution rate. Total concentration of the precipitate particles following the initial decrease, increases with the retrogression time due to the competitive contributions from the precipitation, leading the dissolution process. The subsequent final decrease in the total concentration of particles results from general overall coarsening. This explains the slight

increase of hardness following the initial decrease. The coarsening phenomena has also been supported by Papazian [112], who had observed RRA structure as an over aged structure. However, Park and Ardell [32] observed RRA structure different from T7 structure, because fine particles of strengthening precipitates were present in greater proportion. In addition, the overall precipitate concentration is significantly higher in RRA structure than in T7 structure. Hence, it is expected that RRA structure will show higher hardness value.

4.1f *Natural aging behaviour of retrogressed samples*

Influence of natural aging on retrogressed 1440 and 1441 samples for different immersion time are presented in Figures 4.10 and 4.11 respectively. Natural aging of least retrogressed sample (i.e., corresponding to minimum immersion time) showed maximum response to natural aging as compared to samples subjected to higher immersion times. (Figures 4.10 and 4.11). Natural aging is facilitated due to the presence of δ' Since the least retrogressed sample has more amount of strengthening phase δ' as compared to samples retrogressed for critical time. Presence of δ' phase leads to faster kinetics of precipitation in the least retrogressed samples

In industrial practice there is always an unavoidable delay in starting aging treatment immediately after finishing solutionizing treatment coupled with water quench and cold deformation. Present study has revealed that Al-Li alloys are prone to natural aging. Influence of natural aging on solution treated and cold stretched samples is presented in Figure 4.12. The middle portion of the natural aging curve signifies increased

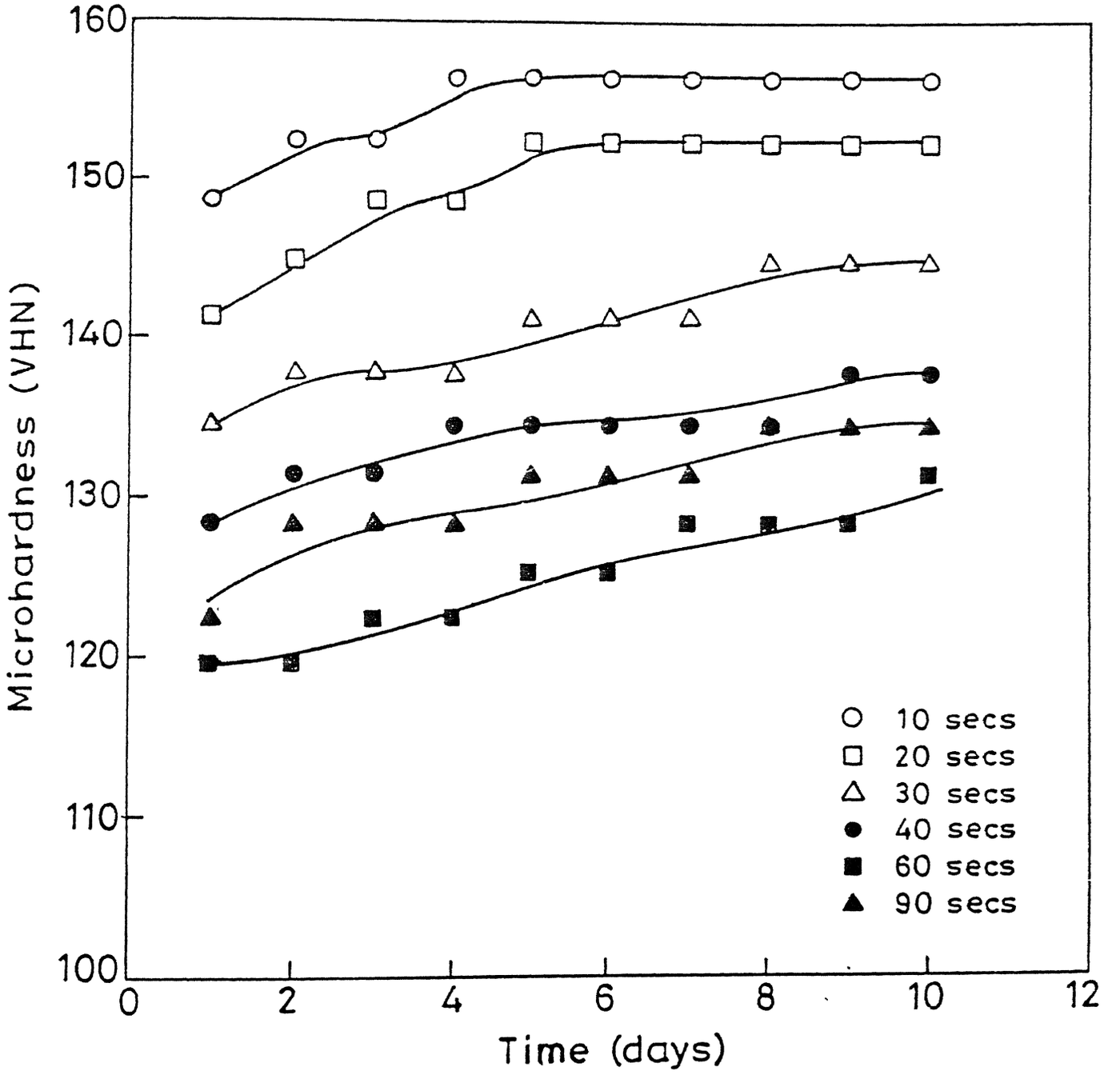

Fig4.10Natural aging behaviour of peakaged 1440 Al-Li alloy after retrogression at 270°C for the indicated times.

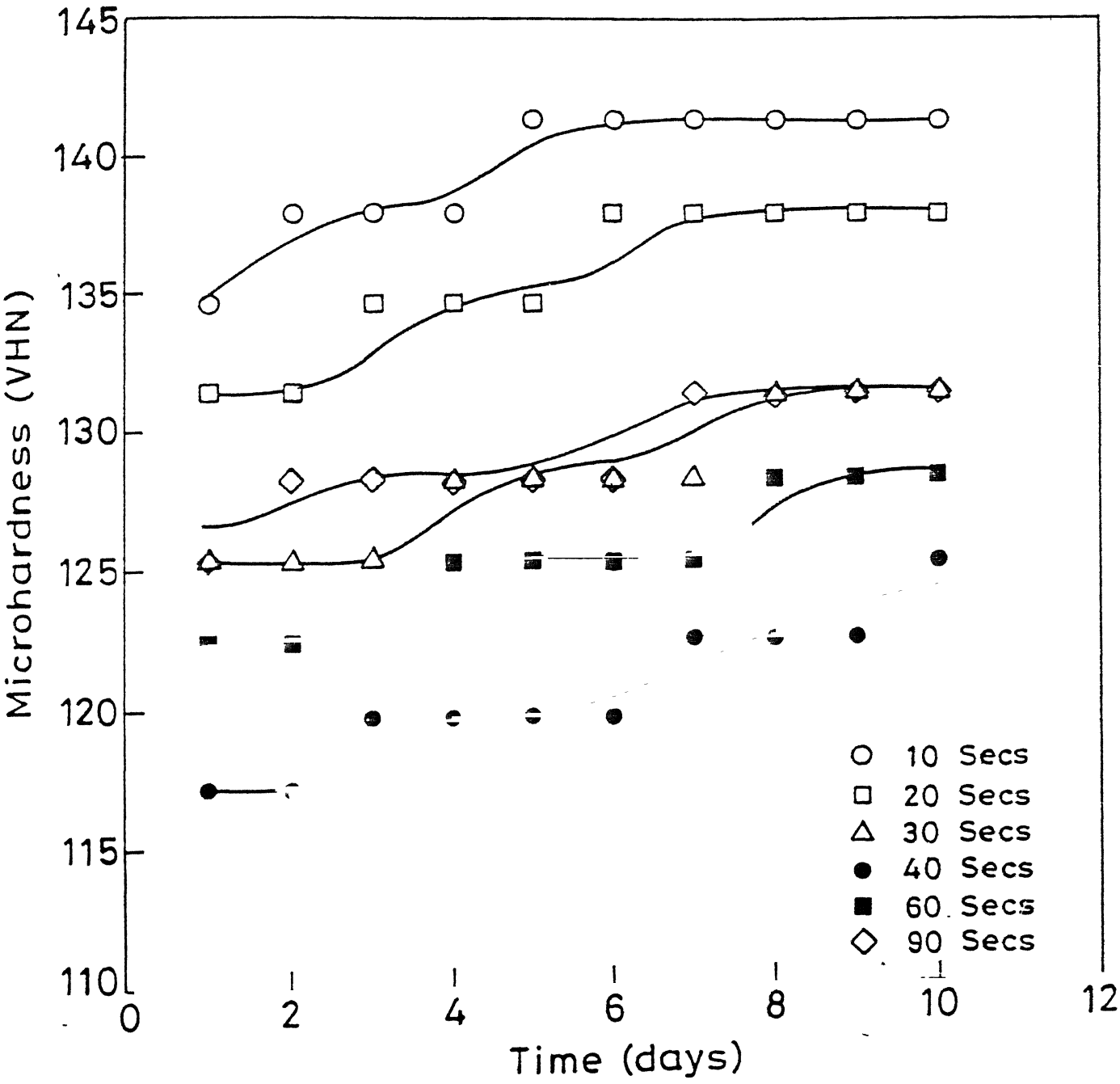

Fig4.11 Natural aging behaviour of peakaged 1441 Al-Li alloy after retrogression at 235°C for the indicated times.

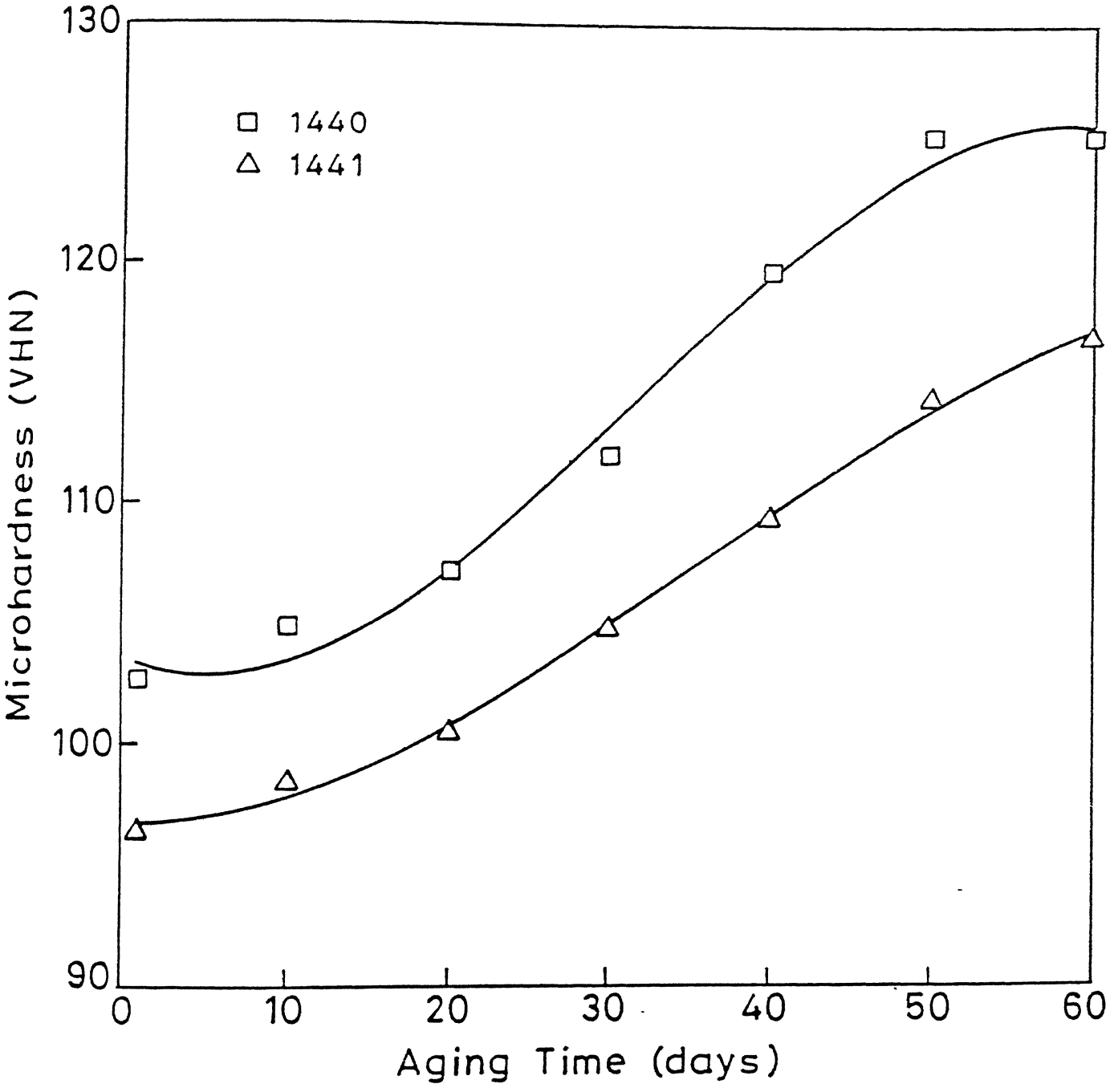

Fig4.12Natural aging behaviour of Al-Li alloys solutionised at 530°C for 1h+WQ+2.5% CW prior to natural aging.

rate of precipitation kinetics compared to the starting and end portion of the curve. The peak hardness value obtained in the case of natural aging is much lower than that of artificial aging.Some amount of natural aging prior to artificial aging may provide more heterogeneous nuclei for the formation of increased number of precipitates during subsequent treatment. As a result, more increase in hardness is expected in age hardened Al-Li alloys.

4.2 *Hydrogen Embrittlement Susceptibility*

The results of the tensile tests conducted on both uncharged and charged specimens (in different heat treatment conditions) are presented in Table 4.1 which also shows the comparative percentage loss in plastic elongation on hydrogen charging. Figure 4.13 shows the histogram of HE susceptibility of the alloys to different heat treatment conditions. Comparative percentage loss (CPL) in plastic elongation (ε_p) is defined as

$$CPL = \frac{\%\varepsilon_{p,uncharged} - \varepsilon_{p,charged}}{\%\varepsilon_{p,uncharged}} \times 100$$

The CPL has been used as the measure of hydrogen embrittlement, as has been used previously by other investigators [15-19], in the following discussions.

The ultimate tensile strength (UTS) decreased by approximately 3 percent after hydrogen charging in all heat treatment conditions but the yield strength (YS) did not exhibit similar consistent behaviour. After RRA treatments, both the YS and UTS was lower than the corresponding values of the initial tempers. Full recovery of the strength could not be achieved upon RRA since the specimens were reaged to the UA temper. Secondly, there is a decrease in the dislocation density upon RRA [28] and

Table 4.1

Alloy Sp. (heat-treatment)	MHv (unch-arged)	YS (MPa) (unch-arged)	YS (MPa) (char-ged)	UTS (MPa) (unch-arged)	UTS (MPa) (char-ged)	$\%\varepsilon_{plastic}(\varepsilon_p)$ (unch-arged)	$\%\varepsilon_{plastic}(\varepsilon_p)$ (char-ged)	%loss in ε_p
1440 UA	138	328	339	412	395	4.9	3.7	24.5
1440 PA	165	376	363	451	420	4.1	3.4	17.1
1440 OA	145	366	342	440	402	6.1	4.7	23.0
1440 URU	131	322	330	409	401	5.1	4.1	19.6
1440 PRU	161	347	341	437	414	3.8	3.4	10.5
1440 ORU	138	320	326	393	382	5.3	4.3	18.9
1441 UA	120	279	285	387	382	14.8	11.8	20.3
1441 PA	145	365	353	433	423	12.0	10.2	15.0
1441 OA	125	362	361	397	396	8.2	6.7	18.3
1441 URU	117	277	282	377	371	15.2	12.4	18.4
1441 PRU	138	347	339	420	410	11.6	10.5	9.5
1441 ORU	120	341	347	381	377	9.1	7.6	16.5

UA ⇒ Underaged
PA ⇒ Peakaged
OA ⇒ Overaged
URU ⇒ Underaged + Retrogressed + Underaged
PRU ⇒ Peakaged + Retrogressed + Underaged
ORU ⇒ Overaged + Retrogressed + Underaged

Tensile test results of reference and hydrogen charged Al-Li-Cu-Mg alloys in different heat-treatment conditions.

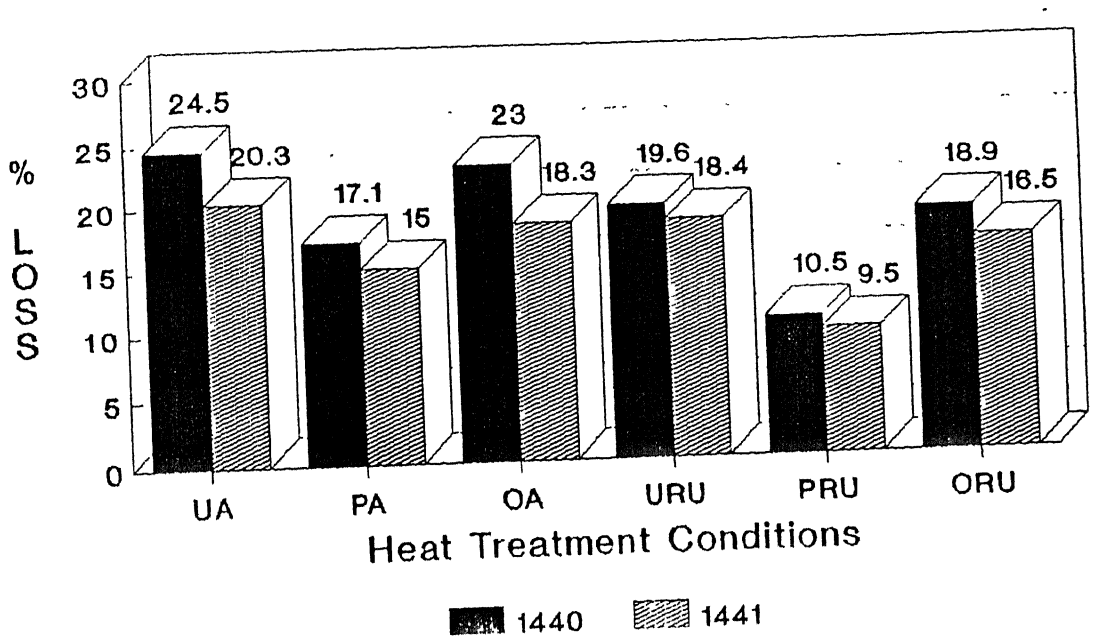

4.13 Histogram showing HE susceptibility of Al-Li alloys to different heat treatment conditions.

therefore the volume fraction of hardening phase (δ′) that precipitates after RRA is lower than in the earlier straight aging case. The decrease in strength upon RRA of UA specimen (Table 4.1) indirectly confirms the second effect.

4.2a *Aging temper*

In the case of both the alloys, the UA temper was the most susceptible to HE, whereas the PA temper was least susceptible to HE. The OA temper occupied intermediate position, in between UA and PA, as regards HE susceptibility. The results of the present study on the effect of aging on HE are consistent with some of the previous investigations [11,15,17,18,79,121-124] and, at the same time, are in contrast to the results obtained in Al-Li alloys by some other investigators [13,14,16,19,33,76,125-129].

EIC susceptibility of conventional Al alloys has been extensively studied. Comparatively little is known about the HE of Al-Li-Cu-Mg-Zr alloys. An extensive review of literature [11,13-19,79,121-129] revealed that there is no consistent trend regarding the effect of aging temper on EIC behaviour of Al-Li alloys. Moreover, the results of conventional Al alloys can not be easily extrapolated to Al-Li alloys as these contain active phases due to the presence of lithium. The extremely active electrochemical behaviour of Li and its possible interaction with atomic hydrogen producing stable alkali hydrides (i.e. LiH and $LiAlH_4$) [42,86] render the HE mechanism in these alloys complex in nature. In addition, it has been reported that the hydrogen content of Al-Li alloys is three to ten times greater than that of conventional Al alloys [130]. Hence, its behaviour is expected to be different from that of the conventional aluminium alloys.

The complexity of HE phenomena in Al-Li alloys arises from factors such as nature and distribution of hydrogen trapping sites, possibility of hydride formation and possible reaction between hydrogen and dislocations, impurities and/or alloying elements. Assuming a critical hydrogen concentration within the alloy lattice, the various mechanisms of HE reported in the literature for Al alloys are hydrogen pressure theory [83], decohesion model [83], hydrogen enhanced localized plasticity (HELP) [84], hydride cracking [42], and hydrogen-dislocation interactions [83]. Disparities amongst the findings of different investigations may be partly due to the different test conditions employed in the studies and partly to their consideration of single HE mechanism. Moreover, the variation in susceptibility of Al-Li alloys in different aging tempers to HE indicates that a universal HE mechanism is quite unlikely. Hence, in the analysis of HE susceptibility of Al-Li alloys to different heat treatment conditions, two or more mechanisms should be considered simultaneously instead of a single one.

Earlier, Meletis *et al.* [121] observed that the PA temper is more resistant to HE than UA and OA tempers for Al-Li alloys. Tien *et al.* [79] also have reported the poor HE resistance of the UA temper. Binsfeld *et al.* [15] and Ohnishi *et al.* [16] observed that HE resistance is poor in the OA temper. In Al-Li alloys, the precipitates at the grain boundary (δ) and the subgrain boundaries (T_1) are active with respect to the matrix [18] and therefore, the severity of intergranular corrosion increases with aging [18,33,124]. The corrosive attack leads to enhanced anodic dissolution of the precipitates as well as to increased hydrogen reduction rates with both the factors affecting EIC [13,14,19].

Although the enhanced intergranular corrosion with aging can not be related directly with EIC, it, nevertheless, does point to the importance of the precipitates at the boundaries in the cracking process.

Pressouyre [27] suggested a universal remedy for HE by controlling the chemistry, morphology and distribution of precipitates in the alloy matrix. According to him, the optimum microstructure should contain a fine and homogeneous distribution of irreversible hydrogen traps in large numbers. Autoradiography studies in tritium-doped Al-Li alloys indicate irreversible trapping of hydrogen by δ' precipitates [131], the major strengthening phase in the alloys. The δ' distribution in the matrix is optimum for the PA condition and hence, the superior HE resistance of the PA temper could be partly attributed to this reason.

The inferior HE resistance observed in UA condition may be attributed to the localization of planar slip. The planar slip conditions favour dislocation-hydrogen transport and this could be one of the reasons for the poor HE resistance of the underaged temper. Moreover, planar slip produces a higher number of slip steps on the surface resulting in larger areas of exposed bare metal. This indirectly provides additional sites for hydrogen reduction (i.e. generation of hydrogen atoms) on the surface.

The increased HE of alloys in OA temper may be attributed to development of strain at the grain boundaries caused by the phase interactions and transformations ($\delta'/\theta' \longrightarrow T_1$), and preferential precipitation of T_1 [126]. Consequently, this strain will increase the critical concentration of hydrogen and thereby HE. The formation of brittle hydride and their subsequent failure can also

play an important role in increasing HE susceptibility in OA temper of the alloy [42]. For example, the interaction of grain boundary δ (AlLi) precipitate with hydrogen may lead to the precipitation of hydride phases which significantly affect ductilities [18]. The testing of hydrogen precharged specimens reflects to a major extent the crack initiation resistance, because once a critical crack has nucleated, the propagation is fairly rapid. This is due to the increasing stress intensity at the crack tip due to the constant elongation rate (strain rate) imposed on the specimen. The two effects, crack initiation and crack propagation, can not be seperated. It is interesting to note that Ricker *et al.* [37] Dorward *et al.* [123] and Vasudevan *et al.* [124] have shown that K_{ISCC} decreased monotonically with either aging or increasing Li content or Li/Cu ratio. This observation was interpreted as being due to the reduced toughness of the OA condition. The increased susceptibility of the OA temper to EIC could be due to lower crack initiation resistance of the OA temper. In the present study, the increased HE in the OA temper can be attributed to easier crack nucleation. Figure 4.14 shows the surface structure of 1441 PA alloy in the uncharged and hydrogen charged conditions. In Figure 4.14(b) crack initiation along the grain boundaries can be noticed, confirming the important role of grain boundary precipitates in HE.

4.2b *RRA*

It is established that the grain boundary precipitates (δ, T_1, and S′) play a significant role in HE of Al-Li alloys [14]. Incidently, RRA of Al-Li alloys has been used by Vasudevan and Doherty [34] as a tool to study the influence of grain boundary

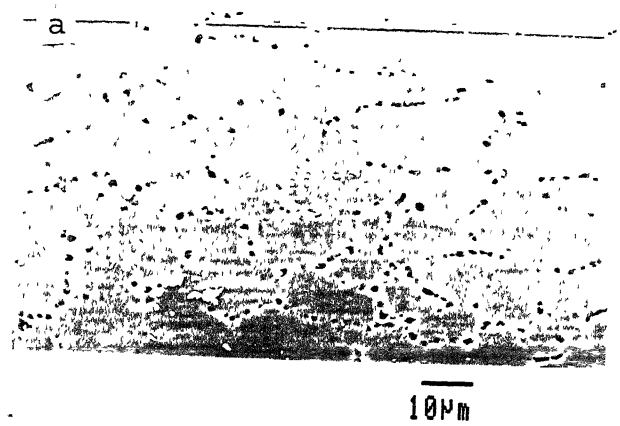

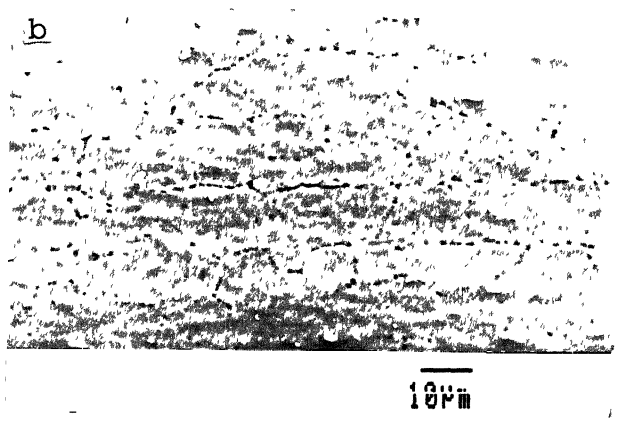

Figure 4.14 SEM photographs of PA 1441 specimen surfaces in the (a) uncharged and (b) hydrogen charged conditions.

precipitates on grain boundary ductile fracture. They observed that the toughness of binary Al-Li alloys is inversely proportional to square root of area fraction of the grain boundary δ (AlLi) precipitate. The retrogression treatment has also been used to control the volume fraction of δ', which causes undesirable planar slip leading to reduced toughness [39]. Moreover, the RRA treatment is supposed to result in low dislocation densities which in turn enhance resistance to EIC [28]. In the present study, therefore, RRA has been adopted to as a means to reduce the dislocation density and to vary the size and amount of grain boundary precipitates while maintaining the matrix structure constant. Ricker *et al.* [37] observed that grain boundary precipitates strongly influence EIC susceptibility of Al-Li alloys, with the critical strain or stress required to initiate EIC decreasing as the grain size and number density increases.

In the present study, the RRA treatment improved the HE resistance of all the samples aged initially to the UA, PA and OA tempers. Out of the several heat treatments employed, the peak-aged + retrogressed + underaging (PRU) treatment resulted in the lowest susceptibility to HE for both alloys. In order to understand the influence of hydrogen charging and RRA treatment on the dislocation structure, four 1440 samples in different heat treatment conditions were observed in the TEM. Figures 4.15(a), 4.15(b), 4.15(c) and 4.15(d) present the dislocation structures of the PA uncharged, the PA hydrogen charged, the PRU uncharged and the PRU hydrogen charged samples, respectively. A decrease in the dislocation density of uncharged peak aged 1440 alloy on RRA treatment (Figures 4.15(a) and 4.15(c)) can be noticed. Hydrogen

charging increases the dislocation density of both the peak aged and PRU samples of the 1440 alloy. However, the increase in dislocation density of the PA alloy after hydrogen charging is more severe compared to that of the RRA sample after hydrogen charging (Figure 4.15). These results are consistent with the observation of Talianker and Cina [28] that dislocation densities in Al alloys are reduced by retrogression and reaging treatment. The general improvement of HE resistance in all of the RRA samples in this study seems to support the suggestion of Talianker and Cina [28] that the reduction in the dislocation density upon RRA leads to enhanced HE resistance.

4.2c *Li content*.

The alloy with a higher Li content (i.e. 1440) was found to be relatively more susceptible to HE under all heat treatment conditions as compared to the alloy with a lower Li content (i.e. 1441). The increased HE resistance of 1441 compared to 1440 alloy may be attributed to lower Li content (or, alternatively lower Li/Cu ratio) and higher Mg content of 1441 alloy as suggested by Holroyd [14] and Vasudevan [124]. Precipitation of Al_2CuMg or Al_2MgLi is favoured in the alloys containing Mg which may increase the crack initiation resistance. The role of Li content in enhancing HE is addressed later.

4.3 *Mechanism of Hydrogen Embrittlement*

Fig. 4.16 shows the SEM photographs of the fractured surfaces of the underaged 1440 alloy in the charged and uncharged conditions. The features for the other alloy were similar. The uncharged specimen exhibited a ductile type of failure throughout

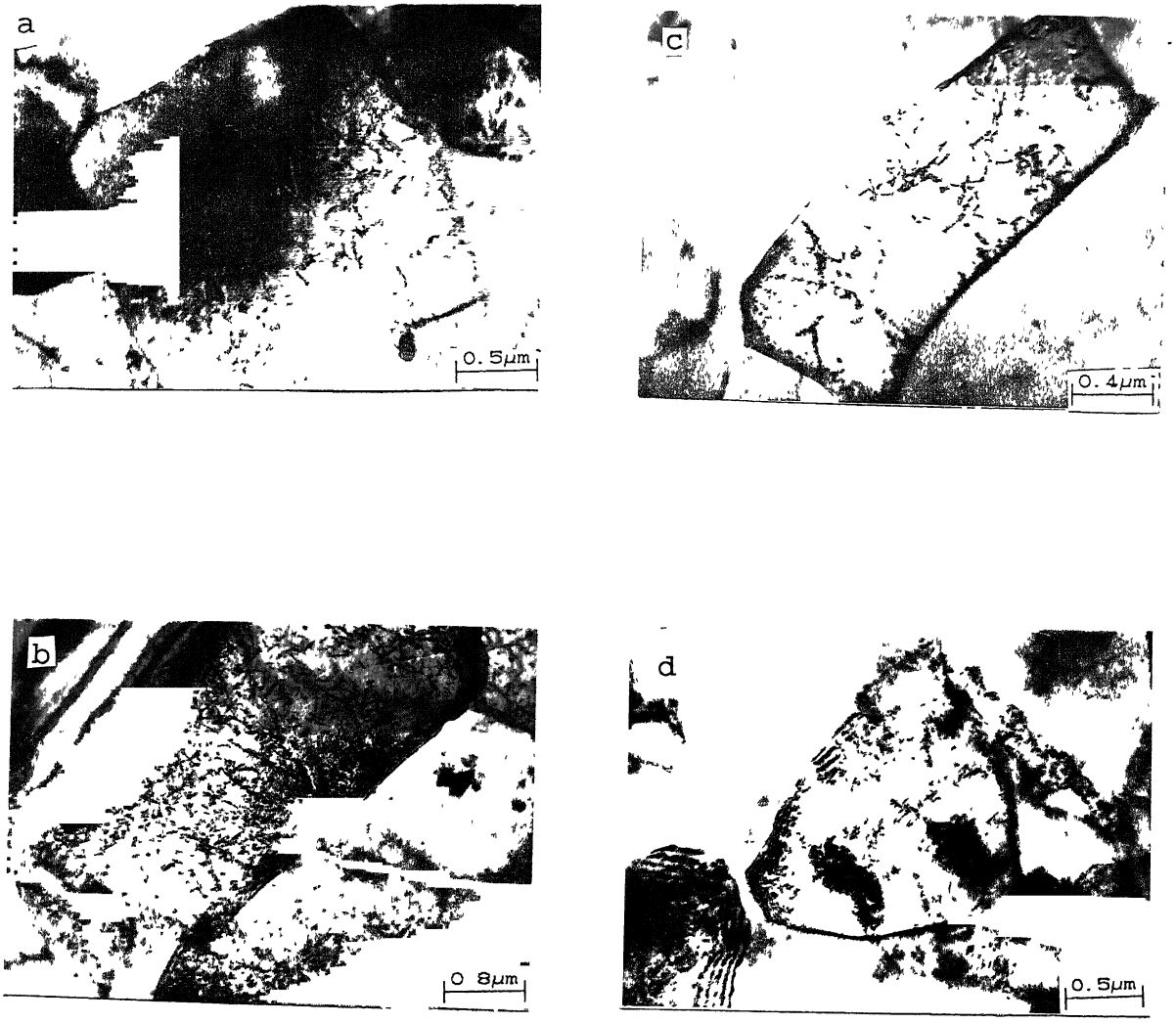

Figure 4.15 TEM micrographs showing the dislocation structure of 1440 alloy in (a) PA uncharged (b) PA hydrogen charged (c) PRU uncharged and (d) PRU hydrogen charged conditions.

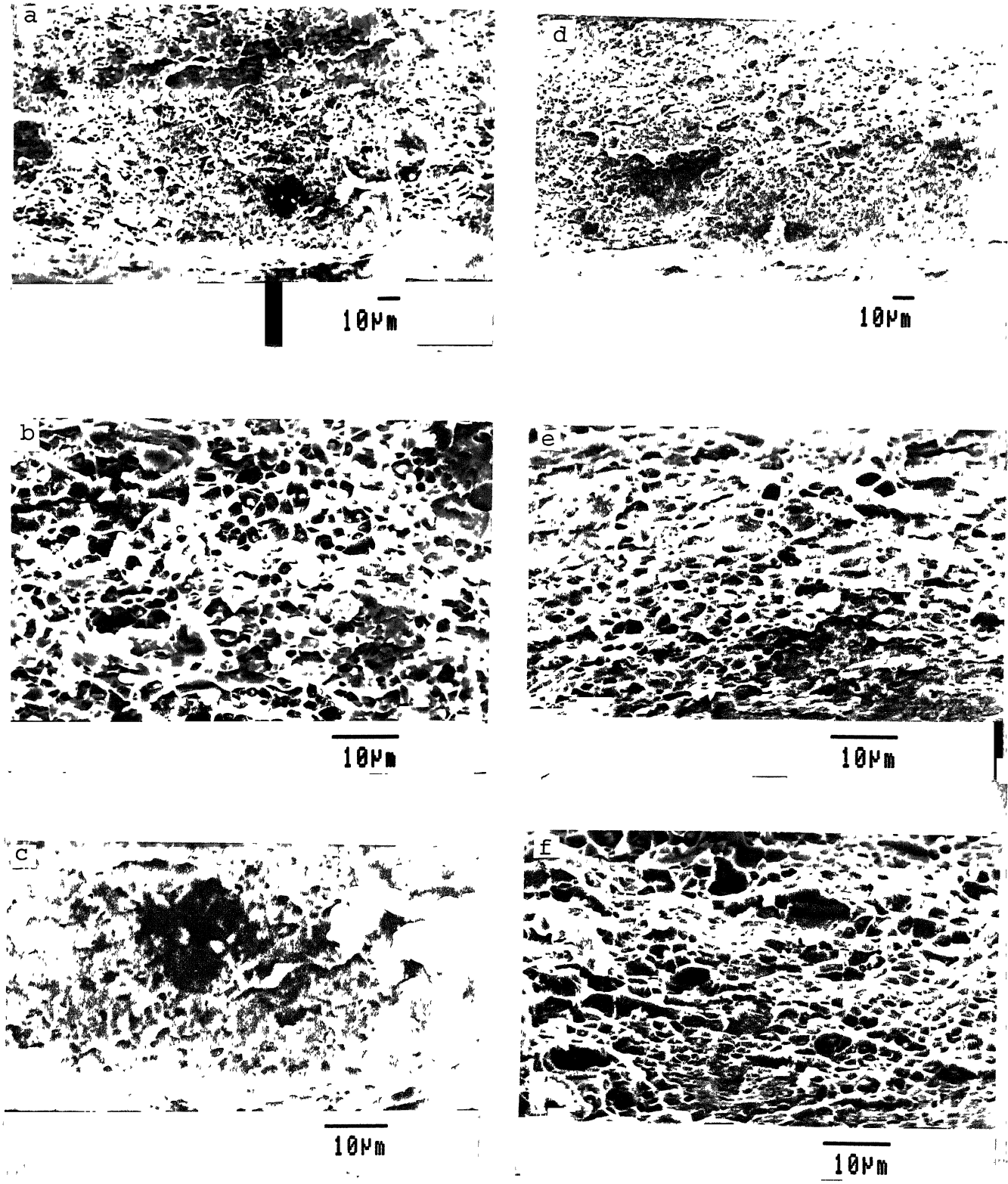

Figure 4.16 SEM fractographs of UA 1440 hydrogen charged (a-c) and uncharged (d-f) specimens; (a), (c), (d) and (f) are fractographs from the surface, while (b) and (e) are from the interior.

the cross-section (Figure 4.16(d) from near the surface of the specimen while Figure 4.16(e) is from the interior). However, the hydrogen charged samples exhibited flat fractographic features near the surface extending approximately 80-100 μm into the material from the surface (Figure 4.16(a)). A higher magnification view of the flat feature is presented in Figure 4.16(c). The fractograph of the inner portion of the hydrogen charged specimen indicate ductile failure (Figure 4.16(b)). The flat fractographic features near the surface of the hydrogen charged specimen and their absence in the reference specimen indicate that hydrogen is responsible for these features.

In order to understand the effect of hydrogen charging on the build-up of hydrogen concentration in the alloys, microhardness (MHv) profiles were obtained across the cross-section of both the PA alloys after hydrogen charging. The average MHv as a function of distance from the surface is presented in Figure 4.17. For both the alloys, the error at each data point is ±2 MHv. The hardness was high at the surface and decreased with depth. Assuming that the hardness is proportional to hydrogen concentration, it is possible to evaluate the hydrogen diffusivities from these profiles [132]. The diffusion depth (80-100 μm) of hydrogen in these alloys corresponds to the depth upto which the flat faceted fracture characteristics were observed in the hydrogen charged tensile specimens (Figure 4.17). Therefore, the enhanced hydrogen concentration at the surface regions of the hydrogen charged specimens leads to these flat fractographic features. Increased faceted appearance of the fracture surface with increased hydrogen pre-charging has also been observed by other investigators in Al-Li alloys [16,17].

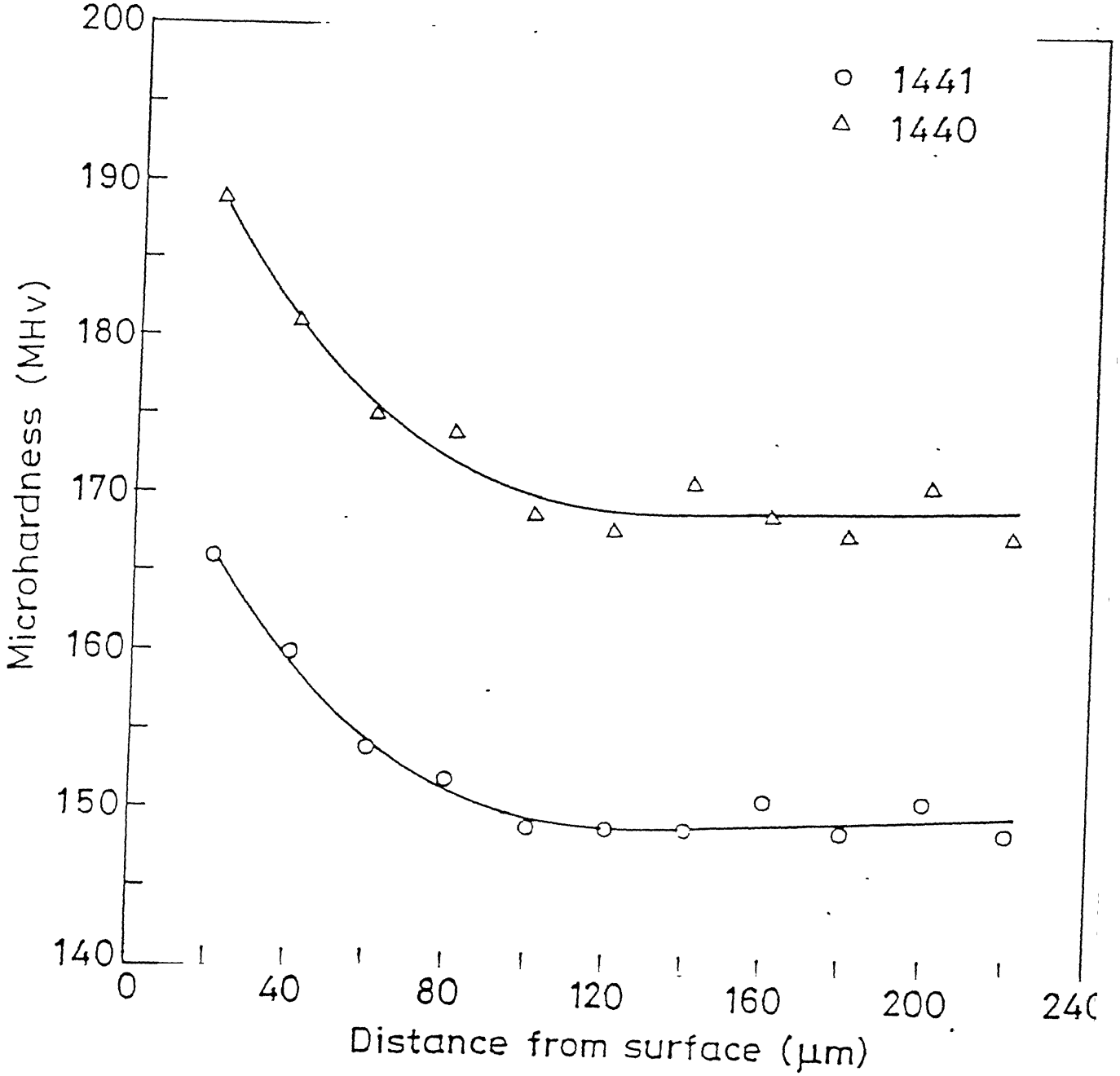

Figure4.17Average microhardness depth profiles of PA 1440 and 1441 alloys after cathodic hydrogen charging in 0.1 mol/l NaOH at 10 mA/cm^2 for 12h.

The faceted appearance of the fracture surfaces of embrittled Al-Li alloys has been attributed to the presence of hydride under HE conditions [18]. This hydride cracking mechanism of EIC in Al-Li alloys has its basis on the unambiguous identification of the hydride $LiAlH_4$ in an embrittled Al-Li-Cu alloy by transmission electron microscopy [42]. The formation of this hydride and LiH was also confirmed by XRD studies on hydrogen charged Al-Li alloys used in the present study [133]. It was found that the $LiAlH_4$ phase was stable once it formed in these alloys, as baking the specimen at room temperature for 168 hours did not lead to its decomposition. This is clearly seen in the XRD patterns of uncharged, freshly hydrogen charged and room temperature baked 1440 PA alloy presented in Figure 4.18. The results for the 1441 alloy were similar (Figure 4.19). The decomposition of these hydrides at temperatures upto 550^{o}C has been extensively studied by XRD [133]. It was found that $LiAlH_4$ decomposes between 130^{o}C and 160^{o}C while LiH was stable even at 500^{o}C. It is reasonable to assume that the concentration of these hydrides in the near surface regions would be larger than in the bulk of the material. If such a situation persists, then the hydrides, especially at the grain boundaries, in the near surface regions would act as potential crack initiation sites (see Figure 4.14) during tensile testing and this would result in lower ductilities for the hydrogen charged specimens. The flat fractographic features in the near surface regions also indicate that the faceted structure could be obtained due to the cracking of the brittle hydrides. This process would result in crack nucleation and its subsequent propagation in the near surface regions. Crack propagation through the material in the inner regions, that contain a lower

concentration of hydrides/hydrogen, would be difficult. Therefore, the ductile nature of the fracture surfaces in the interior of the hydrogen charged specimens indicates that either repeated formation and cracking of the hydride did not occur in front of the crack tip or that the concentration of the hydrides in the interior was low enough that ductile failure results.

It was earlier seen that the 1440 alloy was more susceptible to HE than the 1441 alloy in all the heat treatment conditions.The 1440 alloy with a higher Li percentage contains a lower amount of Cu. It has been reported that Cu addition is deleterious to HE resistance of Al-Li alloys [18]. Although the Cu addition is lower in 1440 compared to 1441, the former is more susceptible to HE. Therefore, the enhanced susceptibility of 1440 alloy must be related to its higher Li content, indicating the importance of the lithium (alumino) hydrides in the embrittlement process.

4.3a *Hydrogen diffusivity in Al-Li alloys*

The diffusion of hydrogen from the surfaces into the alloy determines the buildup of the hydrogen concentration to a critical level at which hydrogen embrittlement occurs [19]. In this regard, the determination of hydrogen diffusivity in Al-Li alloys would be useful. However, data on hydrogen diffusivity in Al-Li alloys is lacking, although limited data is available in the literature for Al and Al alloys [134-140]. Table 4.2presents hydrogen diffusivities in aluminium compiled from various sources [134-138]. Except for Ishikawa and McLellan's data [138], the others have been extrapolated from higher temperatures. This communication reports the determination of hydrogen diffusivities in two Al-Li-Cu-Mg alloys at 298 K by subsurface microhardness

profiling after the specimens were cathodically charged with hydrogen.

Figure 4.17 presents the plots of average microhardness (MHv) as function of distance from the surface for the 1440 and 1441 alloys. The maximum scatter in MHv value at a particular location was ± 2 MHv. Smooth third-order polynomial curves were drawn through the data points. The maximum hardness was obtained at the surface which decreased gradually towards the core of the sample. The depth of hardened subsurface zones were approximately 80 μm. The increase in hardness in the subsurface region of Al-Li alloys upon hydrogen charging has also been observed before [59]. The microhardness variation is due to the variation in hydrogen concentration (which depends upon the diffusion of hydrogen into the alloys), as the microhardness of the uncharged specimens was constant across the crosssections.

The diffusivity of hydrogen in the alloys was estimated from the microhardness profiles. Assuming $(C-C_b)$ to be proportional to increase of MHv over the bulk value $(MHv-MHv_b)$, we obtain

$$\frac{C - C_b}{C_s - C_b} = \frac{MHv - MHv_b}{MHv_s - MHv_b} \qquad 4.1$$

where, C is the hydrogen concentration at a given distance, and subscripts *b* and *s* denote bulk and surface, respectively.

As the specimen surfaces were flat and the depths of diffusion fields were very small compared to the thickness of samples, it may be treated as unsteady diffusion through a semi-infinite flat specimen. Assuming that (i) diffusion occurred through a single phase, (ii) no internal reaction/interaction of hydrogen in the diffusion field, (iii) constant surface concentration (C_s) (i.e. C_s independent of time), and (iv)

constant diffusivity of hydrogen (D_H, in m^2s^{-1}) in the entire diffusion zone, equation (1) can be combined with the standard diffusion equation to obtain

$$\frac{MHv - MHv_b}{MHv_s - MHv_b} = \frac{C - C_b}{C_s - C_b} = 1 - erf\left(\frac{z}{2\sqrt{Dt}}\right) = erfc\left(\frac{z}{2\sqrt{Dt}}\right) \qquad 4.2$$

where z is distance from surface in *m* and t is cathodic hydrogen charging time in *sec*.

The diffusion coefficient was determined using Eq.(2) by the following method [11]. A pair of points on the microhardness vs distance curve was chosen and the parameter Y_{12} was obtained (for two given points 1 and 2) based on Eq.(2).

$$Y_{12} = \frac{(C_1-C_b)/(C_s-C_b)}{(C_2-C_b)/(C_s-C_b)} = \frac{C_1-C_b}{C_2-C_b} = \frac{erfc(z_1/2\sqrt{Dt})}{erfc(z_2/2\sqrt{Dt})} = \frac{(MHv)_1 - (MHv)_b}{(MHv)_2 - (MHv)_b} \qquad 4.3$$

where $(MHv)_1$, $(MHv)_2$ and $(MHv)_b$ are the microhardness values and C_1, C_2 and C_b are the hydrogen concentrations at locations 1, 2 and in the bulk, respectively. D is the only unknown parameter in Eq.(3) for a given experiment. Values of D were obtained using error function table and by trial and error solution. Table 4.3 presents the values of D_H at 298 K in the two alloys obtained by the above procedure. Several pairs of data points were chosen from each curve to obtain a set of diffusivity values. These have also been presented in Table 4.3. It may be noted that the largest and smallest D values for a given alloy differed by approximately a factor of 4. This may be considered as fairly good in view of the many simplifying assumptions used.

Assumptions (i) and (ii) are simplistic and not strictly valid. The peak aged Al-Li-Cu-Mg alloy can not be truely

considered as a single phase material due to presence of different precipitates. However, the volume fraction of the precipitates is low and, moreover, hydrogen primarily diffuses through the continuous matrix phase (solid solution of Mg, Cu and Li in Al). As regards the second assumption, hydrogen in Al-Li alloys can lead to precipitation of hydrides [42] and this would also result in hardening. However, the hydride concentration scales linearly with hydrogen concentration and therefore the hardness profiles reasonably indicate the concentration of hydrogen. It must be mentioned that diffusivity of Li in aged Al-Li alloys has also been obtained by profiling microhardness in the subsurface region after high temperature treatments [107] and similar considerations, implicitly assumed, provided realistic results. As regards the third assumption, the surface concentration of hydrogen would be constant as a constant cathodic hydrogen charging current density was employed. Moreover, the rationale behind the procedure based on equation (3) also eliminates C_s which is an unknown. Finally, since Y_{12} is a ratio, errors on estimated values of D would be partly eliminated due to cancellation effect. Averaging of a set of D values for a profile is expected to reduce estimation errors further.

The average hydrogen diffusivities (D_{av}) in the two Al-Li alloys have also been presented in Table 4.3. The diffusivity of hydrogen in Al-Li alloys is lower than in Al [134-137]. This is reasonable as it has been earlier shown that the presence of lithium lowers the diffusivity of tritium in Al-Li alloys [139,140]. The present results are also self-consistent in that the diffusivity of hydrogen in 1440 alloy (having a higher Li content) is lower than that in 1441 alloy (having lower Li).

Table 4.2 Diffusivity of hydrogen in aluminium at 298 K obtained from the literature.

Investigators [ref]	Diffusivity D (m^2s^{-1})
W.Eichenauer *et al.*[3]	2.1×10^{-13}
W.Eichenauer *et al.*[4]	9.2×10^{-13}
M. Ichimura *et al.*[5]	1.5×10^{-12}
K. Papp *et al.*[6]	1.9×10^{-12}
T. Ishikawa *et al.*[7]	4.6×10^{-14}

Table 4.3 Diffusivity of hydrogen in Al-Li-Cu-Mg alloys at 298 K obtained in the present study.

Alloy	$D_H \times 10^{14}$ (m^2s^{-1})	$D_{H,av} \times 10^{14}$ (m^2s^{-1})
1440	7.52, 8.61, 4.90, 4.28, 2.08	5.48
1441	9.19, 7.00, 6.26, 6.26, 2.08	6.16

4.3b *Hydride Formation*

The XRD patterns of the 1440 alloy in the uncharged and hydrogen charged conditions, and after baking at 25°C for one day are presented in Figures 4.18(a) through 4.18(c), respectively. The patterns for the 1441 alloy under similar conditions are shown in Figures 4.19(a) through 4.19(c). In both the specimens, hydrogen charging clearly resulted in additional peaks which were not eliminated even after baking at room temperature for fairly long times. The interplanar distances obtained from the extra peaks of the charged and baked specimens have been compared with the theoretical interplanar values of several phases including LiH, $LiALH_4$, Li_3AlH_6, $LiAl_4H_{13}$, $LiAl_2H_7$, $LiMg(AlH_4)_3$, AlH_3, $Al(OH)_3$, LiOH, ZrH_2, MgH_2, and $Mg(OH)_2$ phases. The extra diffraction peaks in the XRD patterns of these alloys (freshly charged and baked at 25°C) have been indexed and the results are tabulated in Tables 4.4 and 4.5 for 1440 and 1441 alloys, respectively.

The presence of $LiAlH_4$ in the alloys after room temperature cathodic charging of hydrogen can be directly concluded, whereas the presence of LiH is indirectly indicated. Each of the Figures 4.18(b),(c), and 4.19(b),(c) show a small bump at the base of Al (111) and Al (200) peaks occurring at a slightly lower 2θ value compared to the Al peaks. These bumps have been indexed as LiH (111) and LiH (200) peaks. They have superimposed on the strong Al peaks and therefore, cannot be resolved. The bumps result due to the finite diffraction intensities of the LiH peaks. The identification of LiH is reasonable as the bumps at the base of the Al peaks are not present in the uncharged specimen.

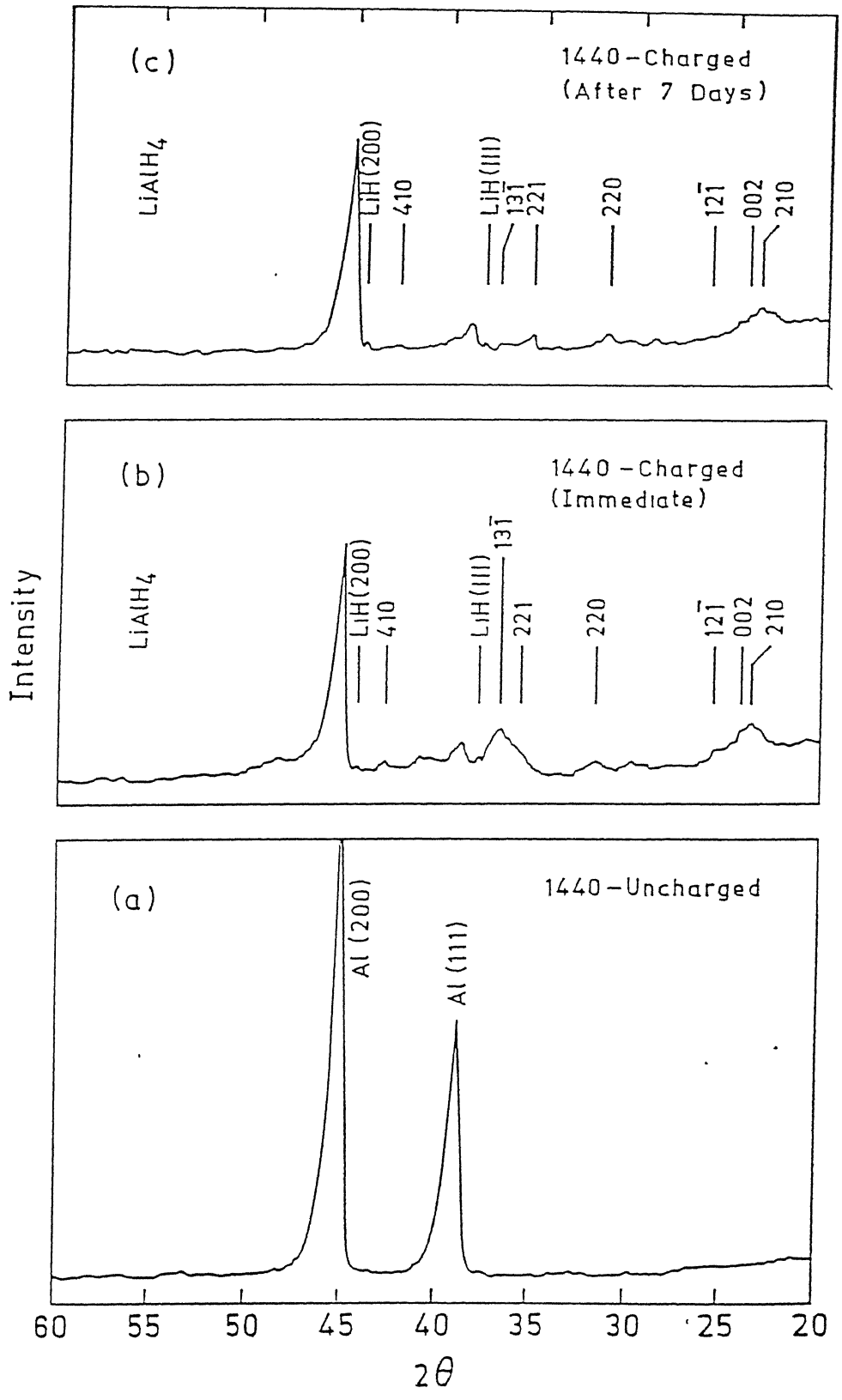

Figure 4.18 XRD patterns of 1440 alloy: (a) uncharged, (b) freshly hydrogen-charged and (c) baked at 25°C for 168 h.

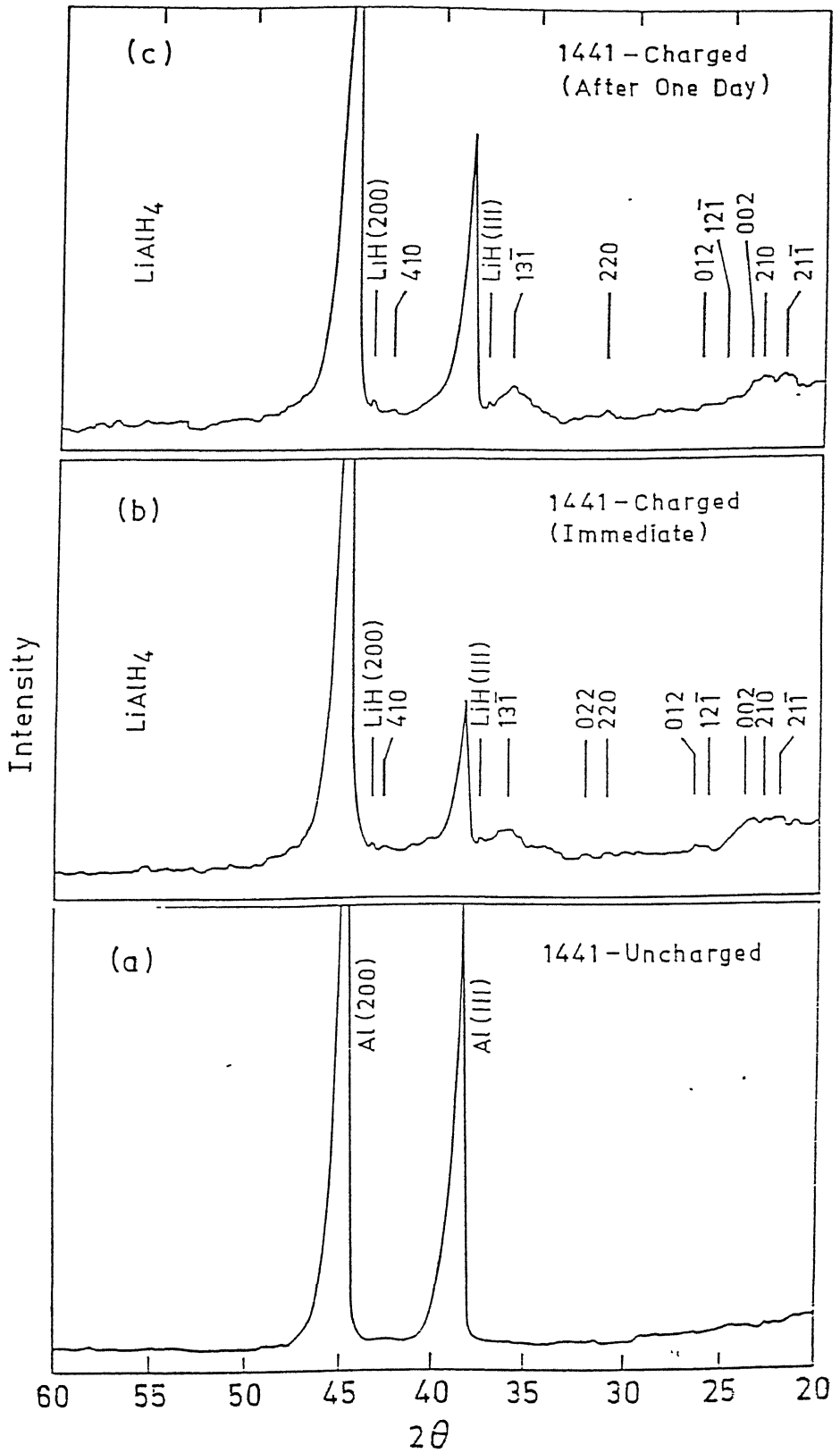

Figure 4.19 XRD patterns of 1441 alloy: (a) uncharged, (b) freshly hydrogen-charged and (c) baked at 25°C for 168 h.

Table 4.4

Observed						Theoretical				
Condition-1			Condition-2							
2θ	d	I/I_1	2θ	d	I/I_1	2θ	d	I/I_1	hkl	possible phase
23.3	3.816	100	23.2	3.834	100	22.9	3.89	100	210	$LiAlH_4$
24.3	3.661	62	24.0	3.708	78	24.2	3.68	25	002	$LiAlH_4$
25.4	3.505	38	25.9	3.440	39	26.0	3.43	10	$12\bar{1}$	$LiAlH_4$
31.2	2.866	35	31.2	2.866	39	30.3	2.95	25	220	$LiAlH_4$
35.4	2.535	57	35.2	2.549	39	35.3	2.54	6	221	$LiAlH_4$
36.5	2.461	93	37.0	2.429	14	36.6	2.45	10	$13\bar{1}$	$LiAlH_4$
37.6	2.391	37	37.8	2.379	35	38.2	2.36	55	111	LiH
42.5	2.126	37	42.3	2.137	17	42.0	2.15	16	410	$LiAlH_4$
44.0	2.057	100	44.0	2.057	100	44.4	2.04	100	200	LiH

Condition-1: Freshly charged sample

Condition-2: hydrogen charged + baked at $25^{o}C$ for 168 h

Analysis of extra diffraction peaks obtained in the freshly hydrogen charged specimen of 1440 alloy and after baking the same specimen at room temperature for 168 hours.

Table 4.5

Observed						Theoretical				
Condition-1			Condition-2							
2θ	d	I/I_1	2θ	d	I/I_1	2θ	d	I/I_1	hkl	possible phase
22.0	4.040	100	22.1	4.022	100	22.2	4.00	2	$21\bar{1}$	$LiAlH_4$
23.0	3.867	100	23.2	3.834	100	22.9	3.89	100	210	$LiAlH_4$
24.0	3.708	100	23.8	3.737	75	24.2	3.68	25	002	$LiAlH_4$
26.0	3.427	52	25.1	3.546	47	26.0	3.43	10	$12\bar{1}$	$LiAlH_4$
26.5	3.363	58	26.3	3.388	47	26.8	3.32	50	012	$LiAlH_4$
31.2	2.866	42	31.2	2.866	40	30.3	2.95	25	220	$LiAlH_4$
32.5	2.754	42	32.5	2.754	30	33.4	2.68	25	022	$LiAlH_4$
36.2	2.481	85	36.4	2.468	83	36.6	2.45	10	$13\bar{1}$	$LiAlH_4$
37.6	2.391	40	37.5	2.398	35	38.2	2.36	55	111	LiH
42.7	2.117	52	42.4	2.132	40	42.0	2.15	16	410	$LiAlH_4$
43.9	2.062	100	44.0	2.057	100	44.4	2.04	100	200	LiH

Condition-1: Freshly charged sample

Condition-2: Hydrogen charged + baked at 25^{o}C for 24 h

Analysis of extra diffraction peaks obtained in thefreshly hydrogen charged specimen of 1441 alloy and after baking the same specimen at room temperature for 24 hours.

It is worth noting that although the XRD patterns in all the figures have been obtained after 70% reduction of the original diffraction patterns, the bumps at the base of Al peaks can still be noticed. Therefore, these small bumps at the base of the strong Al matrix peaks provide evidence for the presence of LiH phase in the hydrogen-charged specimens.

4.3c *Hydride Stability*

The stabilities of the LiH and $LiAlH_4$ hydrides are addressed below. LiH is the most stable of the hydrides that can form in the Al-Li-H system [144] and this has been shown to be the case when Al-Li alloys are annealed at high temperatures in air and hydrogen [87,88]. Dickenson *et al.* [87] explained that LiH is the most stable hydride at 550°C and its formation is thermodynamically favourable, whereas AlH_3 and the various compounds of $LiH:AlH_3$ ($LiAlH_4$, Li_3AlH_6, $LiAl_4H_{13}$) are unstable at 550°C. However, Balasubramaniam *et al.* [42] reported the formation of $LiAlH_4$ in an Al-Li-Cu alloy after slow strain rate testing under cathodic polarization conditions in ambient temperatures. In order to explain the stability of $LiAlH_4$, the hydride phase which was identified by electron diffraction, Balasubramaniam *et al.* [42] computed and compared the stabilities of $LiAlH_4$ and LiH assuming hydrogen to be in the monoatomic form. They showed by thermodynamic calculations that $LiAlH_4$ is more stable than LiH under these conditions. However, Tromans [144] argued that the activities of interacting species were not considered in the analysis of Balasubramaniam *et al.*, and he recalculated the stabilities of LiH, $LiAlH_4$ and AlH_3 by accounting for the activities of Li, Al and hydrogen. He showed that LiH forms at the

lowest limiting activity of hydrogen followed by $LiAlH_4$ and then AlH_3. Moreover, he also noted that the limiting fugacity of hydrogen for LiH formation is slightly lower than that for $LiAlH_4$ formation. In the present case, the actual fugacity of hydrogen is high and could exceed the value for the formation of the less favourable hydrides. The formation of $LiAlH_4$ is therefore possible along with LiH under the condition of high overpotential of hydrogen due to increased hydrogen fugacity during electrochemical charging. The free corrosion potential of these alloys is around -1400 mV Vs SCE and, as mentioned earlier, charging at 10 mA/cm^2 polarizes the specimen to a potential of -1680 mV Vs SCE. It can be easily shown by applying the Nernst equation that the fugacity of hydrogen on the surface, at this negative cathodic potential, should be high. Therefore, the high hydrogen fugacity would have been responsible for stabilizing $LiAlH_4$ in addition to LiH. In this regard, it should be noted that Mikheeva and Arkhipov [147] reported that although the heat of decomposition of $LiAlH_4$ was positive, it did not decompose at ambient temperature even after long exposure times. Incidentally, often a less stable phase can also form because of interfacial energy considerations and most of the analyses of hydride stability in Al-Li alloys do not consider this aspect. Finally, as suggested by Tromans, the actual formation of hydrides could be influenced by kinetic factors.

4.3d *High Temperature Baking Treatments*

In order to further understand the stability of the hydrides formed during cathodic charging, the charged samples were baked at different temperatures. The baking temperatures were chosen on the basis of $LiAlH_4$ decomposition temperature [145-149]. $LiAlH_4$

decomposes in the temperature range 150-430°C and it occurs in three stages. Dilts and Ashby [148] have summarized the thermal decomposition of $LiAlH_4$ to occur as follows:

$$3LiAlH_4 \longrightarrow Li_3AlH_6 + 3H_2 + 2Al \qquad 4.4$$

$$Li_3AlH_6 \longrightarrow LiH + 3/2\ H_2 + Al \qquad 4.5$$

$$LiH + Al \longrightarrow \text{"LiAl"} + 1/2\ H_2 \qquad 4.6$$

$LiAlH_4$ is stable below 150°C and decomposes above this temperature under atmospheric condition [148]. Li_3AlH_6 and LiH are the intermediate products of decomposition of pure $LiAlH_4$. Pure LiH melts with little decomposition at 680°C while LiH in the presence of aluminium metal decomposes at a lower temperature [148].

Figures 4.20(a) through 4.20(c) present the XRD patterns for the 1440 sample that has been baked at 130°C for 25 minutes, subsequently at 160°C for 25 minutes and again the same sample baked at 395°C for 25 minutes, respectively. XRD patterns of the 1441 alloy under similar experimental conditions are presented in Figures 4.21(a) through 4.21(c). It may be noted that the strong (210) $LiAlH_4$ peak is present in the freshly charged sample and after baking at 130°C, for both the alloys. This peak is absent in samples baked at 160°C. Moreover, peaks for Li_3AlH_6 (which is a decomposition product of $LiAlH_4$) could be identified only after baking at 160°C while they are absent after baking at 130°C. These results indicate that the decomposition of $LiAlH_4$ occurs between 130°C to 160°C. Similar findings have been reported by Dilts and Ashby [148].

XRD patterns of specimens successively baked at 510°C, 550°C for 25 minutes in each step and of the specimen directly baked at 550°C after hydrogen charging are shown in Figures 4.22 and 4.23,

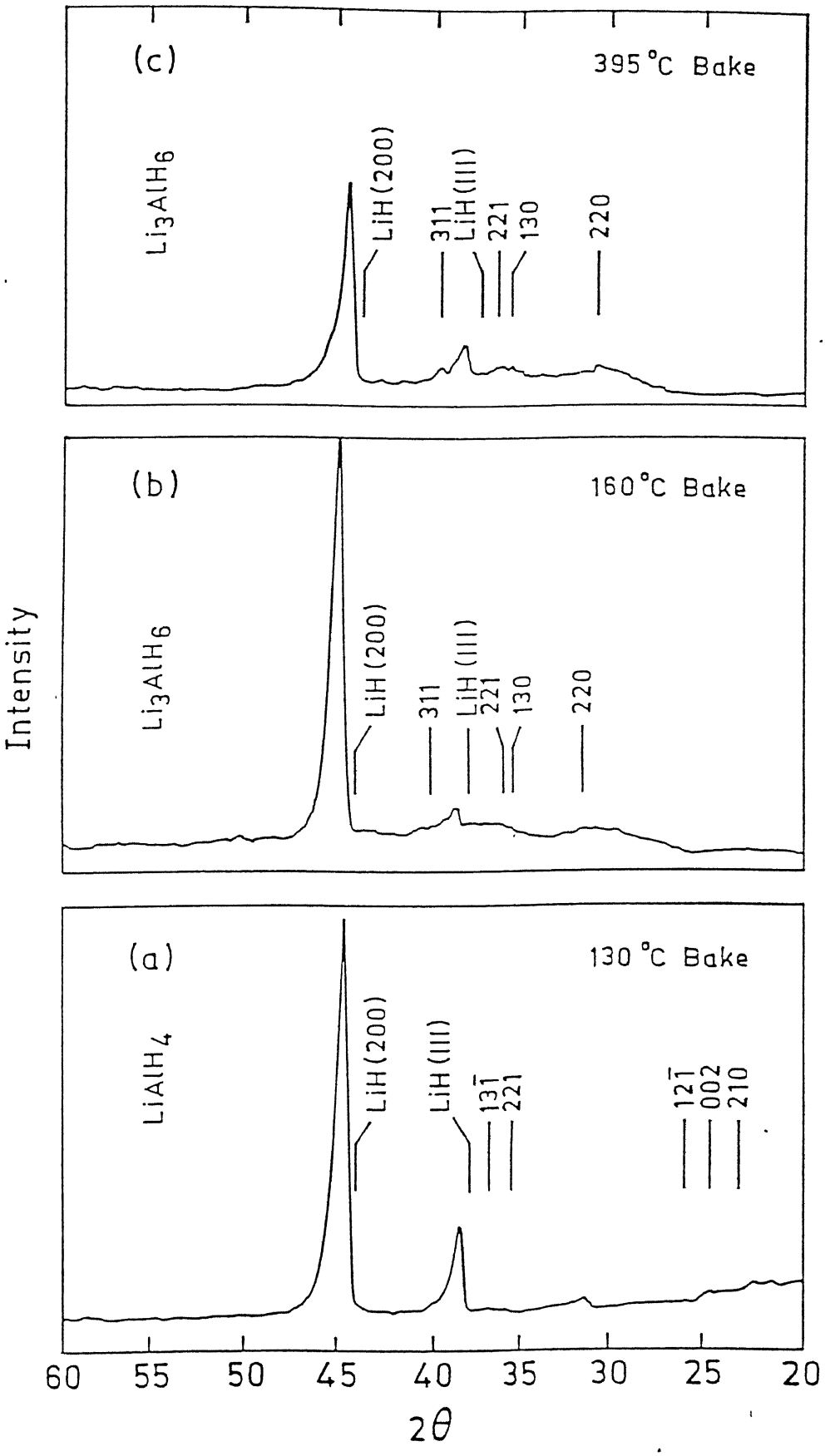

Figure4.20 XRD patterns of 1440 alloy successively baked at: (a) 130°C, (b) 160°C and (c) 395°C for 25 minutes in each case.

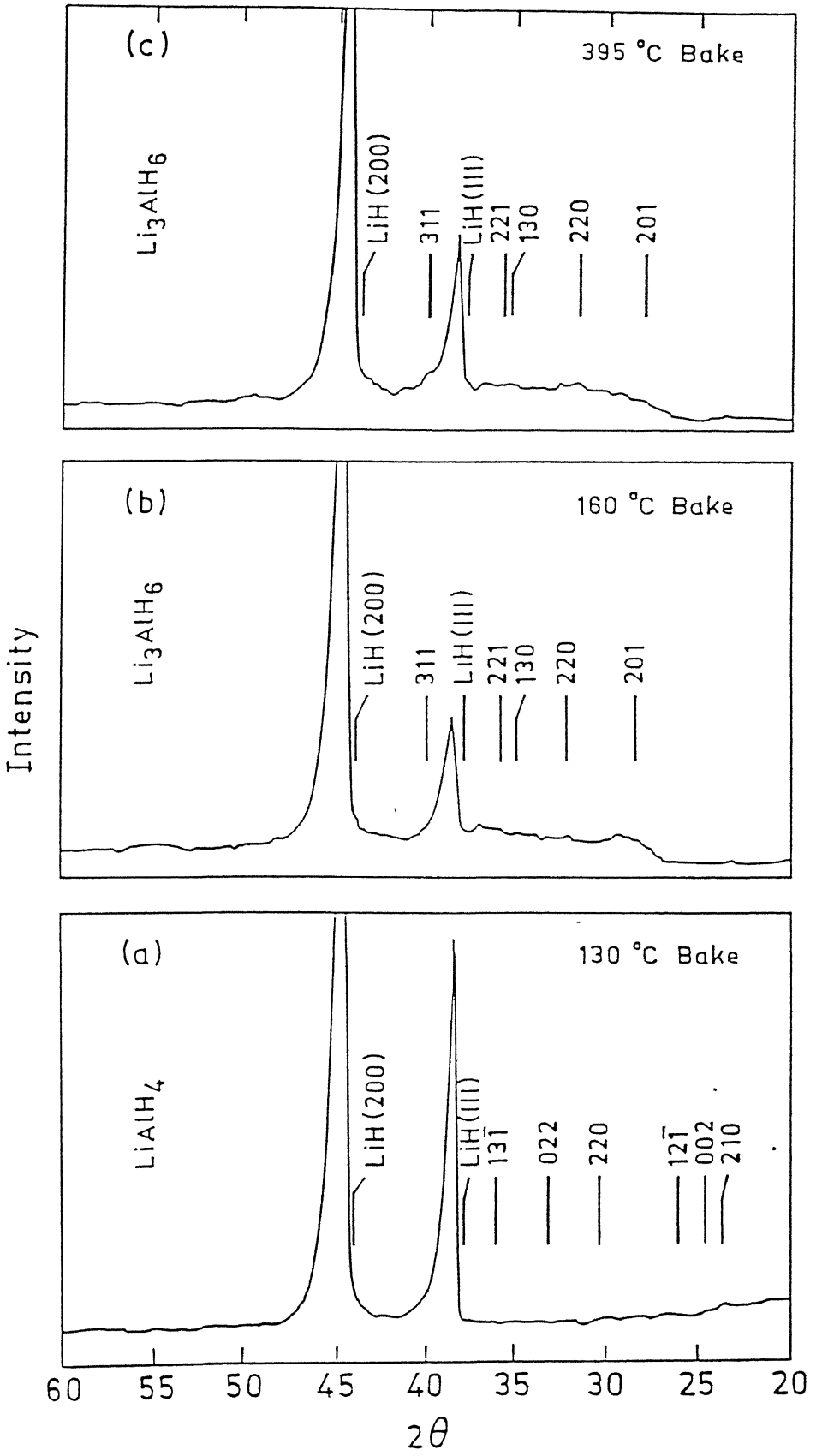

Figure4.21 XRD patterns of 1441 alloy successively baked at: (a) 130°C, (b) 160°C and (c) 395°C for 25 minutes in each case.

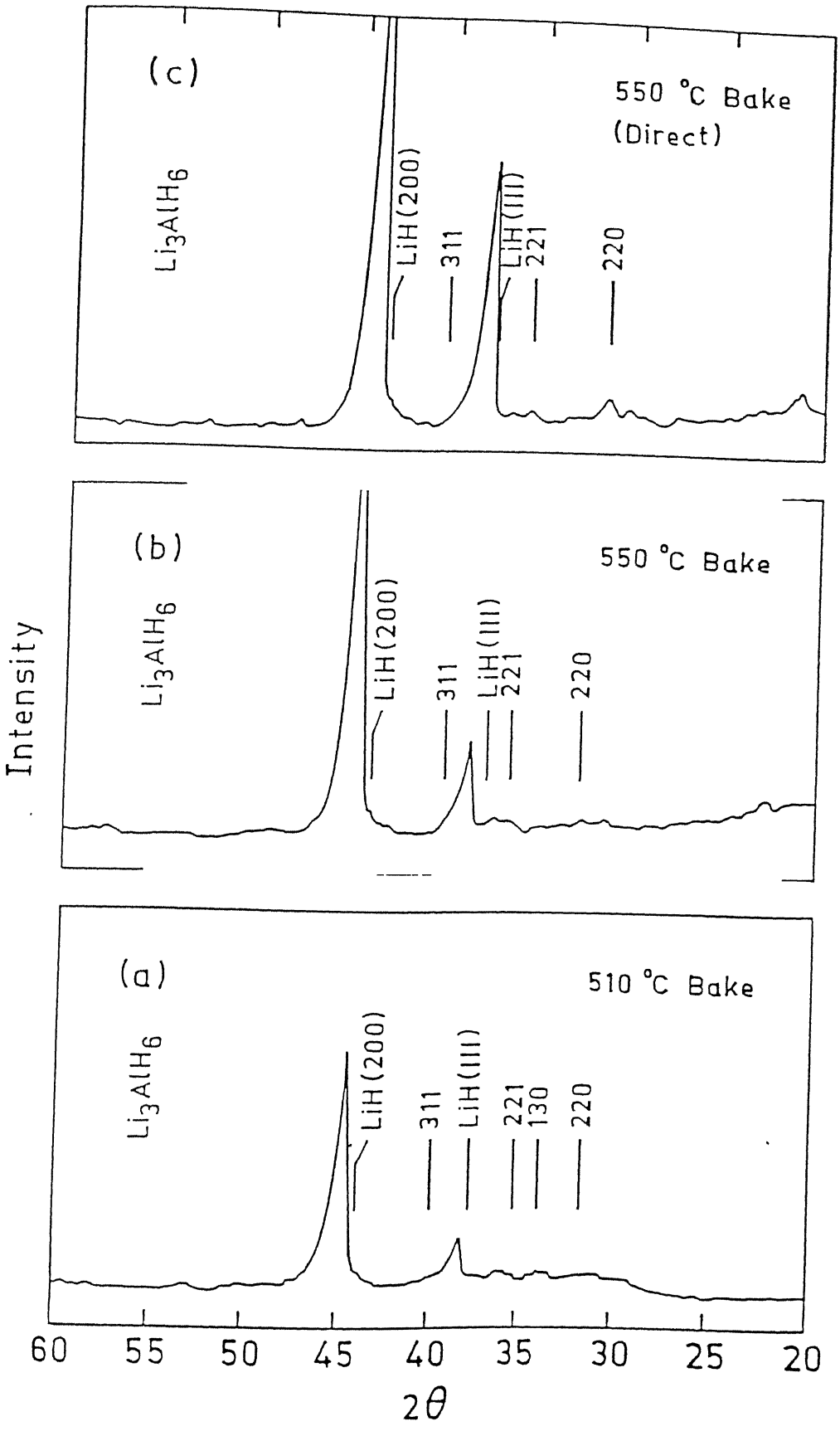

Figure 4.22 XRD patterns of 1440 alloy successively baked at: (a) 510°C and (b) 550°C, and (c) directly baked at 550°C for 25 minutes in each case.

for the 1440 and 1441 alloys, respectively. They indicate that LiH and Li_3AlH_6 are both present in these alloys after these baking treatments. In order to ascertain if the successive baking procedure employed in the study had any effect on the stability of the phases, a sample of each alloy was baked directly at 550°C immediately after room temperature cathodic hydrogen charging. The XRD patterns obtained from these specimens indicated that the same phases (LiH and Li_3AlH_6) obtain even after the direct baking treatment, thereby indicating that Li_3AlH_6 is stable, in addition to LiH, at least up to 550°C. It is reported that Li_3AlH_6 decomposes between 220°C and 430°C [146-148]. In the present study, distinct peaks from the Li_3AlH_6 phase were present in the samples after baking at 395°C (Figures 4.20(c) and 4.21(c)) and even after baking at 550°C. Therefore, the decomposition behaviour of Li_3AlH_6 phase in Al-Li alloys appears to be different from that in its pure form. It was shown earlier by Dilts and Ashby [148] that the decomposition temperature of complex aluminium lithium hydrides is increased in the presence of impurities and other hydrides. Higher Al/LiH ratio, the presence of alloying elements, impurities and other hydrides in the Al-Li alloys may be responsible for the stability of Li_3AlH_6 up to higher temperatures.

CHAPTER 5

SUMMARY

5.1 Conclusions

(1) A solution heat treatment temperature of 530^{o}C with 1 hour soaking is appropriate for 1440 and 1441 alloys. This SHT provides adequate dissolution of the precipitation hardening phases

(2) A 2.5 % cold stretch prior to aging has a beneficial effect on precipitation hardening of both the alloys. This provides higher hardness value than that of unstretched samples, and the aging kinetics are hastened by the cold stretch.

(3) An aging temperature of 170^{o}C with 16~18 hours of aging time provides optimum peak aged hardness for the 1440 alloy. While 18~20 hours aging time provides peak aged hardness for the 1441 alloy at the same temperature. At the aging temperature 190^{o}C overaging of both alloys is much pronounced compared to 150^{o}C aging temperature.

(4) The critical conditions for dissolving the strengthening precipitate δ' into the matrix of 1440 and 1441 alloys, are 60 and 40 secs. of immersion time and 270^{o}C and 235^{o}C retrogression temperature respectively. The least retrogressed samples respond faster to natural aging than the completely retrogressed samples.

(5) In case of natural aging of 1440 and 1441 alloys that have been solution treated and cold stretched, 50 days and 60 days, are required to reach the peak hardness of 125 and 120 VHN , respectively.

(6) Both the 1440 and 1441 alloys were found to be the most susceptible to HE in the under aged temper and least susceptible to HE in the peak aged temper. OA temper occupied intermediate position in between UA and PA as regards HE susceptibility. The improved HE resistance of the PA temper compared to other tempers has been attributed to its microstructure containing a large number of homogeneously distributed irreversible hydrogen traps.

(7) In general, RRA treatment improved the hydrogen embrittlement resistance for all starting aging tempers. TEM studies indicated that there is a reduction in dislocation densities on RRA and this improves the HE resistance of the RRA samples compared to the aged samples.

(8) Amongst the various heat treatments, peak aged + retrogressed + underaged samples provided the lowest susceptibility to HE for both alloys. The alloy containing higher Li or Li/Cu ratio (i.e. 1440) was more susceptible to HE in all heat treatment conditions. The easier crack initiation due to increased hydride formation tendencies resulted in enhanced susceptibility of the alloy with a higher Li content. Identification of hydride phases (LiH and $LiAlH_4$) after cathodic hydrogen charging of 1440 alloy by XRD analysis provides support to hydride cracking mechanism of HE.

(9) Hardening was observed in the subsurface region of two Al-li alloys after cathodic hydrogen charging. The diffusivity of hydrogen in these alloys was determined from the microhardness profiles as 5.48×10^{-14} $m^2 s^{-1}$ for Al-2.30Li-1.24Cu-0.80Mg and, 6.16×10^{-14} $m^2 s^{-1}$ for Al-1.9Li-1.8Cu-1.0Mg alloys. The diffusion coefficient of hydrogen in Al-Li alloys could not be

located in literature for direct comparison. The presence of lithium in Al-Li alloys lowers hydrogen diffusivity.

(10) The presence of LiH and $LiAlH_4$ phases in two cathodically hydrogen-charged Al-Li alloys at room temperature was identified by XRD. $LiAlH_4$ is stable up to 130°C and decomposes between 130°C to 160°C. LiH is stable and does not decompose after baking at 550°C. Li_3AlH_6, a decomposition product of $LiAlH_4$, was obtained on baking the hydrogen-charged specimen at temperatures greater than 130°C and it was present even after baking the specimen at 550°C. The stabilities of these hydrides have been discussed.

5.2 Suggestion for further investigations

(a) Hydrogen concentration across the sample thickness should be measured to understand HE in a better way.

(b) For uniform cathodic hydrogen charging, spiral platinum electrode should be used as counter electrode..

(c) XRD analysis of the specimens subjected to free corrosion potential and subsequently baked at different hydride decomposition temperatures should be carried out to understand the phase transformations.

(d) TEM study of peak aged and retrogressed reaged sample should be carried out for understanding the precipitate chemistry, structure and distribution of various phases.

(e) Analysis of nature and number of specific hydrogen traps in Al-Li alloys using the mathematical model of Pressure and Bernstein must be carried out.

REFERENCES

1. E.A. Balmuth and R.S. Schmidt, in Aluminium-Lithium I, Eds. T.H. Sanders Jr. and E.A. Starke Jr., TMS, Warrendale, USA, p. 69 (1981).
2. E.A. Starke Jr. , T.H. Sanders Jr. and I.G. Palmer, *J of Metals* **33**, 24 (1981).
3. K.K. Sankaran and N.J. Grant, in Aluminium-Lithium I, Eds. T.H. Sanders Jr. and E.A. Starke Jr., TMS, Warrendale, USA, p. 205 (1981).
4. C. Sigli and J.M. Sanchez, *Acta Metall.* **34**, 329 (1986).
5. D. Webster, T.G. Haynes and R.H. Flemming, *Adv. Mat and Process* **133**, 25 (1988).
6. D.B. Williams and J.W. Edington, *Metal Sci.* **9**, 114 (1971).
7. H.K. Hardy, *J. Inst. Met* **84**, 429 (1955-56).
8. B. Noble and G.E. Thompson, *Met. Sci. J.* **8**, 167 (1972).
9. F.S. Lin, S.B. Chakraborty and E.A. Starke Jr., *Met. Trans.* **11A**, 365 (1980).
10. C.R. Brooks, *Metals Handbook*, Volume 4, 9thedition, ASM, Metals Park, USA, p. 843 (1989).
11. R.S. James, *Metals Handbook*, Volume 2, 10thedition, ASM, Metals Park, USA, p. 178 (1989).
12. T.R. Ramchandran, in Proc. of 2nd Int. Conf. on Aluminium, The Al Association of India, p. 583 (1991).
13. L. Christodoulou, L. Struble and J.R. Pickens, in Aluminium-Lithium II, Eds. T.H. Sanders Jr. and E.A. Starke Jr., TMS, Warrendale, USA, p. 561 (1983).

14. N.J.H. Holroyd, A. Gray, G.M. Scamans and R. Hermann, in Aluminium-Lithium III, Eds., C Baker C, P.J. Gregson, S.J. Harris, and C.J. Peel, The Institute of Metals, London, England, p. 310 (1985).

15. F. Binsfeld, M. Habashi, J. Galland, J.P. Fidelle, D. Miannay and P. Rofidal, in Aluminium-Lithium IV, Eds., G.Champier, B. Dubost, D. Miannay and L. Sabetay, J. de Physique Colloque, **48**, C3-587 (1987).

16. T. Ohnishi and T. Ito, *Trans. Japan Inst. Metals* **29**, 642 (1988).

17. E.I. Meletis and W. Huang, in Aluminium-Lithium V, Eds., T H Sanders Jr. and E A Starke Jr., MCE Publications, Oxford, England, p. 1309 (1989).

18. R. Balasubramaniam, D.J. Duquette and K. Rajan, *Acta metall. mater.* **39**, 2597 (1991).

19. Z.F. Wang, Z.Y. Zhu, Y. Zhang and W Ke, *Metall. Trans.* **23A**, 3337 (1992).

20. T. Magnin and M. Rebiere, *Aluminium-Lithium IV*, Eds., G. Champier, B. Dubost, D. Miannay and L. Sabetay, *J. De Physique, Colloque*, **48**, C3-835 (1987).

21. I. Novikov, *Theory of Heat Treatment of Metals*, Mir Publishers, Moscow, p.359 (1978).

22. O. Jensrud and N. Ryum, *Mater. Sci. Engg.* **64**, 229 (1984).

23. T.H. Sanders Jr. and E.A. Starke, *Acta Metall.* **30**, 927 (1982).

24. J. Albrecht, A.W. Thompson and I.M. Bernstein, *Metall. Trans.* **10A**, 1758 (1979).

25. K. Rajan, W. Wallace and J.C. Beddoes, *J Mater. Sci.* **17**, 2817 (1982).

26. L. Christodoulou and H.M. Flower, *Acta metall.* **28**, 481 (1980).

27. G.M. Pressouyre, *Acta metall.* **28**, 895 (1980).

28. M. Talianker and B. Cina, *Metall. Trans.* **20A**, 2087 (1989).

29. B. Cina, *U S Patent 3856584* (December 1974).

30. R.E. Swanson, I.M. Bernstein and A.W. Thompson, *Scripta Met* **16**, 321 (1982).

31. N.C. Danh, K. Rajan and W. Wallace, *Metall Trans* **14A**, 1843 (1983).

32. J.K. Park and A.J. Ardell, *Metall Trans* **15A**, 1531 (1984).

33. A.K. Vasudevan, J. Liu and R.E. Ricker, *Proc. Int. Conf. Environmental Degradation of Engineering Materials*, April 1987, Pennsylvania State Univ, State College, USA, p.321 (1987).

34. A.K. Vasudevan and R.D. Doherty, *Acta Metall* **35**, 1193 (1987).

35. J.C. Huang and A.J. Ardell, *Acta Metall* **36**, 2995 (1988).

36. J.K. Park, *Mater Sci and Engg* **A103**, 223 (1988).

37. R.E. Ricker, J.L. Fink and A.K. Vasudevan, *Met TransA*, **22A**, 264 (1991).

38. P.D. Pitcher, R.J. Stewart, and S. Gupta, *Scripta Met*, **26**, 511 (1992).

39. C.P. Blankenshship, Jr. and E.A. Starke, Jr, *Met TransA*, **24A**, 833 (1993).

40. D.C. Slavik, C.P. Blankenship, Jr, E.A. Starke, Jr. and R.P. Gangloff, *Met.Trans*, **24A**, 1807 (1993).

41. C. Thakur and R. Balasubramaniam, *Metals Materials and Processes*, 1996 (in press).

42. R. Balasubramaniam, D.J. Duquette and K. Rajan, *Acta. metall. Mater.* **39**, 2607 (1991).

43. A.J. Jacobs, *Trans. ASM* **58**, 579 (1965).

44. A.J. Jacobs, *Metall. Progress* **5**, 80 (1966).

45. R.N. Parkins, *J.Metals* **44**, 12 (1992).

46. A.W. Thompson and I.M. Bernstein, *Metallurgical Treatises*, Ed. Tien J K and Elliott J F, TMS AIME, Warrendale, USA, p.589 (1981)

47. E.H. Dix Jr., *Trans ASM* **42**, 1057 (1950).

48. L. Chen, W. Chen, Z.Liu, Y. Shao and Z. Hu, *Metall. Trans*, **24A**, 1355 (1993).

49. J.P. Hirth and H.H. Johnson, Atomistic Fracrure, eds. R.M. Latanision and J.R. Picken, Plenum Press, New York, **5**, p.771 (1983).

50. R.J. Gest and A.R. Troiano, *Corrosion* **30**, 274 (1974).

51. T.F. Klimowicz and R.M. Latanision, *Metall. Trans*, **9A**, 597 (1978).

52. D.A. Hardwick, M. Taheri, A.W. Thompson and I.M. Bernstein, *Metall. Trans*, **13A**, 235 (1982).

53. R.E. Swanson, I.M. Bernstein and A.W. Thompson, *Scripta Metall.*, **16**, 321 (1982).

54. P.P. Pizzo, R.P. Galvin and H.G. nelson, Environment-Sensitive Fracture: Evaluation and Comparison of Test Methods, *ASTM STP 821*, p.173 (1984).

55. S.S. Kim, E.W. Lee and K.S. Shin, *Scripta Metall.*, **22**, 1831 (1988).

56. J.W. Watson, Y.Z. Shen and M. Meshii, *Metall. Trans*, **19A**, 2299 (1988).

57. G. Disson, M. Reboul and C. Fiaud, Aluminum-Lithium Alloys V (Conf. Proc.), Williamsburg, Virginia, USA, MCE Pub. Ltd. Birmingham, UK, p.1261 (1989).

58. A. Ravindra, R. Ambat and E.S. Dwarkadasa, *Proc. 2nd Int. Conf. on Aluminium INCAL91*, Bangalore, p.929 (1991).

59. A.Bandyopadhyay, R. Ambat and E.S. Dwarkadasa, *Bull. Mater. Sci.*, **15**, 311 (1992).

60. C. Thakur and R. Balasubramaniam, *Acta Metall.*, (1996) (communicated).

61. A.J. Bursle and E.N. Pugh, *Environment Sensitive Fracture of Engineering Materials, TMS AIME*, Warrendale, p.18 (1979).

62. A.W. Thompson, and I.M. Bernstein, *Advances in Corrsion Science and Technology,* (ed) *M G Fontana and R W Staechle, Plenum, New York* **7**, p.53 (1980).

63. A.W. Thompson, *Mater Sci Engg,* **43**, 41 (1980).

64. J.A.S. Green, H.W. Hayden, and W.G. Montagne, *Eeffect of Hydrogen on Behavior of Materials,* (ed) Thompson A W and Bernstein I M, *TMS-AIME New York*, p.345 (1976)

65. E.N. Pugh, *Mechanism of Environment Sensitive Cracking of Materials, The Metal Soc, London*, p.493 (1977).

66. G.M. Scamans, and C.D.S Tuck, *Mechanisms of Enviroment Sensitive Cracking of materials, The Metals Soc. London* p.482 (1977).

67. W. Gruhl, and D. Brungs, *Metall* **23**, 1020 (1969).

68. G.M. Scamans, R. Alani, and P.R. Swann, *Corrsion Sci* **16**, 443 (1976).

69. J.L. Nelson, *Met Trans* **6A**, 1459 (1975).

70. J.C. Scully, *Theory of SCC in Alloys, Nato, Brussels*, p.127 (1971).

71. L. Montgrain, and P.R. Swann, *Hydrogen in metals ASM, Metals Park*, p.575 (1974).

72. A.R. Troiano, *Trans ASM* **52**, 54 (1960).

73. J.C.M. Li, R.A. Oriani and L.S. Darken, *Z F Phys Chem* **49**, 271 (1966).

74. H.K. Birnbaum, *Environment Sensitive Fracture of Engg Materials AIME* New York, p.327 (1979).

75. M.O. Speidel and M.V. Hyatt, *Adv Corr Sci Tech*,(ed) M.G. Fontana and R.W. Staehle, Plenum Press, NY, USA, Volume 2. p.115 (1972).

76. R.C. Dorward and K.R. Hasse, *Corrosion* **43**, 409 (1987).

77. A.W. Thompson and I.M. Bernstein, *Reviews on Coatings and Corrosion* **2**, p.3 (1975).

78. M.O.Speidel, *Theory of stress corrosion cracking* (ed) J.C. Scully, Nato Brussels, p.289 (1971).

79. J.K. Tien, A.W. Thompson, I.M. Bernstein and R.J. Richards, *Met. Trans. A* **7A**, 821 (1976).

80. P. Niskanen, T.H. Sanders, M. Marek and J.G. Rinker, Al-Li Alloys ,ed. T.H. Sanders Jr. and E.A. Starke Jr., *TMS-AIME*, Warrendale, p.347 (1987).

81. E.I. Meletis, *Proc Conf Corrosion Cracking*, ed. V. Goel, p.315 (1985).

82. H.C. Rogers, *Trans Am Inst Min Engrs* **218**, 498 (1960).

83. M.R. Louthan Jr., *Corrosion Mechanisms*, ed. F. Mansfeld and Marcel Dekker, New York, USA, p.329 (1987).

84. W. Zhong, Y. Cai and D. Tomanck, *Nature* **362**, 435 (1993).

85. J.J. Moore, *Chemical Metallurgy*, Butterworths, London, p.305 (1981).

86. D.P. Hill, D.N. Williams, and C.E. Mobley, in Aluminium - Lithium II, eds. E.A. Starke Jr. and T.H. Sanders Jr., TMS, Warrendale, USA, p.201 (1983).

87. R.C. Dickenson, K.R. Lawless, and K. Wefers, Scripta Metall., **22**, 917 (1988).

88. R.C. Dickenson, K.R. Lawless and K. Wefers, Aluminium-Lithium V, Eds., T H Sanders Jr. and E A Starke Jr., MCE Publication, Oxford, England, p. 1337 (1989).

89. M.H. Tosten, A.K. Vasudevan and P.R. Howell, *Metall. Trans.* **19A** (1988) 51.

90. P. Sainfort and B. Dubost, in Aluminium-Lithium Alloys IV, Proceedings of the Fourth International Conference on Aluminium-Lithium Alloys, edited by G. Champier, B. Dubost, D. Miannay and L. Sabetay, *Journal De Physique*, Colloque C3,**48** (1987) p.407.

91. R.J. Rioja, P.E. Bretz, R.R. Sawtell, W.H. Hunt and E.A. Ludwiczak, in Aluminium-Lithium Alloys V, Proceedings of the Fifth International Conference on Aluminium-Lithium Alloys, Chameleon Press, London, p.1781 (1989).

92. W.A. Cassada, G.J. Shiflet and E.A. Starke Jr., in Aluminium-Lithium Alloys IV, Proceedings of the Fourth International Conference on Aluminium-Lithium Alloys, edited by G. Champier, B. Dubost, D. Miannay and L. Sabetay, *Journal De Physique*, Colloque C3,**48** p.397 (1987).

93. J. Glazer and J.W. Morris Jr., in Aluminium-Lithium Alloys III, Proceedings of the Third International Conference on Aluminium-Lithium Alloys, edited by C. Baker, S.J. Harris, B. Noble and C.J. Peel, Institute of Metals London, p.191.(1985).

94. M. Niinomi, K. Degau and T. Kobayashi, in Aluminium-Lithium Alloys IV, Proceedings of the Fourth International Conference on Aluminium-Lithium Alloys, edited by G. Champier, B. Dubost, D. Miannay and L. Sabetay, *Journal De Physique*, Colloque C3, **48** p.654 (1987).

95. H.M. Flower and P.J. Gregson, *Mater. Sci. Technol.* **3**, 81 (1987).

96. J.M. Silcock, *J. Inst. Metals* **88**, 357 (1959-60).

97. P. Sanfort and P. Guyot, in Aluminium-Lithium Alloys III, Proceedings of the Third International Conference on Aluminium-Lithium Alloys, edited by C. Baker, S.J. Harris, B. Noble and C.J. Peel, Institute of Metals London, p.420.(1985)

98. S. Suresh and A.K. Vasudevan, *Al-Li Alloys III*, Proceedings of 3rd International Conference on Aluminium-Lithium Alloys, Eds. C.A. Baker, P.J. Gragson, S.J. Haris and C.J. Peel, Institute of Metals, London, p.595 (1986).

99. J. Glazer, T.S. Edgecumbe and J.W. Morris Jr., in Aluminium-Lithium Alloys III, Proceedings of the Third International Conference on Aluminium-Lithium Alloys, edited by C. Baker, S.J. Harris, B. Noble and C.J. Peel, Institute of Metals London, p.369 (1985).

100. D. Venadles, L. Christodoulou and J.R. Pickens, *Scripta Metall.* **17**, 1263 (1983).

101. M. Tatmura, T.Mori and T.Nakamura, *J. Japan Inst. Metals* **34**, 919 (1970).

102. J.C. Huang and A.J. Ardell, in Aluminium-Lithium Alloys III, Proceedings of the Third International Conference on Aluminium-Lithium Alloys, edited by C. Baker, S.J. Harris, B. Noble and C.J. Peel, Institute of Metals London, p.455 (1985).

103. P. Meyer, Y. Cans, D. Ferton and M. Reboul, in Aluminium-Lithium Alloys IV, Proceedings of the Fourth International Conference on Aluminium-Lithium Alloys, edited by G. Champier, B. Dubost, D. Miannay and L. Sabetay, *Journal De Physique*, Colloque C3,**48** p. 131 (1987).

104. D.B. Williams and J.W.Edington, *Metals Sci.* **9**, 529 (1975).

105. D.B. Williams, in *Al-Li Alloys, Proceedings* of First *Int. Conf. on Al.-Li Alloys, eds.* T.H. Sanders Jr., E.A. Starke Jr., TMS AIME, Warrendale, PA, p.89 (1981).

106. K.K. Soni, D.B. Williams, D.E. Newbury, G. Gillen, P. Chi and D.S. Bright, *Metall. Trans.* **24**, 2279 (1993).

107. M.S. Udyavar and E.S. Dwarkadasa, *J. Mater. Sci. Letters* **11**, 490 (1992).

108. M. Ahmad, *Metall. Trans.* **18A**, 681 (1987).

109. J.M. Papazian, *Metall. Trans.* **17A**, 635 (1986).

110. D. Brock and C.W. Balls, *J. Inst. Metals* **99**, 255 (1971).

111. F.W. gayle, N.F. Levoi and J.B. Vadersale, *J. of Metals* **39** No.5 33 (1987).

112. J.M. Papazian, *NASC Report* RE-627, Grumman Aerospace Corp. Bethpage, New York, April 1981.

113. J.D. Kim and J.K. Park, *Metall. Trans.* **24A**, 2613 (1993).

114. B.P. Gu, G.L. Liedl, T.H. Sanders,JR and K. Welpman, *Mater.Sci. and Engg* **76**, 147 (1985).

115. B.P. Gu, K. Mahalingam, G.L. Liedl and T.H. Sanders,Jr, in Aluminium- Lithium Alloys III, Proceedings of the Third International Conference on Aluminium-Lithium Alloys, edited by C. Baker, S.J. Harris, B. Noble and C.J. Peel, Institute of Metals London, (1985) p.360.

116. W.S. Timson, M.H. Tosten, P.R. Howell and D.B. Williams, in Aluminium- Lithium Alloys III, Proceedings of the Third International Conference on Aluminium-Lithium Alloys, edited by C. Baker, S.J. Harris, B. Noble and C.J. Peel, Institute of Metals London, (1985) p.386.

117. F.W. Gayle and J.B. Vandersande, in Aluminium-Lithium Alloys III, Proceedings of the Third International Conference on Aluminium-Lithium Alloys, edited by C. Baker, S.J. Harris, B. Noble and C.J. Peel, Institute of Metals London, p.376 (1985).

118. W. Muller, E. Bubeck and V. Gerold, in Aluminium-Lithium Alloys III, Proceedings of the Third International Conference on Aluminium- Lithium Alloys, edited by C. Baker, S.J. Harris, B. Noble and C.J. Peel, Institute of Metals London, p.435 (1985).

119. T.S. Srivatsan and T.A. Place, *J.Mater.Sci.* **24**, 1543 (1989).

120. E.J. Lavernia, T.S. Srivatsan and F.A. Mohamed, *J. Mater. Sci.* **25**, 1137 (1990).

121. E.I. Meletis, J.M. Sater and T.H. Sanders, Jr., in ***Al Alloys: Physical and Mechanical Properties***, p. 1157. Univ. of Virginia, Charlottesville, USA (1986).

122. E. I. Meletis, *Mater. Sci. Engg.* **93**, 235 (1987).

123. R.C. Dorward and K.R. Hasse, *Corrosion* **44**, 932 (1988).

124. A.K. Vasudevan, P.R. Ziman, S.C. Jha and T.H. Sanders, Jr., in Aluminium-Lithium III, Eds., C Baker C, P.J. Gregson, S.J. Harris, and C.J. Peel, p.303. The Institute of Metals, London (1985).

125. J. B. Lumsden and A. T. Allen, *Corrosion* **44**, 527 (1988).

126. Z. Wang, Z. Zhu, W. Ke, Y. Zhang and Z Hu, *Acta metall.* **58**, 391 (1992).

127. P. Niskanen, T.H. Sanders, M. Marek and J.G. Rinker, *Corr. Sci.* **22**, 283 (1982).

128. J.G. Rinker, M. Marek and T.H. Sanders, Jr., in Aluminium-Lithium II, Eds. T.H. Sanders Jr. and E.A. Starke Jr., p. 597 TMS, Warrendale, USA (1983).

129. G.S. Chen and D.J. Duquette, *Metall. Trans.* **23A**, 1551 (1992).

130. P.N. Anyalebechi, D.E.J. Talbot and D.A. Granger, in *Proc. Conf. on Light Metals,* p.1025. Louisiana, USA (1991).

131. H. Saito, Y. Ishida and H. Yoshida, in Aluminium-Lithium IV, Eds., G. Champier, B. Dubost, D. Miannay and L. Sabetay, J. de Physique Colloque, **48**, C3-535 (1987).

132. C. Thakur and R. Balasubramaniam, *J. Mat. Sci. Lett.* (1996), communicated.

133. C. Thakur and R. Balasubramaniam, *Scripta mater.* (1996) communicated.

134. W. Eichenauer and A. Pebler, *Z. Metallk.* **48**(1957)373.

135. W. Eichenauer, K. Hattenbach and A. Pebler, *Z. Metallk.* **52**, 682 (1961).

136. M. Ichimura, M. Imabayashi AND M. Hayakawa, *J. Japan Inst. Metals* **44**, 1053 (1980).

137. K. Papp and E. Kovacs-Cseteny, *Scripta Metall.* **15**, 161 (1981).

138. T. Ishikawa and R.B. McLellan, *Acta Metall* **34**(6), 1091 (1986).

139. M. Nakashima, M. Saeki, Y. Aratono and E. Tachikawa, *J. Nuclear Mater.* **116**, 141 (1983).

140. T. Hayashi, K. Okuno and H. Kudo, *J.Less-Common Metals* **141**, 169 (1988).

141. T.K. Roy, R. Balasubramaniam and A Ghosh, *Scripta Metall. Mater.*, (in press).

142. R. Balasubramaniam and D.J. Duquette, in Aluminium-Lithium VI, Eds., M. Peters and P.J. Winkler, DGM Information, Oberursel, Germany, 767 (1992)..

143. F. Bernard, A. Elbouri, E. Sciora and N. Gerard, J. Alloy Compd. **177**, 245 (1991).

144. D. Tromans, Scripta Metall. Mater., **27**, 217 (1992).

145. W.E. Garner and E.W. Haycock, Proc. Roy. Soc., **A211**, 335 (1952).

146. R. Ehrlich, A.R. Young, G. Rice, J. Drovak, P. Shapiro and H.E. Smith, J. Am. Chem. Soc., **88**, 858 (1966).

147. V.I. Mikheeva and S.M. Arkhipov, Russ. J. Inorg. Chem. **12**, 1066 (1967).

148. J.A. Dilts and E.C. Ashby, Inorg. Chem. , **11**, 1230 (1972).

149. Yu.N. Shevechenko, N.N. Mal'tseva, V.A. Nazarenko, A.I. Golovanova and N.T. Kuzentsov, Dokl Akad Nauk USSR **296**, 362 (1987).

APPENDIX A

POLARIZATION BEHAVIOR OF Al-Li ALLOYS IN NaOH

Abstract

The nature of surface films that form under free corrosion conditions and their effect on the subsequent polarization behavior of an Al-1.90Li-1.80Cu-1.00Mg-0.09Zr alloy in 0.1 mol/l NaOH solution at 35°C has been studied. The variation of the free corrosion potential (FCP) as a function of time is characteristic for the alloy in the electrolyte. It initially changes in the noble direction with time when the specimen surface becomes totally enveloped by a black coating and later, the black coating is punctured at some localized regions and the FCP shifts towards the active direction and stabilizes at an active value of -1450 mV vs SCE. XRD analysis of the surface film layer deposited over the specimen indicates that it consists of essentially lithium aluminum hydroxide at short immersion times, and lithium aluminium hydroxide and copper hydroxide after long immersion in the electrolyte. The nature of the scale morphology has been studied by scanning electron microscopy. The presence of Cu in the scale results in enhanced passivity behavior (i.e. lower primary and complete passivation potentials and lower critical and passive current densities) during polarization measurements. It was also observed that the hydride $LiAlH_4$ forms in the surface regions of the alloy under free corrosion conditions.

The effect of electrolyte temperature on the polarization characteristics of the Al-Li alloy has also been studied.The electrolyte temperature was the equilibrium temperature established due to the prevailing weather conditions at different times in the year. The alloy exhibited active-passive behavior at all the temperatures. The zero current potential and the free corrosion potential were nobler with decreasing temperature. The corrosion current density, the critical current density and passive current density increased with temperature indicating the activated nature of the electrochemical process. The passive range was higher at 35°C compared to the other temperatures. The temperature effect on the polarization behavior has been also been explained by considering the dissolved oxygen concentration in the electrolyte at different temperatures.

Introduction

Rising energy costs and the advent of tough composites have stimulated the development of advanced aluminum-lithium alloys for aircraft applications. The attractive combination of weight saving benefits and increased stiffness of Al-Li alloys has generated interest in these alloys[1,2]. The substitution of Al-Li alloys in place of conventional 7XXX series Al alloys in aircraft components would entail a saving of 8 to 10 percent of the structural weight along with an increase of 15 percent in the elastic modulus, therefore providing an extra margin of safety for critical aerospace applications.

In addition to fuel efficiency, aircraft structures are also required to be corrosion resistant for safe and long service life. In this regard, several studies have shown that Al-Li alloys are susceptible to environmental degradation[3-7]. The influence of Li additions on the corrosion properties of Al alloys is of interest. The presence of active element Li has rendered these alloys different in corrosion behavior from conventional Al alloys. They have been observed to be more susceptible to corrosion by Niskanen *et al.*[8,9] and Ricker *et al.*[10]. Moreover, lithium bearing precipitates in Al-Li alloys interact with hydrogen and hence render the mechanism of hydrogen embrittlement (HE) complex in nature. In a detailed study of HE of aged and retrogressed-reaged Al-Li-Cu-Mg alloys, tensile specimens were precharged with hydrogen by electrochemical means at constant cathodic current density in an alkaline solution of 0.1M NaOH[11]. Similarly, S.S. Kim *et al.*[12] and L. Chen *et al.*[13] have also used the same

electrolyte for hydrogen pre-charging. That the specimen surface turns black in color after cathodic hydrogen charging was observed by several investigators [7,14]. In addition, the phase transformations that occur in the near surface zone of the Al-Li alloys has been also been characterized by X-ray diffraction analysis[15]. The permeation of hydrogen into the alloys depends on surface film characteristics. Finally, it has been experimentally observed in the case of Al-Li-Cu-Mg alloys that the pH of electrolyte within pits is alkaline in nature, in contrast to acidic pit environment in the case of conventional Al alloys[16]. Pits act as initiation sites for environment induced cracking (EIC) of Al-Li alloys[17] and therefore, the surface film formation characteristics under alkaline conditions are also important in understanding the environmental degradation of Al-Li alloys by EIC. A thorough search of the literature revealed that polarization studies have not been conducted in pure NaOH solution as most of the investigators have used 3.5% NaCl electrolyte[16-25]. Hence, there was a need to understand the film forming characteristics under open circuit, potentiodynamic and cathodic hydrogen charging conditions. In the present study, the corrosion behavior of Al-Li-Cu-Mg alloys has been studied in alkaline solution of 0.1M NaOH using potentiodynamic polarization technique and the surface film formed under free corrosion and polarization conditions was characterized by X-ray diffraction (XRD) and scanning electron microscopy (SEM). Moreover, the effect of ambient temperature on the polarization characteristics were also studied.

Experimental Procedure

The Al-Li alloy (designated as 1441) used in the present study were supplied by the Defense Metallurgical Research Laboratory, Hyderabad. The composition of the 1441 alloy was 1.90% Li, 1.80% Cu, 1.00% Mg, 0.09% Zr and balance Al. Incidentally, the film formation characteristics and polarization behavior on another Al-Li alloy of composition Al-2.30Li-1.24Cu-0.80Mg-0.12Zr (designated as 1440) was also studied and as its behavior was similar to that reported in this communication for the 1441 alloy, the 1440 alloy is not discussed in this communication. Peak aged (aged at 170^{o}C for 18h) coupons of 1 cm^{2} cross-sectional area were sectioned from the sheet and later all the surfaces were ground to 600 grit surface finish. Specimen coupons were connected with a conductive wire and this assembly was mounted in a cold setting epoxy. Specimen surfaces were polished to 1 micron surface finish and were thoroughly cleaned with acetone prior to each polarization experiment. Polarization experiments were performed in a one litre electrochemical cell controlled by a potentiostat interfaced with a personal computer. A platinum foil of 1 cm^{2} area was used as counter electrode. A 0.1 mol/l NaOH solution of pH=13 was the electrolyte used in the present study as this was the solution in which cathodic hydrogen precharging was conducted for HE studies[11]. In the case of polarization studies for understanding film characteristics, the temperature of the electrolyte was that of the ambient temperature (35^{o}C). The free corrosion potential was monitored continuously immediately from the time of immersion, versus saturated calomel electrode (SCE).

Before the start of each polarization experiment, the specimen was allowed to attain a stable potential. The data of potential versus time was obtained. After having obtained the steady free corrosion potential, the potential was scanned at the rate of 1mV/sec from -1800 mV to +1800 mV followed by reverse scan from +1800 mV to -1400 mV. X-ray diffraction (XRD) patterns were obtained before (for reference purposes) and after immersion for different times (2h, 15h and 7 days) in the NaOH electrolyte in a Rich Seifert X-Ray Diffractometer 2002 using Cu K_{α} radiation. In some experiments, XRD patterns were also obtained after removing the surface scale by mechanical polishing with fine emery paper.In all the XRD experiments, the intensity of scaling, recorder chart speed, and sample rotation rate were maintained constant. Square (one cm on the side) specimen coupons were used for this purpose. After the XRD patterns were obtained from the surface of the above specimens, the microstructural features of the surface film were observed in a JEOL 840A scanning electron microscope. Electrical charging of the the surface film during observation in the SEM was avoided by coating the film with a thin Ag layer by sputtering prior to insertion in the SEM.

Surface Film Formation Characteristics

Free Corrosion Potential vs Time:

The nature of variation of free corrosion potential (FCP) with time of immersion in the alkaline solution is presented in Figure A.1 for the alloy 1441. It is seen that the FCP stabilizes only after a fairly long time (about 6 hours). The FCP is at a

very active value immediately upon immersion (-1550 mV) and then rapidly rises in initial period to about -1400 mV. This initial steep rise is due to ohmic drop and charging of the double layer next to the surface[26]. The potential continues to rise even after this value is reached but the rate of increase is much slower. The free corrosion potential reaches its maximum value (-1250 mV) after approximately 5 hours. The following observations were made visually as regards the nature of the surface of the specimen after immersion in the electrolyte. The specimen surface was very clean and appeared bright before immersion. With increasing immersion time, the surface appeared tarnished and acquired a black layer on the surface. This black layer completely covered the surface and it was tenacious. The black layer coverage was stable (i.e. did not show any ruptures) till the maximum in the FCP was obtained. Then, an interesting feature was observed in all the experiments. The black layer was punctured at a few locations which appeared as pin-holes and vigorous bubble evolution was observed to take place from these ruptured locations. When such a state was observed on the surface, the free corrosion potential decreased rapidly until it reached a value of about -1450 mV. The number of ruptured pin-holes (or localized reaction sites), interestingly, still remained the same while the potential fell rapidly towards active potentials. After the fall of potential, the free corrosion potential stabilized and remained the same even for long immersion (>14 hours). The number of pits still remained the same when the free corrosion potential stabilized and bubble evolution was observed from these localized rupture sites.

Moreover, it was observed that the color of the film had turned greenish or greenish-yellow after attaining the stable FCP. It is important to note that this behavior was observed in a number of independent experiments. Interestingly, Craig *et al* [16] in their study of the local chemistry of pits in Al-Li-Cu-Mg alloys observed that after a long time of immersion, the pits were packed with greenish hydrous deposits with both metallic Cu and oxidized copper particles in and around the pits. In summary, the free corrosion potential did not stabilize immediately after immersion but exhibited a characteristic behavior described above. Interestingly, it was earlier observed by Colvin *et al.*[27] that a ternary Al-Li-Ge alloy took fairly long times (18-36 hrs) for stabilization in deaerated 3.5% NaCl solution. Apart from this reference source, there has been no mention of the nature of the stabilization of the free corrosion potential of Al-Li alloys as most of the investigators have stated that the free corrosion potentials stabilized in fairly short times in NaCl solutions[16-25].

Potentiodynamic Polarization:

In order to understand the effect of the surface film on the corrosion behavior of the alloy, potentiodynamic polarization experiments were conducted at the following two conditions: when the FCP attained a value of (a) -1300 mV after 2 hours immersion and (b) -1450 mV after 14 hours immersion. The polarization curves for these two conditions are presented in Figures A.2 and A.3, respectively. In both the cases, the polarization scan was begun

from an active potential of -1800 mV and scanned in the noble direction upto +1800 mV, at a constant scan rate of 1 mV/sec. In some experiments, the scanning direction was reversed after the noble potential of +1800 mV was reached and the potential scanned in the active direction. The potentiodynamic polarization curves for the two conditions exhibited active-passive behavior and these did reveal some changes. Interestingly, the nature of curve was similar for the other Al-Li alloy studied and also in different heat treatment conditions (i.e. underaged, peakaged and overaged). This implies that the polarization behavior did not depend upon the composition of the Al-Li-Cu-Mg alloys and also did not depend upon the heat treatment condition.

Table A.1 presents the various parameters obtained from the polarization curves for the specimens after 2 and 15 hour immersion, when the free corrosion potential was -1300 and -1450 mV, respectively. The zero current potential in the forward scan (ZCP_f) was nobler for condition (a). However, the potentials for primary passivation and complete passivation for condition (a) were active compared to condition (b), thereby implying the enhanced passive behavior of the specimen immersed in the solution for 15 hrs, which is also reflected by the nature of the polarization curves obtained for the two conditions (Figures A.2 and A.3). The enhanced passivity is also observed in the lower critical (i_{crit}) and passive (i_{pass}) current densities obtained for condition (b) compared to condition (a) (Table A.1). Incidentally, the i_{crit} and i_{pass} are comparable to that obtained by Ambat and Dwarakadasa for a number of Al-Li alloys in alkaline

pH[16]. Upon further increasing the potential, the current density does not vary with the potential and this is indicative of the passive region. The passive film is stable up to the breakdown potential after which the specimen pits at a few localized locations. The breakdown potentials for the condition (a) is higher than that for condition (b). Ambat and Dwarakadasa[16] have observed that the breakdown potential of several Al-Li alloys to be about -500 mV in alkaline pH=12 NaCl solution and this is understandable as the presence of chloride ions leads to earlier destabilization of passive films on the surface of Al[28]. Moreover, the passive range obtained for the specimen immersed in the solution for 15 hours is comparable to that obtained for the specimen immersed in the solution for 2 hours although the i_{crit} is higher for the later. Upon reversal of scan after reaching +1800 mV, it is seen that the reverse scan closely follows the path of the forward scan, thereby indicating the good re-passivation behavior of these alloys in the alkaline pH.

The reverse scan intersects the forward scan and zero current potential is obtained at the potential ZCP_b. On reversal of scan, it was observed that the ZCP is obtained at a much more noble potential compared to the ZCP on the forward scan. This can be explained by the fact that corrosion occurring under free corrosion conditions and in the transpassive region (during polarization) causes the surface to be enriched with Cu due to dealloying of Al and Li[22]. The specimen that had been immersed for 15 hours appears to have a higher amount of enriched Cu on the surface which may probably be due longer immersion at the free

corrosion potential rather than occurring during polarization as it observed that the specimen immersed for 2 hours has a lower amount of surface Cu enrichment (reflected by its active ZCP_b) although it corrodes faster according to the polarization characteristics (Table A.1). The enrichment of Cu on the film for longer immersion times has been observed by SEM and this is discussed later. Moreover, Craig *et al*[16] have also observed Cu enrichment on the surface of Al-Li-Cu-Mg alloys exposed to alkaline environments. Therefore, during the return scan, the exchange current density for hydrogen reduction reaction is increased due to the surface being richer in Cu because the exchange current density for hydrogen evolution reaction is higher on Cu than on Al[29]. Therefore, the zero current potential is shifted to positive potentials. A similar explanation was evoked by Buchheit and Stoner[22] to explain the cyclic polarization behavior of Al_2CuLi in NaCl solution.

Characterization of surface film:

Figures A.4(a) and (b) present the XRD patterns for 1441 PA samples immersed for 0 and 7 days in NaOH solution at 25°C. The extra peaks observed in Figure A.4(b) were compared with the theoretical peaks of the hydrides, oxides and hydroxides of Al, Li, Cu and Mg. The extra peaks matched with the reported peaks of $Cu(OH)_2$ and $LiAl_2(OH)_7\ 12H_2O$ and the peaks in Figure A.4(b) have been indexed accordingly. It has been hypothesized that the black film that forms under cathodic charging conditions is $Al(OH)_3$+LiOH[23] and the present study reveals the exact nature of

the scale. It has been reported that the color of the $Cu(OH)_2$ is bluish green in color. The bluish green color of the powder from surface film layer indirectly confirms the presence of copper hydroxide in the film. A greenish surface deposit in the pits of Al-Li-Cu-Mg alloys was also reported by Craig *et al* [16]. It was also noticed that the intensities of the peaks from the $Cu(OH)_2$ phase is higher after the 15 hour immersion than after the 2 hour immersion. XRD patterns obtained from the surface of the alloy after cathodic hydrogen charging at 10 mA/cm^2 also revealed the presence of these two phases. Interestingly, some of the peaks obtained corresponded to that of the hydride phase $LiAlH_4$. In most of the polarization experiments conducted, it was noticed that as soon as the cathodic polarization was begun, severe hydrogen evolution was observed over the green-filmed specimen surface. As the potential approached the ZCP, the green layer generally peeled off from certain locations on the surface. As the potential was scanned beyond the ZCP into the anodic polarization region, the color of the specimen further changed to dark green and remained the same till the end of the experiment. The green layer that had peeled off from the specimen during the polarization experiment was carefully filtered out from the test electrolyte, dried and analyzed by XRD. The analysis of the film revealed that it essentially consisted of $Cu(OH)_2$ and $LiAl_2(OH)_7$ $12H_2O$ as observed earlier for the scales formed under immersion conditions. In order to understand the presence of $LiAlH_4$, the surface film that had formed under immersion condition was removed by careful mechanical polishing with fine emery paper so that the surface

again appeared bright and shiny. Care was taken to remove all the film from the surface. XRD patterns were obtained from the cleaned specimens and one such pattern obtained from the clean surface of the specimen immersed for 7 days is provided in Figure A.4(c). The interesting feature that was revealed was that the maximum intensity peak of the $LiAlH_4$ phase can be seen, thus indicating that this hydride forms under free corrosion conditions in Al-Li alloys. The presence of this hydride phase was also noticed in the 2h and 15h immersion specimens after their surface films had been removed; however, the intensity of the peak was much weaker compared to the present case. The presence of this phase in Al-Li alloys after cathodic hydrogen charging has earlier been confirmed by transmission electron microscopy[30] (in the presence of stress) and by XRD[31] (in the absence of stress). The present study further reveals that this hydride can also form under free corrosion conditions and this is due to the availability of hydrogen resulting from the reduction reactions that occur on the specimen surface during immersion in the electrolyte. An interesting observation that was made in connection with hydrogen evolution was that when few shavings of the Al-Li alloy were placed in the NaOH electrolyte kept in a petri dish, the shavings were observed to move on their own due to buoyancy created by vigorous hydrogen evolution. The present identification of the hydride under free corrosion condition is an important result as regards EIC of Al-Li alloys as the presence of hydrides in the near-surface regions of the alloys would have deleterious consequences as they would act as potential crack initiation sites during EIC[17].

The samples that were immersed for 2h, 15h and 7d were observed on the scanning electron microscope after the XRD experiment was performed in order to understand the topology and nature of the film formed on their surfaces. The sample that had been immersed for 2 hours revealed the presence of islands of the film on the surface (Figures A.5a and A.5b). Moreover, the islands appeared as faceted implying that they grew on the surfaces with some orientation relation with the substrate. The relatively thick scale did not appear to have covered the entire surface of the specimen and therefore the higher values of i_{crit} were observed in the polarization experiment for this condition. The composition of the scale was analyzed by the energy dispersive analysis by x-rays (EDAX) facility of the SEM and it consisted essentially of Al. On the other hand, the specimen that had been immersed for 15 hours revealed that the surface film completely covered the surface and that there appeared two types of films on the surface: continuous, large grained and fine grained (Figure A.6a and A.6b). Moreover, the film had ruptured in some places as can be seen from Figure A.6. The areas from the film that appeared dark were continuous and spot analysis obtained by EDAX revealed that it consisted essentially of Al and Mg with trace amounts of Cu. In contrast, the fine grained portion of the film revealed that Cu was also significantly present in addition to Al and Mg in the scale. The surface film on the 7 day immersion specimen was uniform all throughout the surface (Figure A.7a). The grain size of the film was coarser in this case compared to the earlier cases and moreover, the scales appeared to have cracked from the center of

the grains (Figure A.7b). The scale consisted essentially of Al and Cu, as analyzed by EDAX. It must be mentioned that EDAX cannot indicate the presence of Li as it can only analyze elements beyond atomic number 6. However, the presence of Li in the scale as hydrated lithium aluminum hydroxide can be concluded as the XRD analysis clearly provided the composition of the scale.

The results of the SEM and XRD studies can be explained as follows. Intitally the composition of the scale formed on the surface is rich in Al and Li and this is mostly due to the formation of the $LiAl_2(OH)_7$ $12H_2O$ phase due to the dissolution of Al and Li from the surface. Lithium has been shown to be incorporated in the oxide film of Al-Li alloys [25,31]. The source of Li enhancement in the film is the leaching out of Li from the alloys and, under suitable condition, it becomes incorporated in the film[25,31]. The enrichment has also been experimentally verified by testing in Li containing solution and characterizing the passive film by secondary ion mass spectroscopy[25]. Moreover, the oxides of Al are generally grey in color and this compares well with the observation that the initial scale formed on the surface is greyish in color. With increasing time, the scale is enriched in Cu and this could either happen by Cu getting corroded out of the specimen or by the re-precipitation of Cu that was dissolved initially from the alloy onto the surface. In this regard, dealloying of Cu from Al-Li-Cu alloys has been observed[22]. It has been suggested that dissolved Cu ions are transported from dissolution sites and re-deposited on the surface where they can be favorably reduced[22]. Therefore, the visual

greenish appearance of the scale only after long periods of immersion reveals that this process seems to be likely occurring for the present Al-Li alloy. Moreover, this is also in conformity with the findings of green deposits in the pits of Al-Li alloys by Craig *et al* [16].

Effect of Electrolyte Temperature

It was observed that the nature of the polarization curve depended upon the season in which the experiments were conducted, i.e. it was different when the experiments were conducted in winter and when conducted in summer. The polarization curves were themselves highly reproducible in any particular season. The only difference in the experiments conducted during these times was the ambient temperature ($15^{o}C$' in the winter and $35^{o}C$ in the summer). The electrolyte's temperature was similar to that of the ambient temperature. Therefore, this was the main variable in the experiments conducted in the different seasons. The effect of this variable on the polarization characteristics is addressed below.

Potentiodynamic polarization experiments were performed at different seasons when the temperature of the electrolyte was $15^{o}C$, $25^{o}C$ and $35^{o}C$. The temperature of the electrolyte used in the polarization cell was not controlled and therefore it was allowed to equilibrate with the ambient temperature of the environment. In all the cases, the polarization scan was begun from an active potential of -1800 V and scanned in the noble direction upto +1800 mV, at a constant scan rate of 1 mV/sec. The scanning direction was reversed after the noble potential of +1800

mV was attained and the potential scanned in the active direction. The potentiodynamic polarization curves for the 1441 alloy in 0.1 mol/l NaOH at temperatures of 15°C and 35°C are provided in Figures A.8 and A.9, respectively. In these above two figures and Figure A.3 (for temperature 25°C), it can be noticed from the forward polarization scan that the alloy exhibited active-passive behavior in this electrolyte at all the temperatures. On reversing the scan, the polarization scan nearly traces the original forward polarization curve and this is indicative of the good re-passivation nature of the alloy in this electrolyte.The behavior of the 1440 alloy was similar and therefore its polarization curves are not being reported here. Interestingly, the nature of polarization curve was also similar in different heat treatment conditions' (i.e. underaged, peakaged and overaged) of the alloys and very minor variations were observed in the parameters of the polarization curve for the different ageing conditions.

Table A.2 presents the various parameters obtained from the polarization curves for the 1441 alloy in electrolytes at temperatures of 15°C, 25°C and 35°C. The zero current potential during the forward scan (ZCP_f) and the stabilized FCPs become active with increasing solution temperature. The primary passivation potential (E_{pp}) and the complete passivation potential (E_{cp}) are similar at the different temperatures. The critical current density (i_{crit}) and the passive current density (i_{pass}) increases with increasing solution temperature, indicating that the corrosion process is an activated phenomenon. Moreover, the

corrosion current density (i_{corr}), estimated by Tafel extrapolation in the active region, increases with increasing solution temperature (Table A.2). Incidentally, this is the normal effect of temperature on these parameters of the anodic polarization curve of an active-passive metal (Jones 1990). The order of i_{crit} and i_{corr} are comparable to the the critical current density and corrosion rate obtained by Ambat and Dwarakadasa[18] for a number of Al-Li alloys in alkaline pH. The passive range is similar at 15°C and 25°C, but lower than the range at 35°C. Ambat and Dwarakadasa[18] have observed that the breakdown potential of several Al-Li alloys to be about -500 mV in alkaline pH=12 NaCl solution and this is lower than the breakdown potentials obtained in this study as the presence of chloride ions leads to easier destabilization of passive films on the surface of Al-Li alloys[28]. On reversing the scan, the ZCP_b is nobler in the case of the solution at 15°C than in the case of the solution at 25°C. In the case of the solution maintained at 35°C, the ZCP_b was not attained as the scanning was stopped at -1000 mV due to memory limitations of the potentiostat, but nevertheless it must be at a more active value than for the other two cases.

The change in the parameters of the potentiodynamic polarization curves obtained in the solution of different temperatures can be explained by considering the activated nature of the corrosion process, as it was observed that i_{corr}, i_{crit} and i_{pass} increase with increasing temperature. Moreover, the dissolved oxygen content, which depends upon the temperature of the electrolyte, could also affect the polarization behavior. It

is well known that the polarization behavior of Al is influenced by the oxygen content in the electrolyte[33,34]. The solution at a higher temperature contains a lower amount of dissolved oxygen than the solution at the lower temperature. For example, the oxygen concentration in fresh water or water of low salinity is 11.3 ppm at $10^{o}C$ and 6.5 ppm at $40^{o}C$[35]. The effect of oxygen content is also reflected by the observation that the i_{crit} for passivation is lower with increasing oxygen concentration in the solution thereby implying the easy formation and establishment of passivity (by the formation of a hydrated oxide) on the surface of the alloy immersed in a solution with higher dissolved oxygen concentration. Moreover, the stabilized free corrosion potential and ZCP_f are nobler with increasing oxygen concentration in the solution (Table A.2). Ricker and Duquette[10] have found that the aeration of solution reduced the passive current density and increased the ZCP of Al-Li-Mg alloys. Moreover, Tsao and Pizzo[36] studied the effect of oxygen content (between 0.5 and 15 ppm) on the polarization behavior of several Al-Li-Cu alloys and showed that the ZCP shifts to noble values with increasing oxygen concentration with E_{pp} remaining essentially unaffected. The results of the present study (Table A.2) are in conformity with these earlier studies. The shift in the ZCP as a function of aeration has been explained by Pourbaix[33] by the mixed potential theory. It was earlier noted that the stabilized free corrosion potentials obtain only after long period of immersion in the electrolyte. One of the characteristic features when the corrosion potential had stabilized was that there were thin ruptures on the

surface film from which vigorous hydrogen evolution took place. It is reasonable to assume that the presence of oxygen in higher amounts in the electrolyte would result in a lower amount of rupturing thereby stabilizing the potentials at a nobler value.

The nature of the curves obtained can be explained by the mixed potential theory. The cathodic polarization curve (due to oxygen reduction and/or hydrogen reduction) intersects the anodic polarization in the active region and therefore, the specimen is in a state of active corrosion on immersion in the electrolyte. On reversal of scan, it was observed that the ZCP_b is obtained at much a more noble potential compared to the ZCP_f obtained during the forward scan. This can be explained by the fact that corrosion occurring during the forward scan causes the surface to be enriched with Cu due to dealloying of Al and Li[22] and during the return scan the exchange current density for hydrogen reduction reaction is increased due to the surface being richer in Cu and also due to the fact that the exchange current density for hydrogen evolution reaction is higher on Cu than on Al[29]. Therefore, the ZCP_b is shifted to positive potentials. It is interesting to note that a similar explanation has been provided by Buchheit and Stoner[22] to explain the shift of ZCP on reverse scan for Al_2CuLi in NaCl solution. Incidentally, the enrichment of Cu on the surface film formed on the Al-Li alloy used in the present study under free corrosion conditions has been experimentally verified by x-ray diffraction analysis and scanning electron microscopy. The amount of Cu, present as $Cu(OH)_2$, on the surface was minimal at small times of immersion and it became

significant with increasing time of immersion. Moreover, it was visually observed that the film on the surface of the Al-Li alloy turned greenish in color after stabilization of free corrosion potential and greenish-yellow after polarizing the specimen past the passive region during the forward polarization scan. The color change is indicative of Cu enrichment as copper compounds are generally green in color. Craig *et al*[16] in their study of local chemistry of pits in Al-Li-Cu-Mg alloys noticed that the solution in the pits became alkaline, unlike conventional Al alloys, and also that under these conditions the pits were packed with a greenish hydrous material with both metallic copper and oxidized copper particles in and around the pits. Therefore, Cu enrichment occurs on the surface of Al-Li-Cu-Mg alloys exposed to alkaline environments and the shift in the ZCP_b in the active direction during reverse polarization can be explained. The shift is more pronounced when the electrolyte temperatures are lower and this implies that the amount of Cu ennoblement on the surface is higher in this case, thereby resulting in nobler ZCP on reversal of scan. This would at first sight appear anomalous since the corrosion rate in the active state is higher at higher temperatures (Table A.2). However, this can be resolved by noticing Figures A.3, A.8 and A.9 that the alloy remains in the transpassive state for a longer time during the polarization scan at the lower temperatures due to the lower breakdown potentials in these cases compared to that at $35^{o}C$. The surface ennoblement of Cu arises due to this reason.

References

1. K.K. Sankaran, N.J Grant *Mater.Sci.Engg.* 44 (1980):p. 213
2. E.J. Lavernia, T.S. Srivatsan, F.A. Mahamed, *J. Mater. Sci.* 25 (1990):p. 1137
3. L. Christodoulou, L. Struble and J.R. Pickens, in Aluminium-Lithium II, ed. T.H. Sanders Jr., E.A. Starke Jr. (Warrendale,PA:TMS, 1983), p. 561
4. N.J.H. Holroyd, A. Gray, G.M. Scamans, R. Hermann, in Aluminium-Lithium III, ed. C Baker C, P.J. Gregson, S.J. Harris, C.J. Peel (London:The Institute of Metals, 1985), p. 310.
5. F. Binsfeld, M. Habashi, J. Galland, J.P. Fidelle, D. Miannay, P. Rofidal in Aluminium-Lithium IV, ed. G. Champier, B. Dubost, D. Miannay, L. Sabetay, J. de Physique Colloque, 48 (1987):p. C3-587
6. Z.F. Wang, Z.Y. Zhu, Y. Zhang, W Ke, *Metall. Trans.* 23A (1992):p. 3337
7. E.I. Meletis, W. Huang, in Aluminium-Lithium V, ed. T H Sanders Jr., E A Starke Jr.(Oxford, UK:MCE Publications, 1989), p. 1309.
8. P. Niskanen, T.H. Sanders, Jr. , M. Marek, J.G. Rinker, in Aluminium-Lithium Alloys, ed. T.H. Sanders Jr., E.A. Starke Jr. (Warrendale, PA:TMS, 1981), p. 347.
9. P. Niskanen, T.H. Sanders Jr., J.G. Rinker, M. Marek, *Corr. Sci.* 22 (1982):p. 283.

10. R.E. Ricker, D.J. Duquette, in Aluminium- Lithium II, ed. T.H. Sanders Jr., E.A. Starke Jr., (Warrendale,PA:TMS, 1983), p. 581.
11. C. Thakur, R. Balasubramaniam, *Acta Metall. Mater.* (1996) Communicated.
12. S.S. Kim, E.W. Lee, K.S. Shin, *Scripta Metall.* 22 (1988): p. 1831.
13. L. Chen, W. Chen, Z. Liu, Y. Shao, Z. Hu, *Metall. Trans.* 24A (1993):p. 1355.
14. A. Bandyopadhyay, R. Ambat, E.S. Dwarkadasa, *Bull. Mater. Sci.* 15 (1992):p. 311.
15. C. Thakur and R. Balasubramaniam, *Scripta. Metall. Mater.* (1996) Communicated.
16. J.G. Craig, R.C. Newman, M.R. Jarrett, N.J.H. Holroyd, in Aluminium-Lithium IV, ed. G. Champier, B. Dubost, D. Miannay, L. Sabetay, J. de Physique Colloque, 48 (1987):p. C3-825.
17. R. Balasubramaniam, D.J. Duquette and K. Rajan, *Acta Metall. Mater.* 39 (1991):p. 2597.
18. R. Ambat, E.S. Dwarakadasa, *Corr. Sci.* 33 (1992):p. 681.
19. P.P. Pizzo, R.P. Galvin, H.G. Nelson in "Environment-Sensitive Fracture: Evaluation and Comparison of Test Methods," ASTM STP *821,* ed. S.W Dean, E.N. Pugh and G.M. Ugiansky, (Philadelphia,Pa:ASTM,1984) p. 173.
20. J.B. Lumsden, A.T. Allen, *Corr. Sci.* 44 (1988):p. 527.
21. C.T. Tsao, P.P. Pizzo, *Corrosion'*85, paper no. 69, NACE, Boston, USA (25-29 March 1985).

22. R.G. Buchheit, G.E. Stoner in Aluminium-Lithium V, ed. T H Sanders Jr., E A Starke Jr. (Oxford, UK:MCE Publications, 1989).

23. R.S. Piascik, R.P. Gangloff in Environmental Cracking of Metals, ed. R.P. Gangloff, M.B. Ives, (Houston,TX:NACE,1989).

24. T. Magnin, M. Rebiere in Aluminium-Lithium IV, ed. G. Champier, B. Dubost, D. Miannay, L. Sabetay, J. de Physique Colloque, 48 (1987):p. C3-835.

25. J. Gui, T.M. Devine, *Scripta Metall.* 21 (1987):p. 853.

26. I. Epelboin, M. Keddam in Passivity of Metals, ed. R.P. Frankenthal, J. Kruger, (Princeton,NJ:The Electrochemical Society,1978), p. 184.

27. E.L. Colvin, G.L. Cahen, Jr., G.E. Stoner, E. A. Starke, *Corrosion* 42 (1986):p. 416.

28. S. Schnuriger, G. Mankowski, Y. Roques, G. Chatainier, F. Dabosi, in Aluminium-Lithium IV, ed. G. Champier, B. Dubost, D. Miannay, L. Sabetay, J. de Physique Colloque, 48 (1987): p. C3-851.

29. G.Kortum, J.O.M. Bockris in "Textbook of Electrochemistry" Vol II, (Amsterdam:Elsevier, 1951).

30. R.Balasubramaniam, D.J.Duquette, K.Rajan, *Acta Metall. Mater.* 39 (1991):p. 2607.

31. C.Thakur, R. Balasubramaniam, *Scripta Mater,* communicated.

32. J.P. Moran, E.A. starke, G.E. Stoner, G.L. Cahen Jr., *Corrosion* 86, paper no. 203, NACE, Houston (17-21 March 1986).

33. M. Pourbaix, *Corrosion* **27** (1971):p. 449

34. K. Tohma and Y. Takeuchi, *J Jpn Inst Light Met.* **29** (1979):p. 232

35. S.K. Garg in *Environmental Engineering* Volume II (New Delhi:Khanna Publishers) 1990 p 589

35. C.H. Tsao and P.P. Pizzo in *Corrosion 85*, March 25-30, Boston USA, 1985, paper 69.

36. Z.F. Wang, Z.Y. Zhu, Y. Zhang and W.Ke *Metall. Trans.* **23A** (1993):p 3337

LIST OF FIGURES

LIST OF TABLES

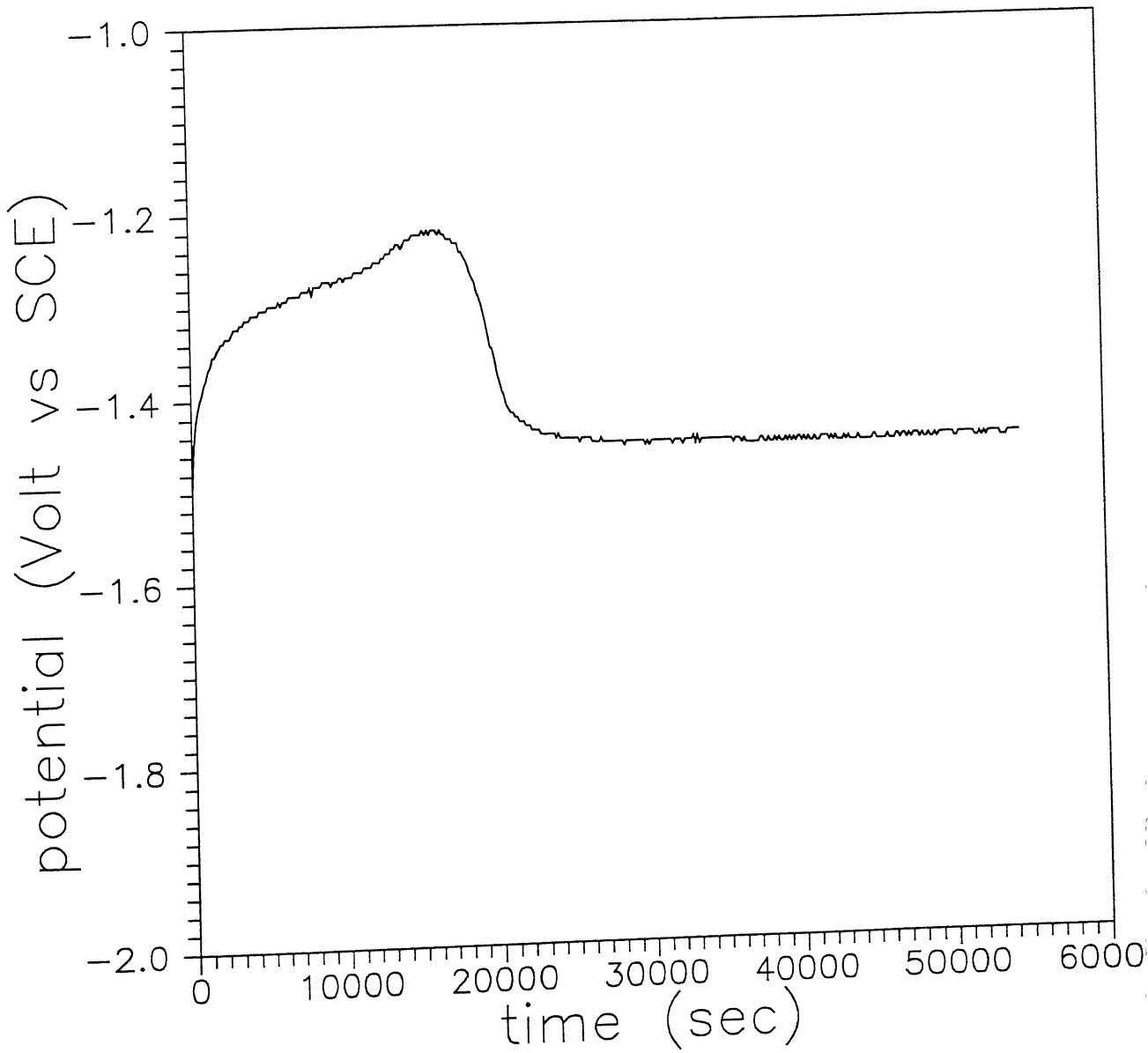

FIG A.1. Variation of free corrosion potential as a function of time for 1441 alloy in 0.1 mol/l NaOH solution at 25°C.

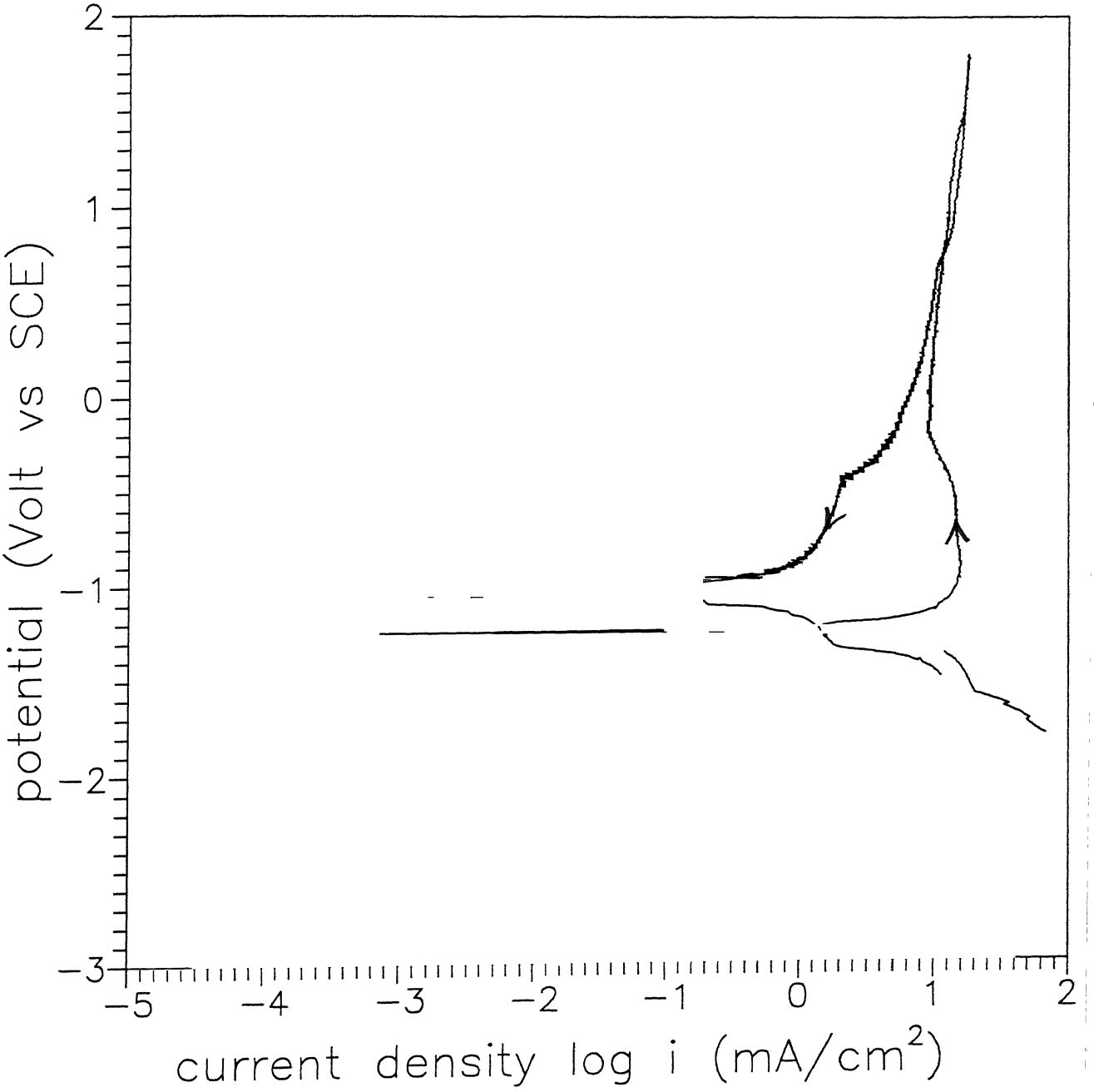

FIG A.2. Cyclic potentiodynamic polarization curves for 1441 alloy in 0.1 mol/l NaOH solution after 2 hour immersion at 25°C.

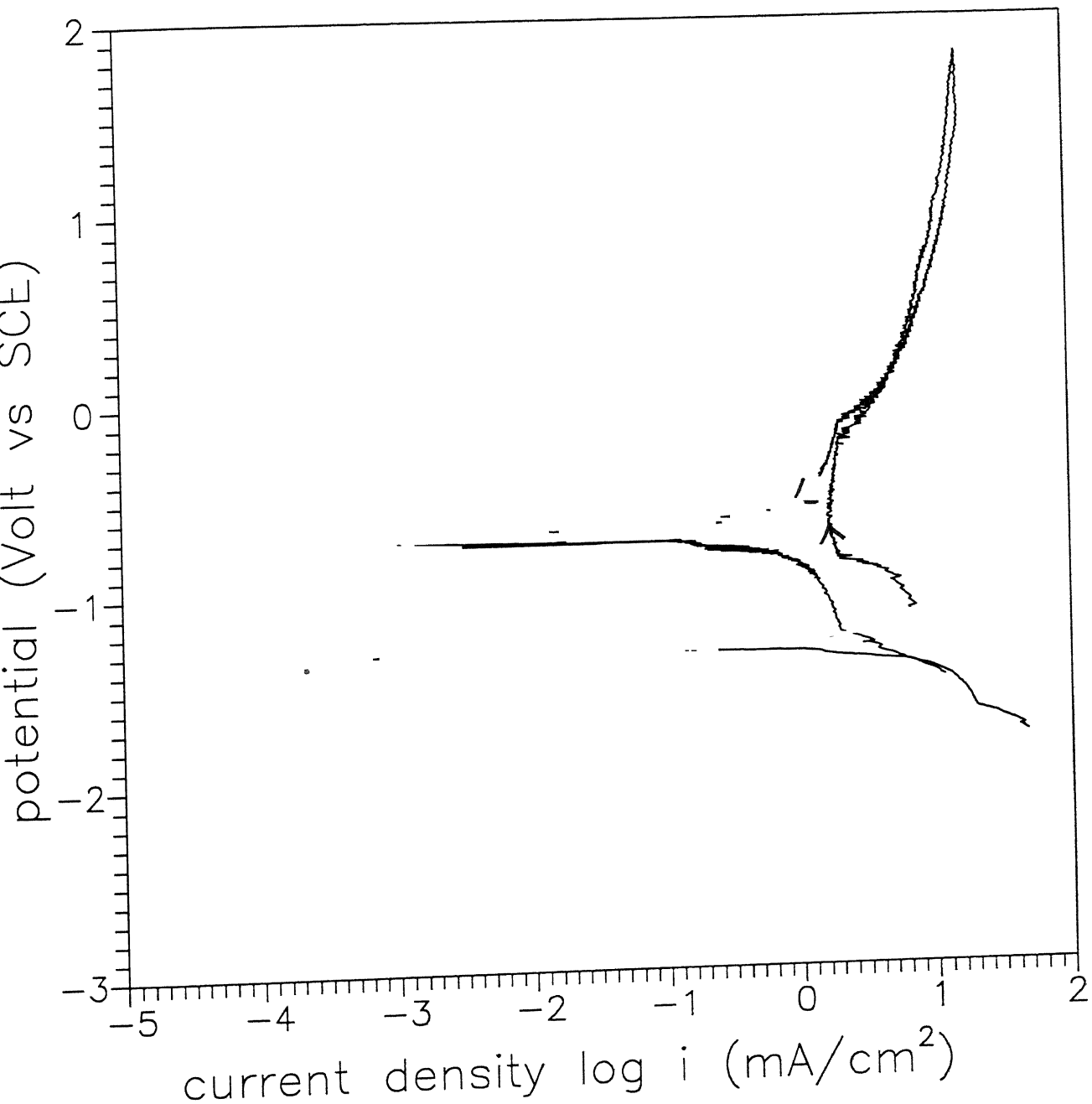

FIG A.3. Cyclic potentiodynamic polarization curves for 1441 alloy in 0.1 mol/l NaOH solution after 15 hour immersion at 25°C.

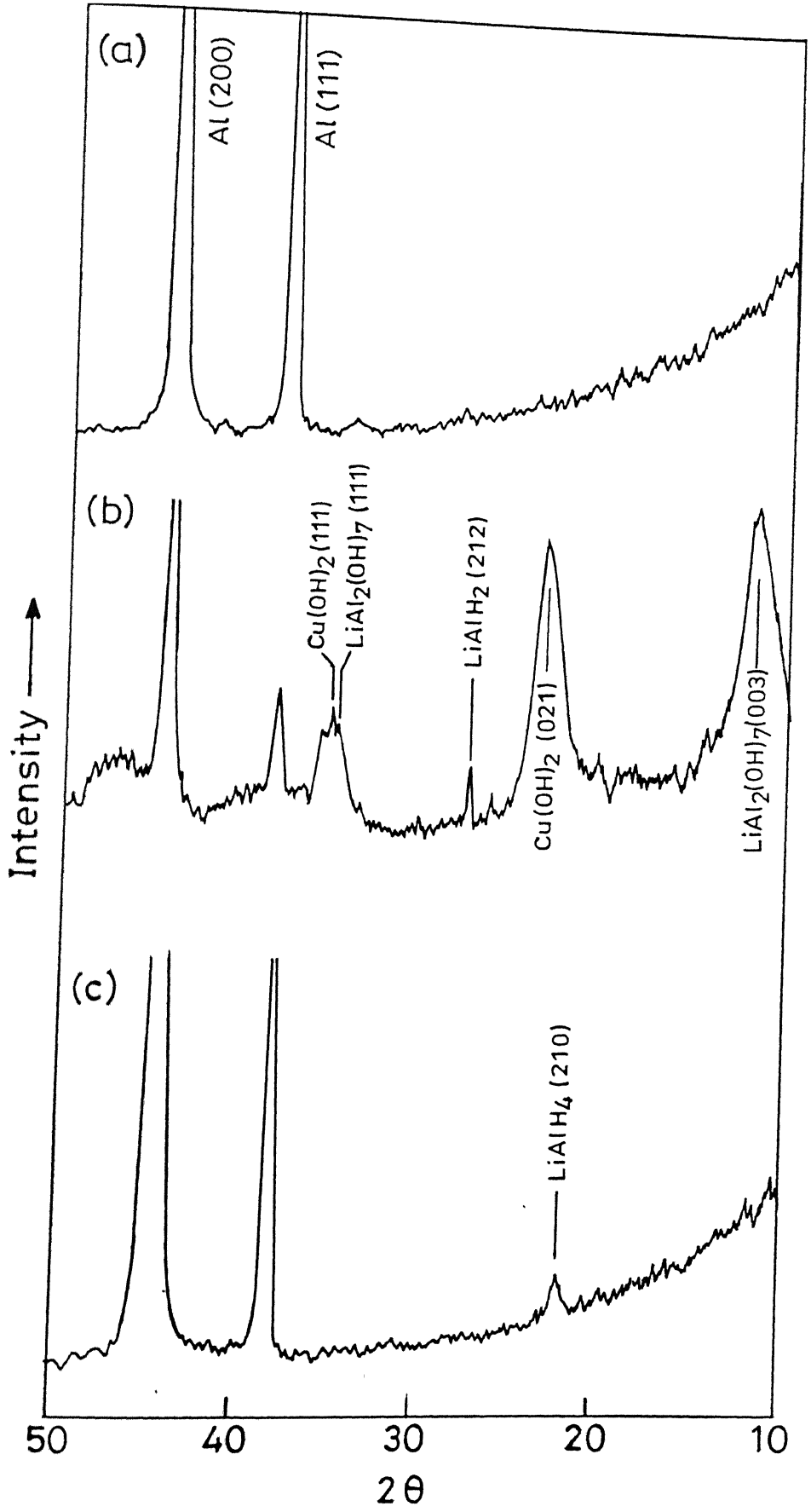

FIG A.4. X-ray diffraction patterns of the 1441 alloy (a) before and after (b) 7 days immersion in 0.1 mol/l NaOH solution, and (c) after removal of the scale from the surface of the specimen immersed for 7 days.

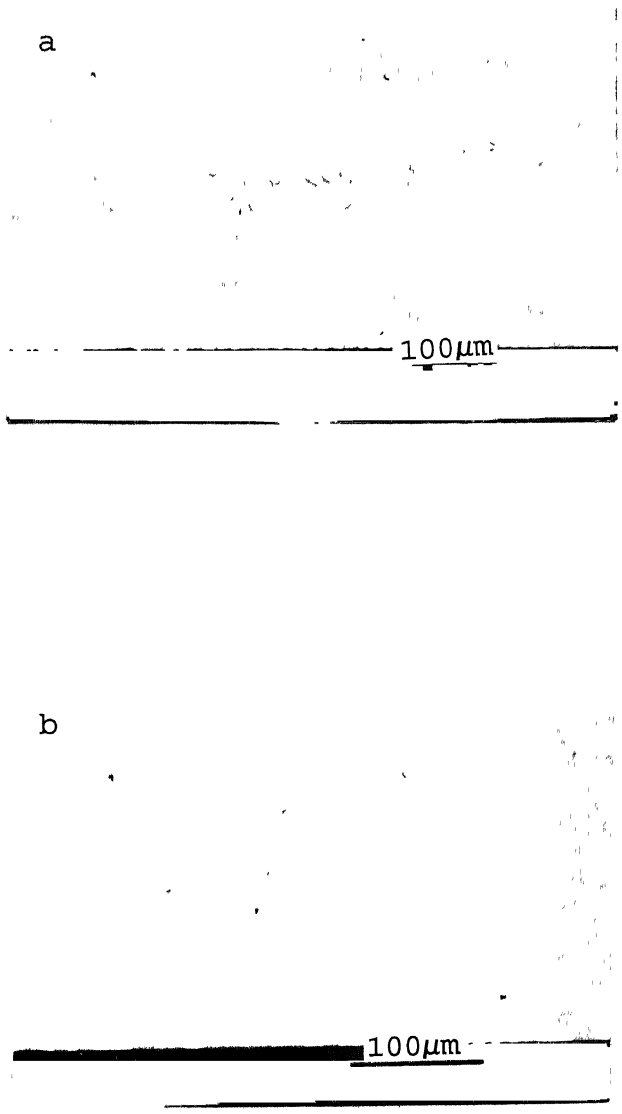

FIG A.5. Scanning electron micrographs of the film formed on 1441 alloy after 2 hour immersion in 0.1 mol/l NaOH solution at (a) low and (b) high magnification.

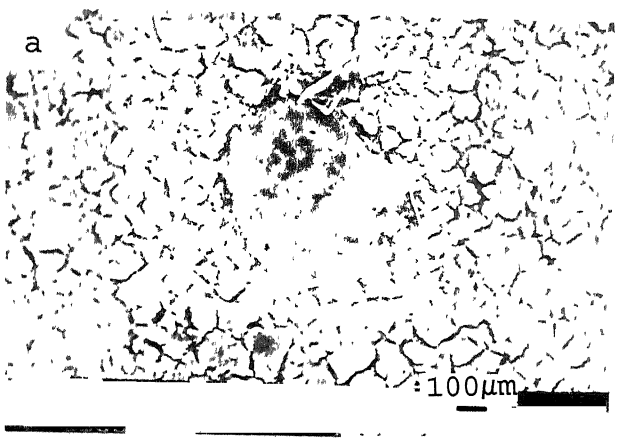

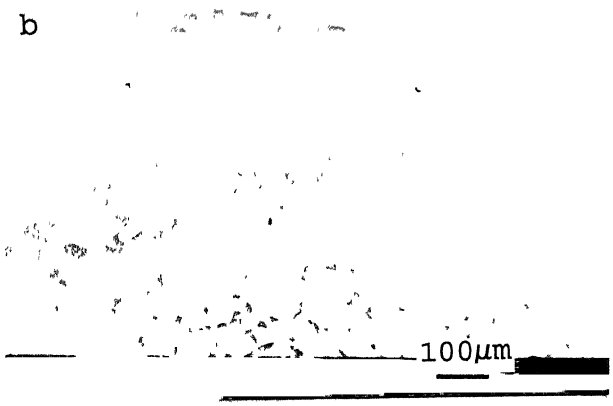

FIG A.6. Scanning electron micrographs of the film formed on 1441 alloy after 15 hour immersion in 0.1 mol/l NaOH solution at (a) low and (b) high magnification.

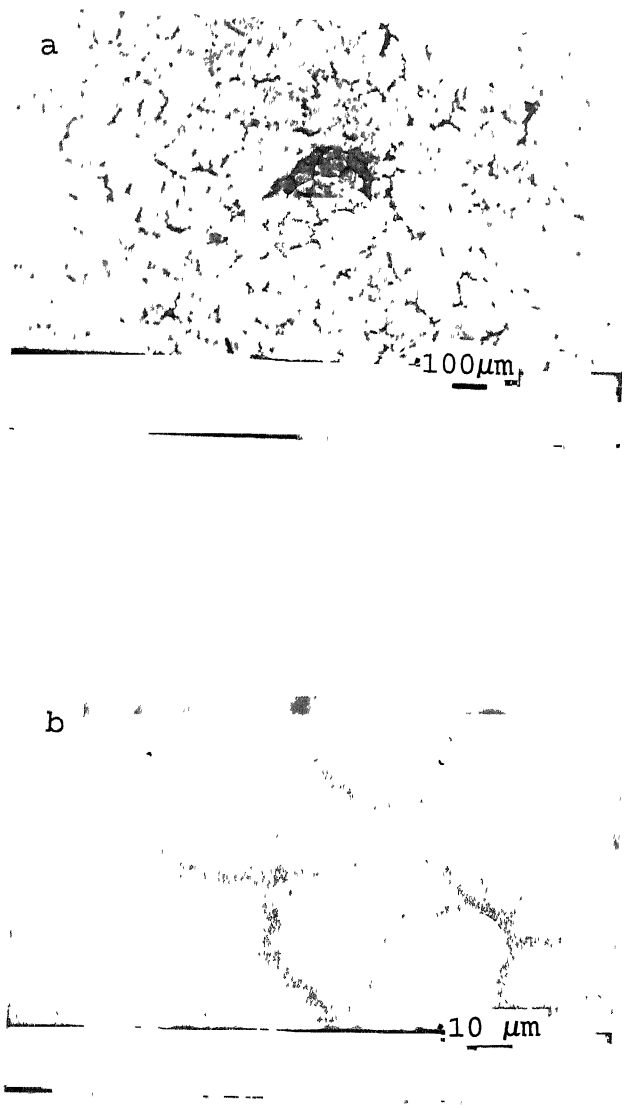

FIG A.7. Scanning electron micrographs of the film formed on 1441 alloy after 7 days immersion in 0.1 mol/l NaOH solution at (a) low and (b) high magnification.

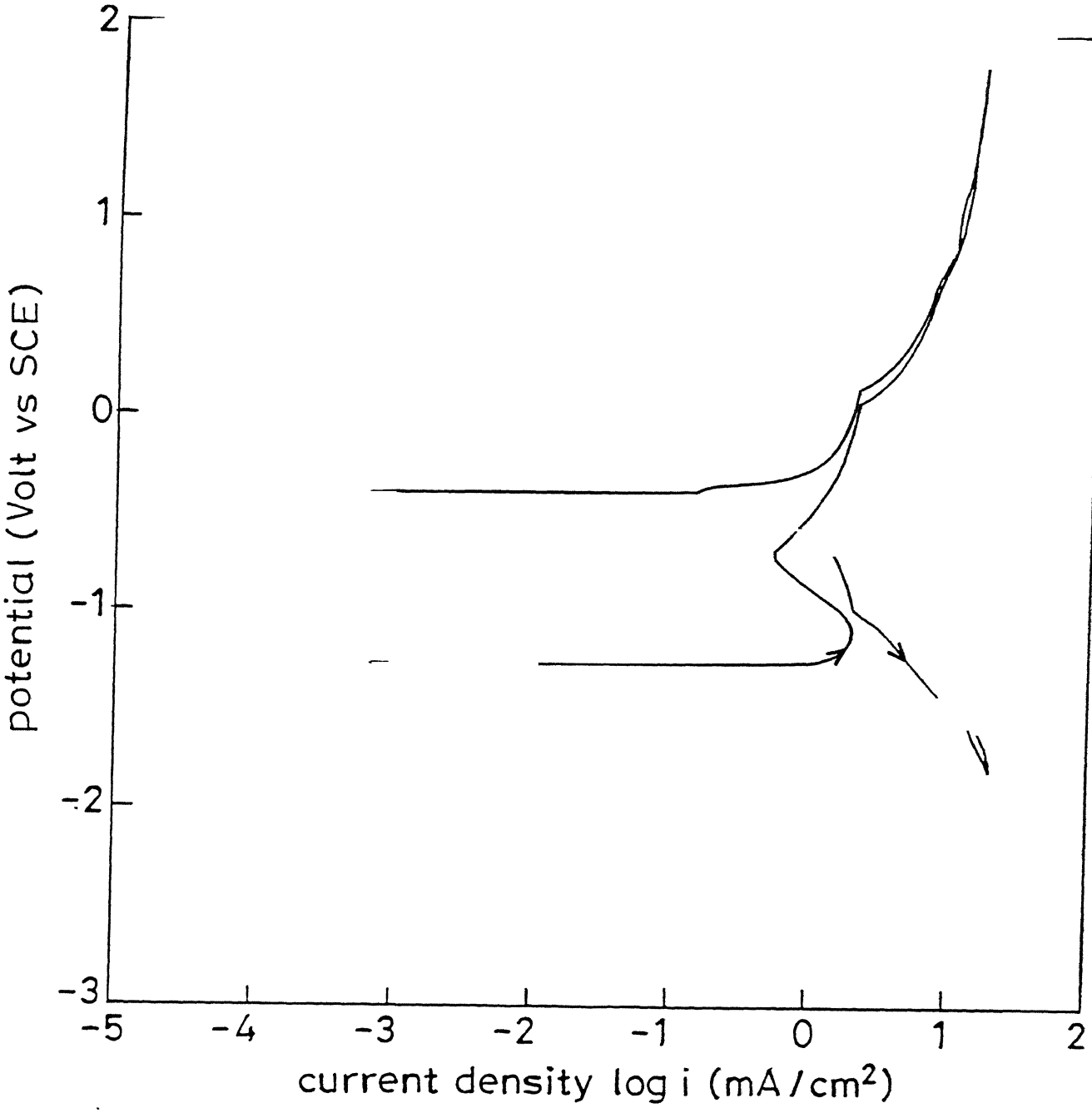

FIG A.8 Cyclic potentiodynamic polarization curve in 0.1 mol/l NaOH solution at 15°C.

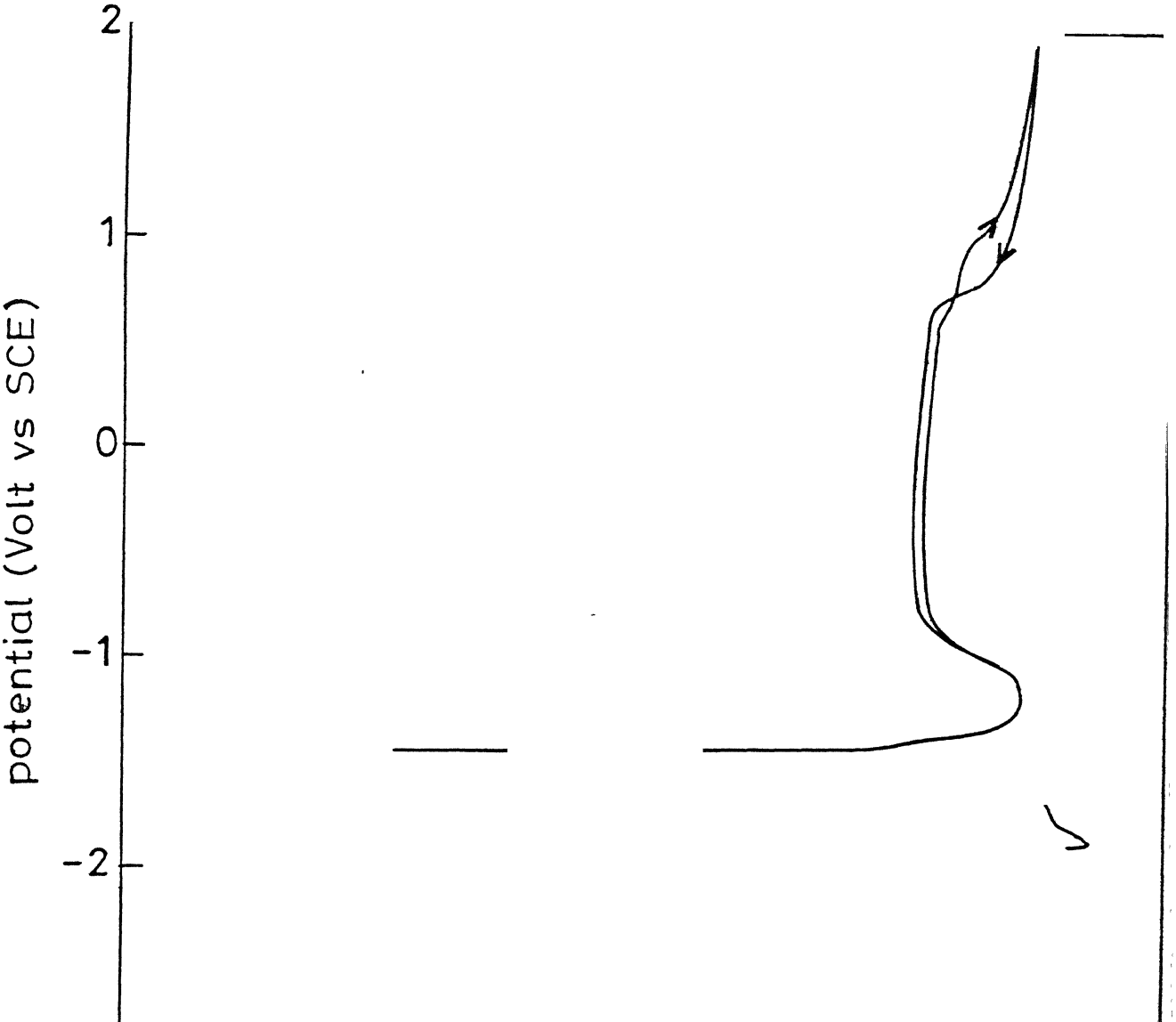

FIG A.9 Cyclic potentiodynamic polarization curve in 0.1 mol/l NaOH solution at 35°C.

TABLE A.1

Electrochemical polarization charateristics of the 1441 alloy in 0.1 mol/l NaOH solution after 2 and 15 hour immersion at 25°C.

Immersion Time (h)	FCP mV vs SCE	ZCP_f mV vs SCE	ZCP_b mV vs SCE	Epp mV vs SCE	Ecp mV vs SCE	i_{crit} A cm^{-2}	i_{pass} mA cm^{-2}
2	-1300	-1250	-1050	-950	-200	15.9	10.0
15	-1458	-1320	-720	-1200	-900	6.3	1.6

TABLE A.2

Electrochemical parameters obtained from the polarization curves of the Al-Li alloy in 0.1 mol/l NaOH solution at different temperatures.

Temp (°C)	FCP mV vs SCE	ZCP_f mV vs SCE	Passive Range mV	i_{crit} mA cm^{-2}	i_{pass} mA cm^{-2}	i_{corr} mA cm^{-2}
15	-1450	-1250	700	1.8	0.5	0.3
25	-1458	-1320	700	6.3	1.6	0.5
35	-1520	-1450	1550	10.0	2.0	0.8

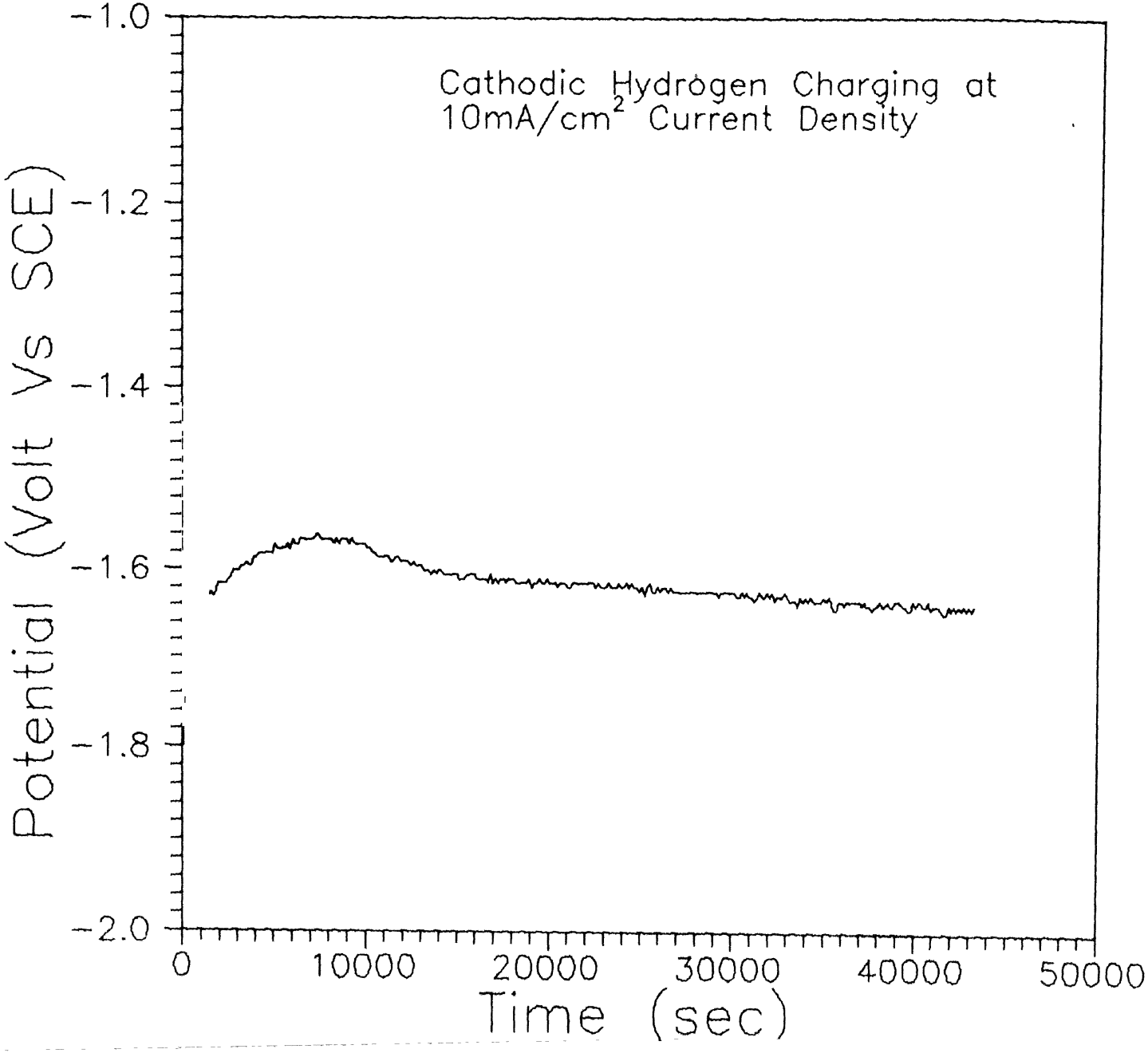
Cathodic Hydrogen Charging at
10mA/cm^2 Current Density
Potential (Volt Vs SCE)
-1.0
-1.2
-1.4
-1.6
-1.8
-2.0
0
10000
20000
30000
40000
50000
Time (sec)